

D3.3. Lab Testing and Validation of the Thermal Management System



Reinventing High-performance pOwer converters for heavy-Duty electric trAnSpot

Grant Agreement Number 101056896

Deliverable name: Lab Testing and Validation of the Thermal Management System
Deliverable number: D3.3
Deliverable type: Report (R)
Work Package: WP3: Thermal Management System
Lead beneficiary: BOSMAL (BOS)
Contact person: Rafał Sala;
rafal.sala@bosmal.com.pl
Piotr Bielaczyc;
piotr.bielaczyc@bosmal.com.pl
Dissemination Level: PU - Public
Due date for deliverable: August 31st, 2024



Funded by the
European Union

DOCUMENT CONTROL PAGE

Author(s):	Rafał Sala, Michał Heseck, Piotr Bielaczyc, Arman Fathollahi
Contributor(s):	BOSMAL, AU, UPC
Reviewer(s):	Jørgen Houe Pedersen, Arman Fathollahi, Corneliu Barbu, David Lumbreras, Luis Romeral
Version number:	v.11
Contractual delivery date:	31-08-2024
Actual delivery date:	03 – 03 – 2025
Status:	Submitted

REVISION HISTORY

Version	Date	Author/Reviewer	Notes
v.0	30 – 07 – 2024	Michał Heseck	Creation, First Draft
v.1	18 – 09 – 2024	Rafał Sala	Comments and review
v.2	19 – 11 – 2024	Arman Fathollahi	First Draft of Sections 3-4
v.3	2 – 12 – 2024	Jørgen Houe Pedersen/ Arman Fathollahi	Review/Revise Sections 3-4
v.4	12 – 02 – 2025	Michał Heseck	Added final TMS testing results, incorporated AU report, minor formatting changes
v.5	15 – 02 – 2025	Rafał Sala	Deliverable Review/Revise
v.6	15 – 02 – 2025	Arman Fathollahi	Deliverable Revise
v.7	15 – 02 – 2025	Rafał Sala	Added additional description, minor corrections
v.8	24 – 02 – 2025	Corneliu Barbu	Reviewed. Submitted.
v.9	24 – 02 – 2025	David Lumbreras	Reviewed. Executive Summary and sections 1.2 shortened. Sections 1.3 and 1.4 removed. Future Directions and Recommendations section removed.
V.10	27 – 02 – 2025	Jose Saez	Reviewed. Format adjustments. List of acronyms
V.11	02 – 03 – 2025	Luis Romeral	Final Version. Submitted

ACKNOWLEDGEMENTS

The work described in this publication was subsidised by Horizon Europe (HORIZON) framework through the Grant Agreement Number 101056896.

DISCLAIMER

Funded by the European Union. Views and opinions expressed are however those of the author(s) only and do not necessarily reflect those of the European Union or CINEA. Neither the European Union nor the granting authority can be held responsible for them.

TABLE OF CONTENTS

LIST OF ACRONYMS	6
EXECUTIVE SUMMARY	7
1 INTRODUCTION.....	8
1.1 DESCRIPTION OF THE DOCUMENT and its purpose.....	8
1.2 WPS AND TASKS RELATED WITH THE DELIVERABLE	8
2 HEATSINK GEOMETRY DESIGN OPTIMIZATIONS	9
2.1 LOW-POWER CONVERTER AIR-COOLED HEATSINK.....	9
2.2 HIGH-POWER CONVERTER LIQUID-COOLED HEATSINK	12
2.3 KEY DIFFERENCES BETWEEN HEATSINKS	27
3 THERMAL MANUFACTURING PROCESS OF LIQUID-COOLED HEATSINKS FOR HIGH-POWER CONVERTER	27
4 THERMAL MANAGEMENT SYSTEM UNDER TEST	30
5 TEST PROGRAM DESCRIPTION	31
5.1 TEST PHASES	31
5.1.1 PHASE 1: COMPONENT-LEVEL TESTING	31
5.1.2 PHASE 2: SYSTEM-LEVEL VALIDATION.....	32
6 COMPONENTS TESTING	33
6.1 RADIATOR THERMAL PERFORMANCE TEST	33
6.1.1 TEST OBJECT IDENTIFICATION	33
6.1.2 SCOPE OF THE TEST	33
6.1.3 TEST STAND INSTRUMENTATION	33
6.1.4 TEST RESULTS AND DISCUSSION.....	35
6.2 FAN SYSTEM FUNCTIONAL CHARACTERISTIC TEST	38
6.2.1 TEST OBJECT IDENTIFICATION	38
6.2.2 SCOPE OF THE TEST	39
6.2.3 TEST STAND INSTRUMENTATION	39
6.2.4 TEST RESULTS AND DISCUSSION.....	40
6.3 COOLANT PUMP PERFORMANCE TEST	45
6.3.1 TEST OBJECT IDENTIFICATION	45
6.3.2 SCOPE OF THE TEST	46
6.3.3 TEST STAND INSTRUMENTATION	46
6.3.4 TEST RESULTS AND DISCUSSION.....	47
6.4 HEATSINK FUNCTIONAL CHARACTERISTIC TEST	48

6.4.1	TEST OBJECT IDENTIFICATION	48
6.4.2	SCOPE OF THE TEST	49
6.4.3	TEST STAND INSTRUMENTATION	50
6.4.4	TEST RESULTS – HEATSINK SAMPLE 1	51
6.4.5	TEST RESULTS - HEATSINK SAMPLE 2.....	55
6.5	THERMAL MANAGEMENT SYSTEM FUNCTIONAL CHARACTERISTIC TEST	62
6.5.1	TEST OBJECT IDENTIFICATION	62
6.5.2	SCOPE OF THE TEST	62
6.5.3	TEST STAND INSTRUMENTATION	63
	The test stand instrumentation is presented in Table 23.	63
6.5.4	TEST RESULTS – TMS.....	65
7	ANALYSIS OF THE THERMAL PERFORMANCE OF THE LIQUID-COOLED HEATSINK.....	67
7.1	ALUMINUM VS. COPPER HEATSINK PERFORMANCE.....	67
7.2	DATA ANOMALIES IN SAMPLE 2.....	67
7.3	PERFORMANCE EVALUATION OF THE ALUMINUM HEATSINK....	68
7.4	SYSTEM CHARACTERIZATION AND WORST-CASE SCENARIO...	68
8	CONCLUSION	71

LIST OF ACRONYMS

ACRONYM	DESCRIPTION
CAE	Computer Aided Engineering
CFD	Computational Fluid Dynamics
EV	Electric Vehicles
GaN	Gallium Nitride
IMD	Integrated Motor Drive
PCB	Printed Circuit Board
SiC	Silicon Carbide
TMS	Thermal Management System

EXECUTIVE SUMMARY

This deliverable D3.3 reports on the laboratory testing of the Thermal Management System (TMS) for a 150 kW High-Power Converter (HPC). Two prototype heatsinks, one made of copper and the other of aluminium, were tested. The aluminium heatsinks showed significant weight reduction while maintaining heat dissipation efficiency. The TMS is integral to the RHODAS project's 150 kW Integrated Motor Drive (IMD), ensuring optimal temperature for power converters in electric vehicles. The TMS, including the aluminium heatsink module, radiator, fan system, coolant pump, and piping, demonstrated effective performance under various thermal loads in laboratory conditions.

Supported by Computer Aided Engineering (CAE) and Computational Fluid Dynamics (CFD) analyses, the TMS design proved to be robust and scalable. Test results will guide future optimizations to enhance thermal efficiency and system integration for vehicle applications. The TMS is critical in preventing overheating, improving reliability, and extending the lifespan of components in electric vehicles (EVs).

1 INTRODUCTION

1.1 DESCRIPTION OF THE DOCUMENT AND ITS PURPOSE

The purpose of this document is to provide a comprehensive overview of the testing and validation program performed on the TMS developed under the RHODAS project. Effective thermal management is required for achieving target performance and longevity of power converters employed in electric vehicle powertrains. The power converters are responsible for electrical energy conversion process which generates significant amount of energy losses in the form of heat. The TMS is essential to dissipate such heat and maintain appropriate thermal conditions for optimal system performance.

This document outlines the objectives, methodologies, test results and conclusions of the testing program focusing on the following aspects:

- **Test Object Identification:** TMS components description, schematics and of the liquid-cooled heatsink module, radiator, fan system and coolant pump.
- **Test Program Description:** A structured breakdown of the testing phases, including component and system-level testing for thorough evaluation of the TMS performance.
- **Components Testing:** Test results and analysis of individual TMS components focussing on the development heatsink module performance.
- **Thermal Management System Validation:** Evaluation of the integrated TMS at selected points of thermal loading, simulating worst-case scenarios.
- **Conclusions and Recommendations:** Summary and insights gained from the testing activities to further refine and scale up the TMS for applications of above 150 kW.

1.2 WPS AND TASKS RELATED WITH THE DELIVERABLE

This deliverable refers to Task T3.6 included in WP3: Development and Validation of the Thermal Management System.

2 HEATSINK GEOMETRY DESIGN OPTIMIZATIONS

The geometry of liquid-cooled heatsinks is crucial for enhancing thermal management efficiency, especially in high-power applications where effective heat dissipation is essential. The heatsink design, including fin shapes, channel arrangements and overall surface area, directly influences its ability to remove heat from high-power semiconductor modules. A well-designed geometry increases surface contact with the liquid, allowing for an even and effective distribution of temperature. This not only prevents localized hotspots but also improves the lifespan and performance of the system, as components remain within safe operational temperatures.

Optimizing heatsink geometry impacts the heat dissipation process by enabling faster and uniform cooling. By fine-tuning aspects like fin spacing, thickness, and flow paths, designers can enhance the flow rate and heat absorption of the cooling fluid, maximizing the thermal transfer efficiency. Improved geometry also reduces fluid pressure drop, minimizing energy consumption for fluid movement while maintaining optimal cooling. These optimizations ensure that high-power systems operate at peak efficiency, maintain stability, and reduce the risk of thermal overload, ultimately supporting system reliability and energy efficiency.

This section introduces various heatsink designs along with their iterative optimization process. Additionally, the optimized geometry is presented, accompanied by a sensitivity analysis of the heatsink material and key design parameters. Finally, we review the results of the heatsink pressure test on the final version to ensure it meets the requirements for industrial application.

2.1 LOW-POWER CONVERTER AIR-COOLED HEATSINK

In the initial phase, the AU team designed a set of three heatsinks for the low-power converter (15kW) developed by UPC in WP2.

The low-power converter is a modular T-type converter, where each phase has its own power and control PCB. The prototype incorporates SiC and GaN semiconductors and the converter is designed to handle power levels up to 15 kW, as specified in D2.4. The modulation technique used in the converter plays a critical role in determining power losses thus, influences the requirements for the heatsink designs. In case of low-power converter the efficiency of 96% was assumed corresponding to 200 W of heat loss per phase.

Based on the converter's power losses and to balance cooling system complexity with heat dissipation needs, AU designed an air-cooled heatsink. Figure 1 illustrates the geometry configuration and boundary conditions for this air-cooled low-power heatsink. The heat rates indicated in the figure result from power losses within the GaN and SiC modules of the RHODAS low-power converter. Additionally, a height step was incorporated in the heatsink design to align with the height differences of the GaN and SiC power board areas on the converter board. In order to validate the heatsink performance, the design was simulated by the Finite Element Method using COMSOL Multiphysics software, applying the same boundary conditions and parameters as shown in the Figure.

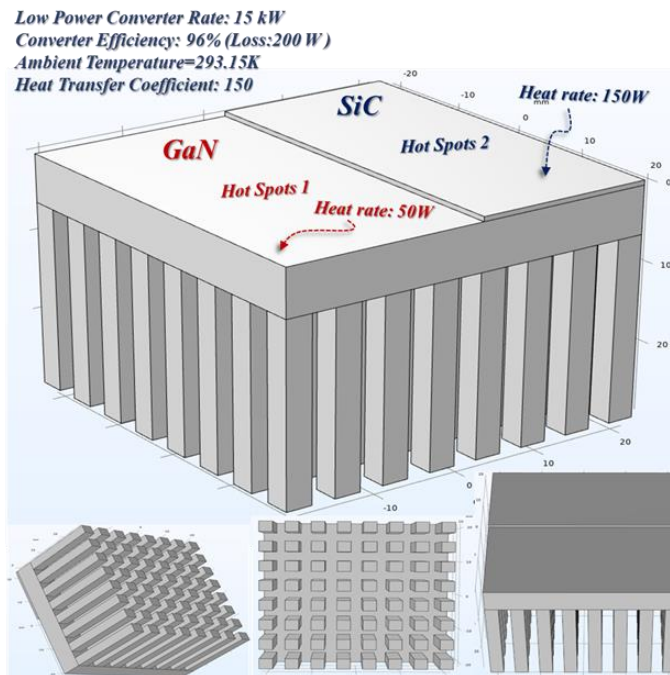


Figure 1 - Geometry configuration and boundary conditions for the air-cooled low-power heatsink

Figure 2 presents the meshing arrangement used in the simulation and the resulting element quality histograms.

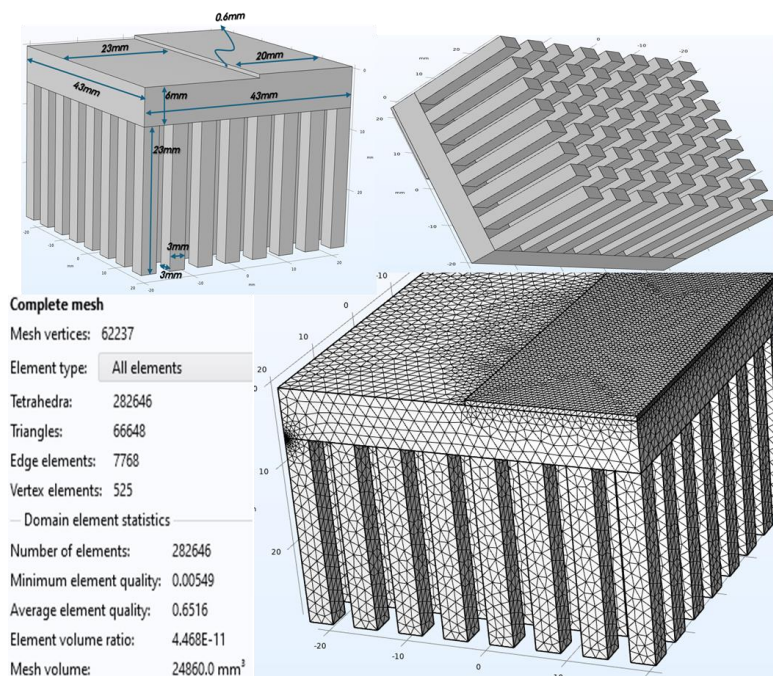
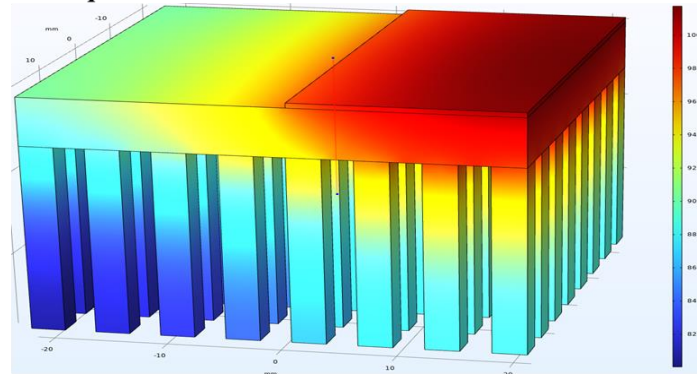


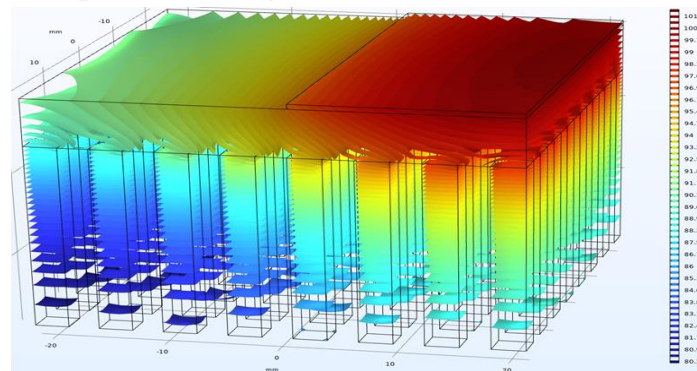
Figure 2 - Geometry configuration and boundary conditions for the air-cooled low-power heatsink

The results of the Multiphysics simulations are shown in Figure 3 and Figure 4, which presents the temperature distribution in the heatsink body and cold plate, demonstrating the efficient heat dissipation of this copper heatsink. The figure also displays heat dissipation isosurfaces, illustrating the heat flow from the top to the bottom layers of the heatsink. Temperature limits for the SiC module (175 °C) and GaN module (150 °C) were

maintained, with maximum temperatures observed at 97.0309 °C for the GaN cold plate and 101.740 °C for the SiC cold plate, both within the required limits for safe operation.

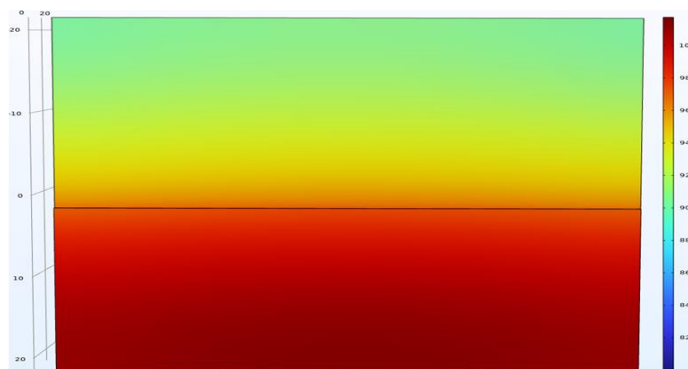


(a)



(b)

Figure 3 - Multiphysics analysis of the air cooled copper heatsink: a) Temperature distribution results b) heat dissipation isosurfaces



(a)

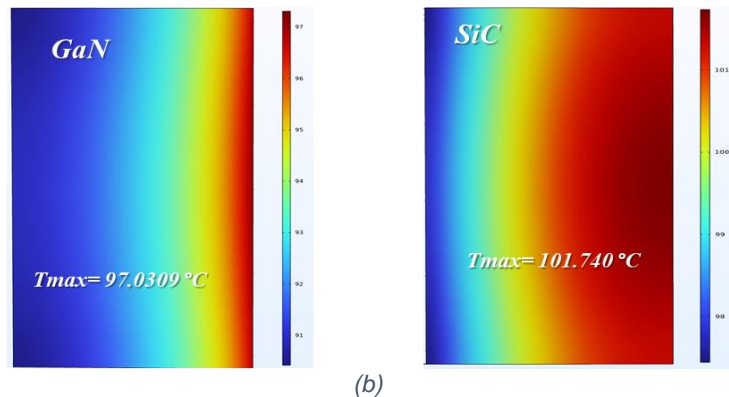


Figure 4 - Multiphysics analysis of the air-cooled copper heatsink: a) Temperature distribution results in the top b) Temperature distribution results in the cold plates

In the next phase, given that the heat transfer coefficient provided by the fan (which will direct air to the cold plate) significantly impacts heat dissipation efficiency, a sensitivity analysis was conducted on the heatsink.

Figure 5 shows the results of this analysis, where the heat transfer coefficient was varied from 200 W/(m²·K) to 350 W/(m²·K), resulting in a reduction in the maximum cold plate temperature from 84.472 °C to 62.041 °C.

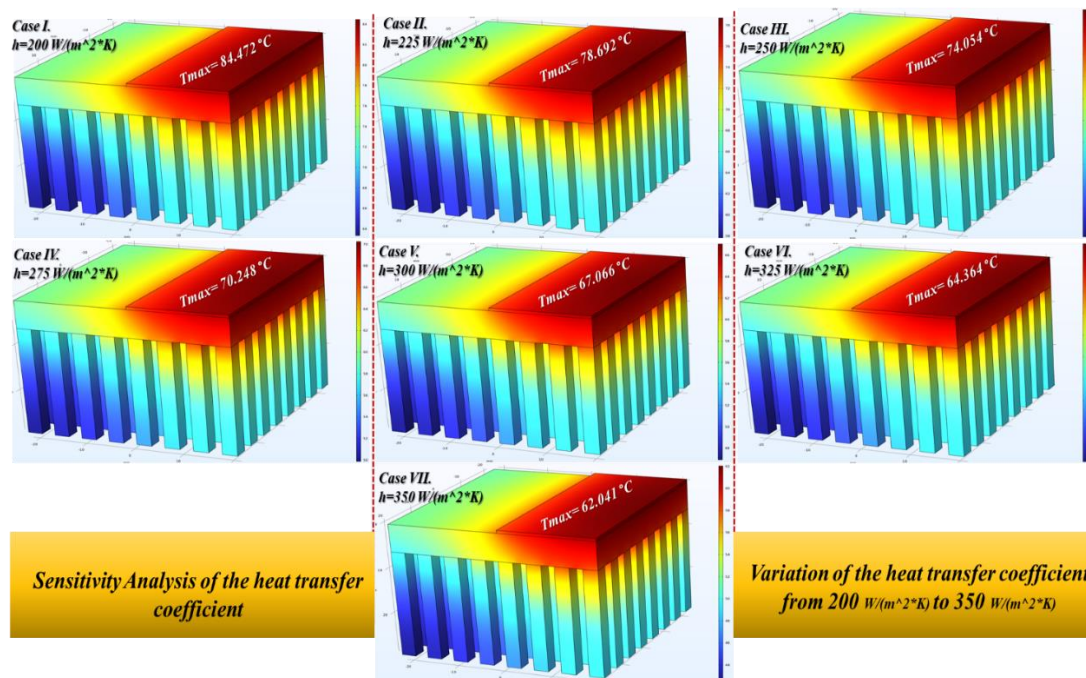


Figure 5 - Sensitivity analysis of heat dissipation efficiency in the air cooled heatsink, showing variation in maximum cold plate temperature as the heat transfer coefficient is adjusted from 200 W/(m²·K) to 350 W/(m²·K).

2.2 HIGH-POWER CONVERTER LIQUID-COOLED HEATSINK

As part of Task T3.5 in WP3, AU aims to design and manufacture a set of three heatsinks for the high-power converter developed by AIT. The structure of hybrid high-power T-type multilevel converter included main power board with GaN semiconductors, SiC

power modules and sensors. The prototype heatsinks underwent extensive laboratory testing protocols to ensure their effective functionality.

Based on the required heat dissipation capacity and the TMS developed in Tasks T3.1 and T3.2 of WP3, the AU team decided to design a liquid-cooled heatsink. Given that nearly two-thirds of the total power losses in each phase of the high-power converter come from the operation of SiC modules, AU designed the first draft of the high-power heatsink to accommodate the characteristics of the SiC modules, as specified in their data sheet.

Figure 6 and Figure 7 show the initial design for this high-power heatsink, characterized based on the real SiC CAB450M12XM3 module. Figure 6 illustrates the geometry of this liquid-cooled heatsink, which utilizes a long pin arrangement to enhance efficiency. Note that the initial parameters used in the simulation are depicted in Figure 5 (a), including the average inlet velocity, inlet temperatures, cold plate temperatures and the assumption of laminar flow and suppressed backflow at the heatsink outlet.

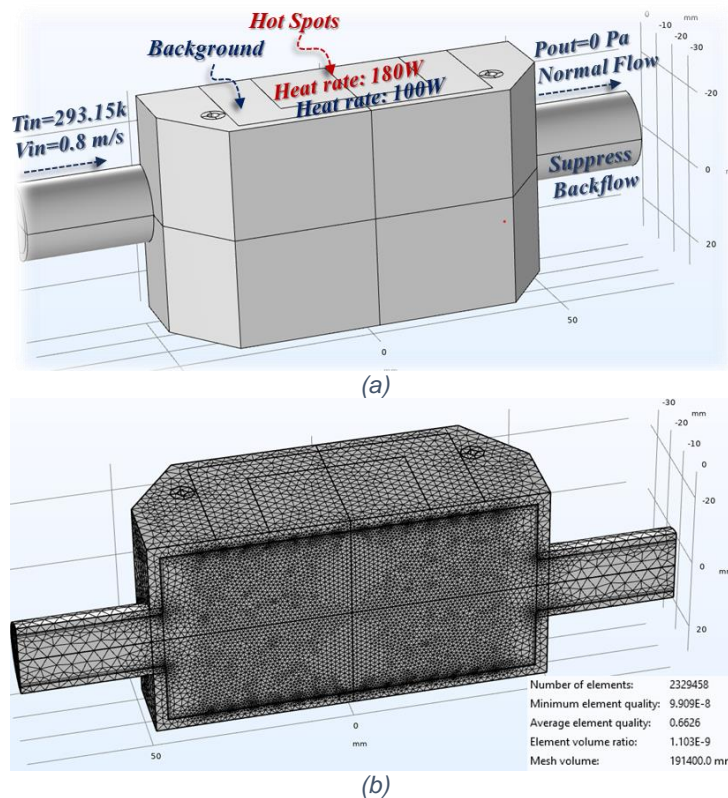


Figure 6 - First version of the high-power heatsink design, based on specifications of the SiC CAB450M12XM3 module: a) Geometric Configuration and Boundary Conditions b) Meshing Arrangement and Results

C. Geometry Components and Definitions

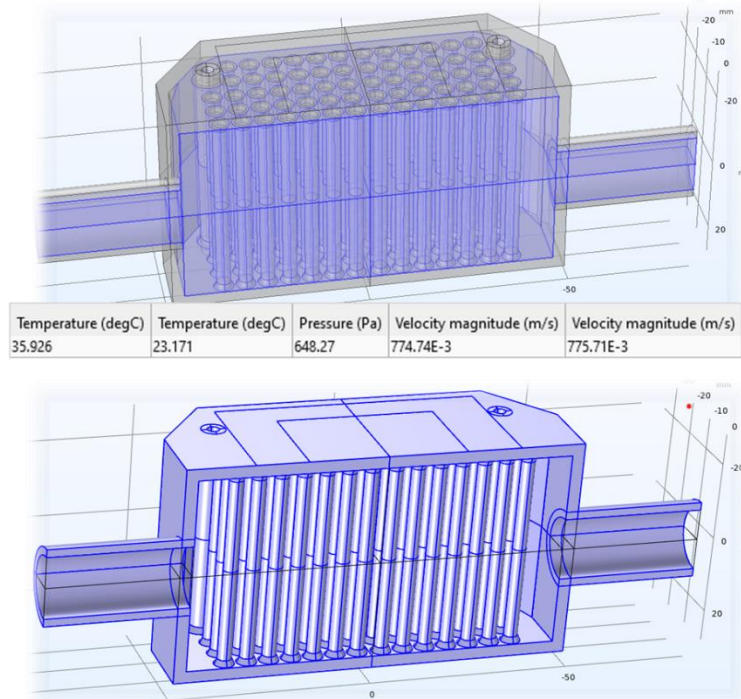


Figure 7 - First version of the high-power heatsink design, based on specifications of the SiC CAB450M12XM3 module: Geometry Components and Definitions

Figure 8 and Figure 9 present the temperature ($^{\circ}\text{C}$) and velocity distributions (m/s) in the top half of the heatsink, including the temperature distribution on the cold plate and along a line from one corner of the heatsink to the midpoint of the cold plate.

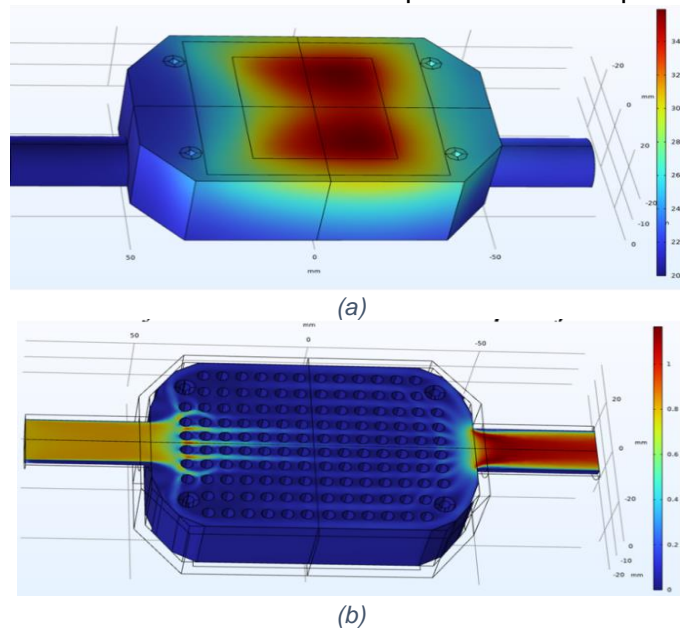


Figure 8 - First version of the high-power heatsink design, based on specifications of the SiC CAB450M12XM3 module: a) Temperature Distribution Results in the Top Half, b) Velocity Distribution Results in the Top Half

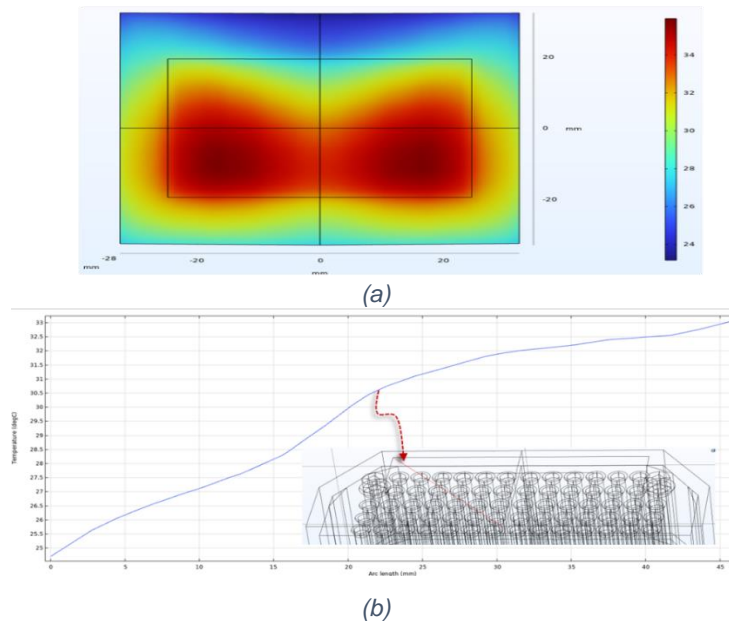
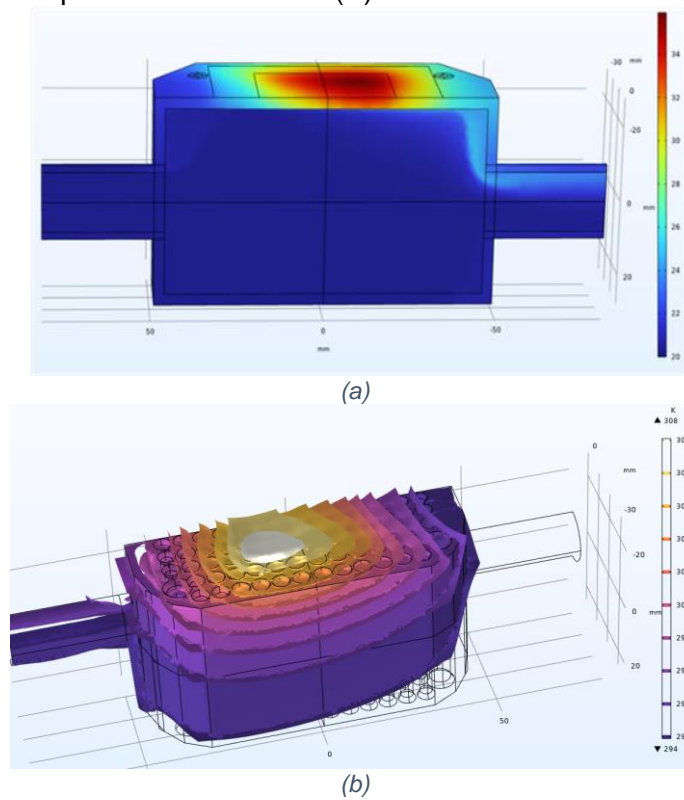
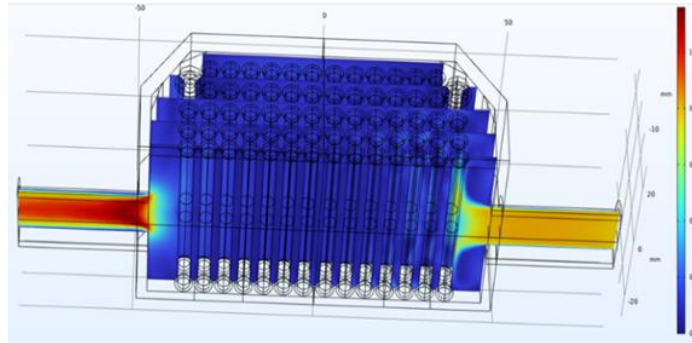


Figure 9 - First version of the high-power heatsink design, based on specifications of the SiC CAB450M12XM3 module: a) Temperature Distribution Results in the Cold Plate, b) Temperature Distribution Results in the Defined line

To further examine heat dissipation from the top cold plate to the bottom of the heatsink, Figure 10 shows temperature isosurfaces (K) within the heatsink.





(c)

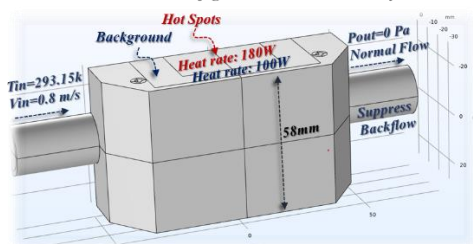
Figure 10 - First version of the high-power heatsink design, based on specifications of the SiC CAB450M12XM3 module: a) Temperature Distribution Results inside the Heatsink, b) Temperature Isosurface Results inside the Heatsink, c) Velocity Distribution Results inside the Heatsink

One of the most critical aspects in designing a liquid-cooled heatsink is optimizing its geometry, specifically determining the ideal size and shape of the heatsink. This design process must also consider mechanical constraints, as well as size limitations imposed by related designs, such as the power converter board and converter housing.

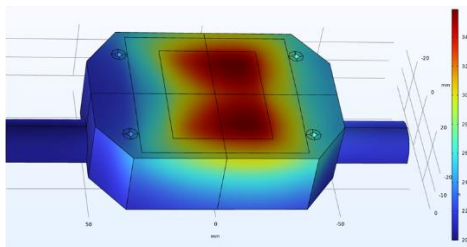
In this phase, AU conducted a scenario-based optimization, examining and simulating various design options to improve the heatsink heat dissipation characteristics, thereby reducing the maximum temperature on the heatsink top surface or cold plate. Figure 11 displays the results of a comparison between heatsinks of different heights. The temperature distribution in the top half of the heatsink indicates that a shorter heatsink height can improve heat dissipation, resulting in a lower maximum temperature on the heatsink.

Additionally, the results for velocity distribution and temperature distribution within the heatsink demonstrate enhanced liquid flow and more effective heat dissipation with optimized geometry.

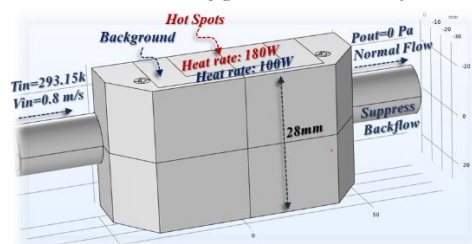
Case I. Geometric Configuration and Boundary Conditions



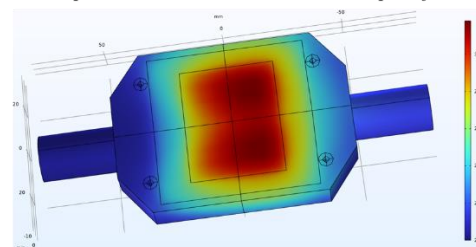
A. Temperature Distribution Results in the Top Half



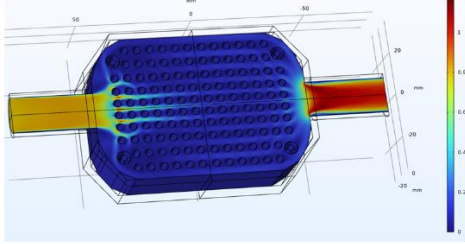
Case II. Geometric Configuration and Boundary Conditions



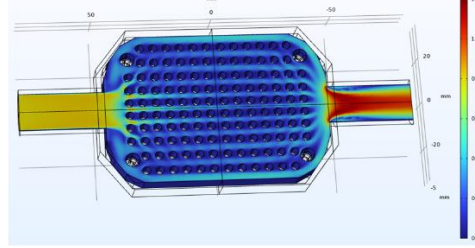
A. Temperature Distribution Results in the Top Half



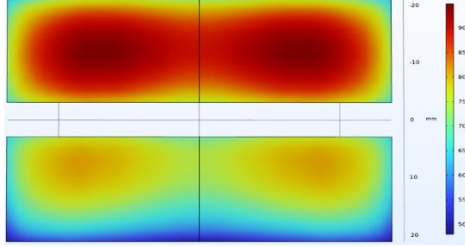
B. Velocity Distribution Results in the Top Half



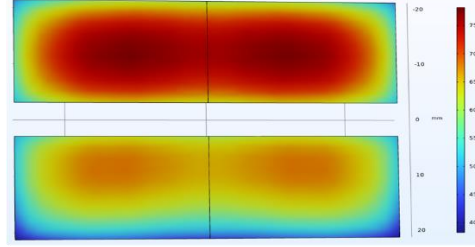
B. Velocity Distribution Results in the Top Half



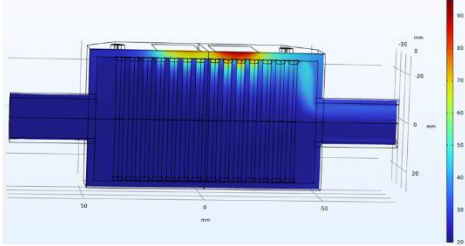
C. Temperature Distribution Results in the Cold Plate



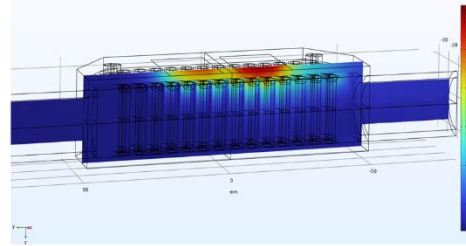
C. Temperature Distribution Results in the Cold Plate



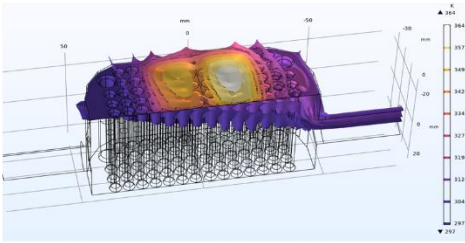
D. Temperature Distribution Results inside the Heatsink



D. Temperature Distribution Results inside the Heatsink



E. Temperature Isosurface Results inside the Heatsink



E. Temperature Isosurface Results inside the Heatsink

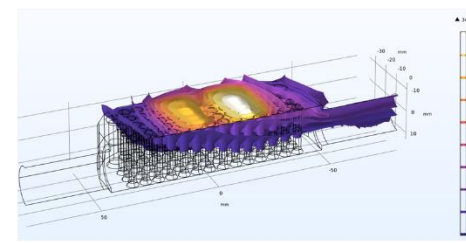
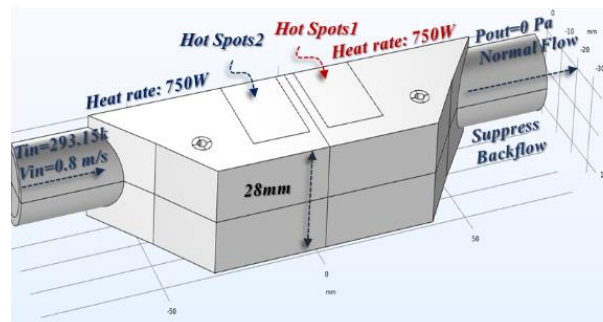
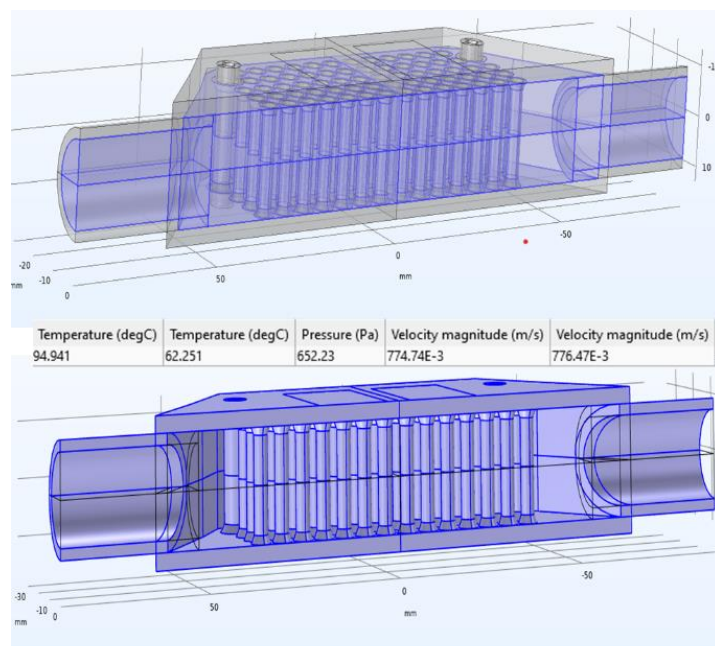


Figure 11 - Comparison of temperature distribution in heatsinks of varying heights, illustrating improved heat dissipation and lower maximum temperature with a shorter heatsink height.

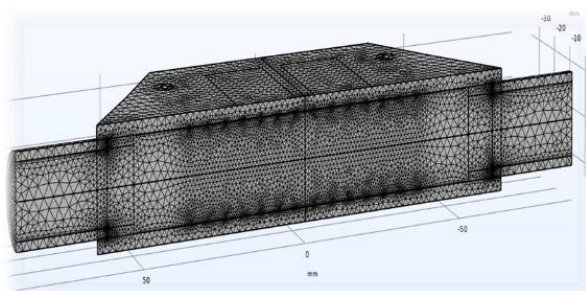
In the next phase of optimization, the AU team focused on refining the body shape of the high-power heatsink. Results from the previous heatsinks' velocity distributions indicated that, due to the current shape, two areas near the inlet and outlet remained inactive. To address this issue, the AU team modified the geometry around the inlet and outlet areas, as shown in Figure 12, to improve flow distribution and maximize heat dissipation.



(a)



(b)



(c)

Figure 12 - Modified heatsink geometry near the inlet and outlet areas: a) Geometric Configuration and Boundary Conditions, b) Geometry Components and Definitions, c) Meshing Arrangement and Results

As shown in Figure 13, adjusting the heatsink body shape transformed these previously inactive areas near the inlet into active regions, enhancing heat dissipation. Additionally, the flow distribution near the outlet demonstrated improved efficiency with this new design.

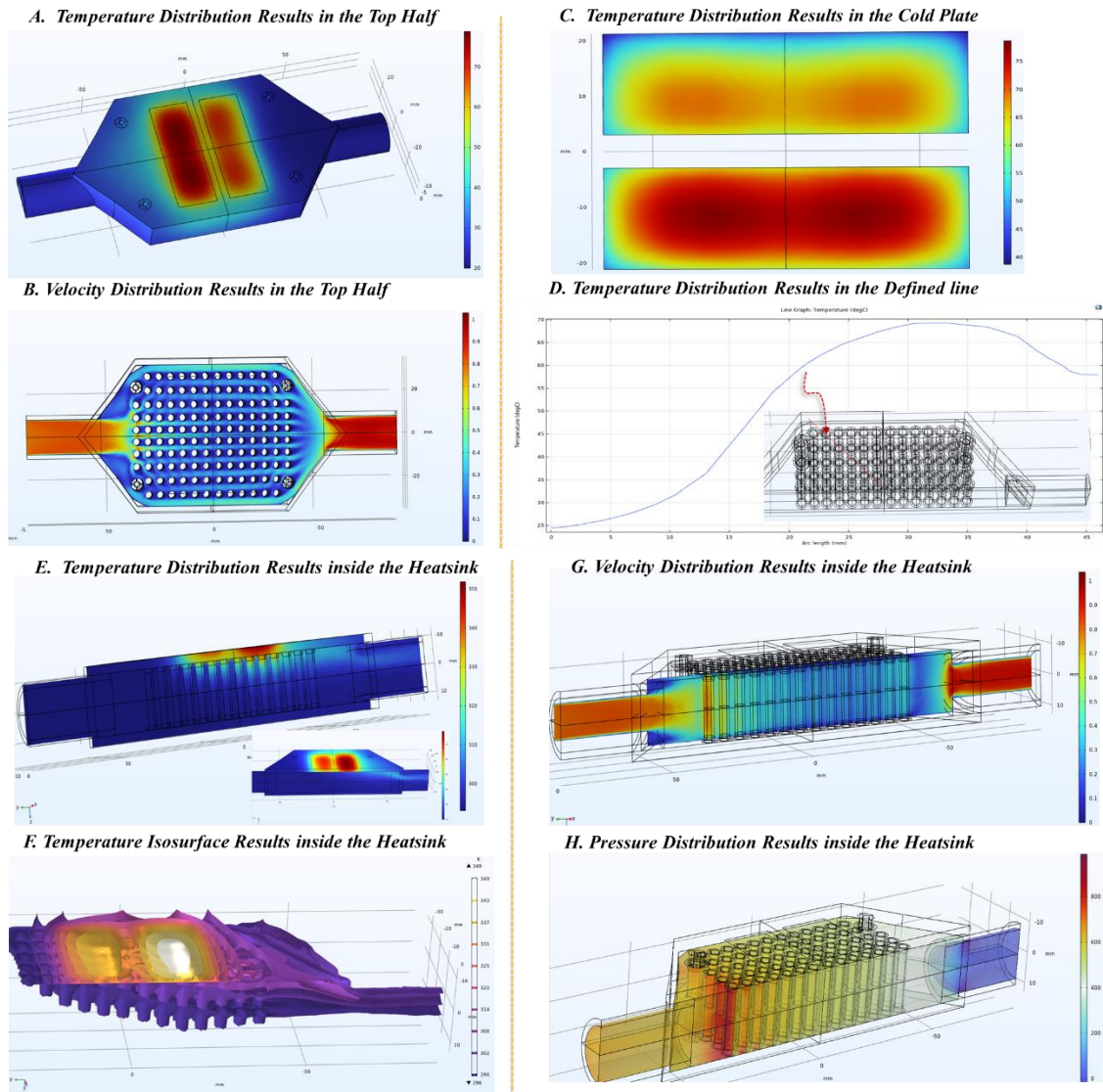


Figure 13 - Improved flow and heat dissipation in the redesigned heatsink, with previously inactive areas near the inlet transformed into active regions, enhancing overall performance.

It is important to note that we investigated several design scenarios, and only those that positively enhanced heatsink performance are reported here. For instance, one scenario that did not yield positive results involved varying the height difference between the inlet and outlet pipes.

The idea was to position the inlet closer to the top surface of the heatsink, encouraging fluid circulation near the cold plate and utilizing gravity to accelerate the fluid's exit from the outlet positioned near the bottom of the heatsink.

Figure 14 summarizes the geometry and results of this Multiphysics simulation, conducted in COMSOL. The findings indicate that increasing the heatsink's height to accommodate this different placement of the inlet and outlet did not enhance heat dissipation efficiency.

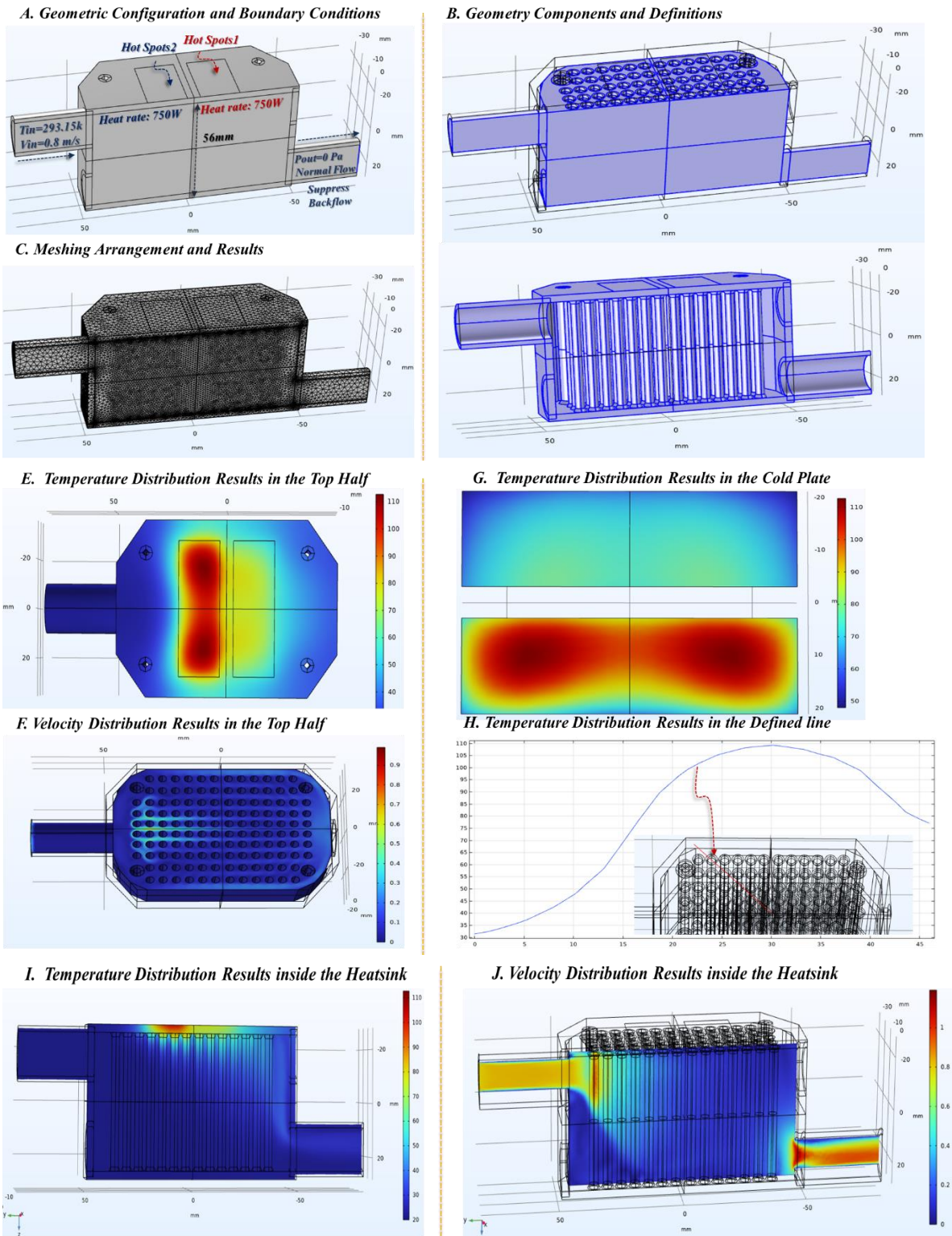


Figure 14 - Geometry and simulation results for a design scenario with varying inlet and outlet heights, showing that this configuration did not improve heat dissipation efficiency.

The arrangement of cooling pins in a liquid-cooled heatsink plays a crucial role in optimizing thermal management by enhancing heat transfer efficiency. A well-designed pin configuration ensures an even distribution of coolant around heat-generating components, preventing hotspots and reducing thermal gradients. An effective pin

arrangement increases the surface area in contact with the liquid, promoting turbulent flow and maximizing heat dissipation.

Figure 15 compares two different pin arrangements within the designed heatsink geometry. By changing from a symmetrical to an asymmetrical arrangement - where the pin lines are shifted every second row - the simulation results, summarized in Figure 15, show that the asymmetrical configuration not only improves velocity distribution but also reduces the overall and maximum temperatures on the cold plate.

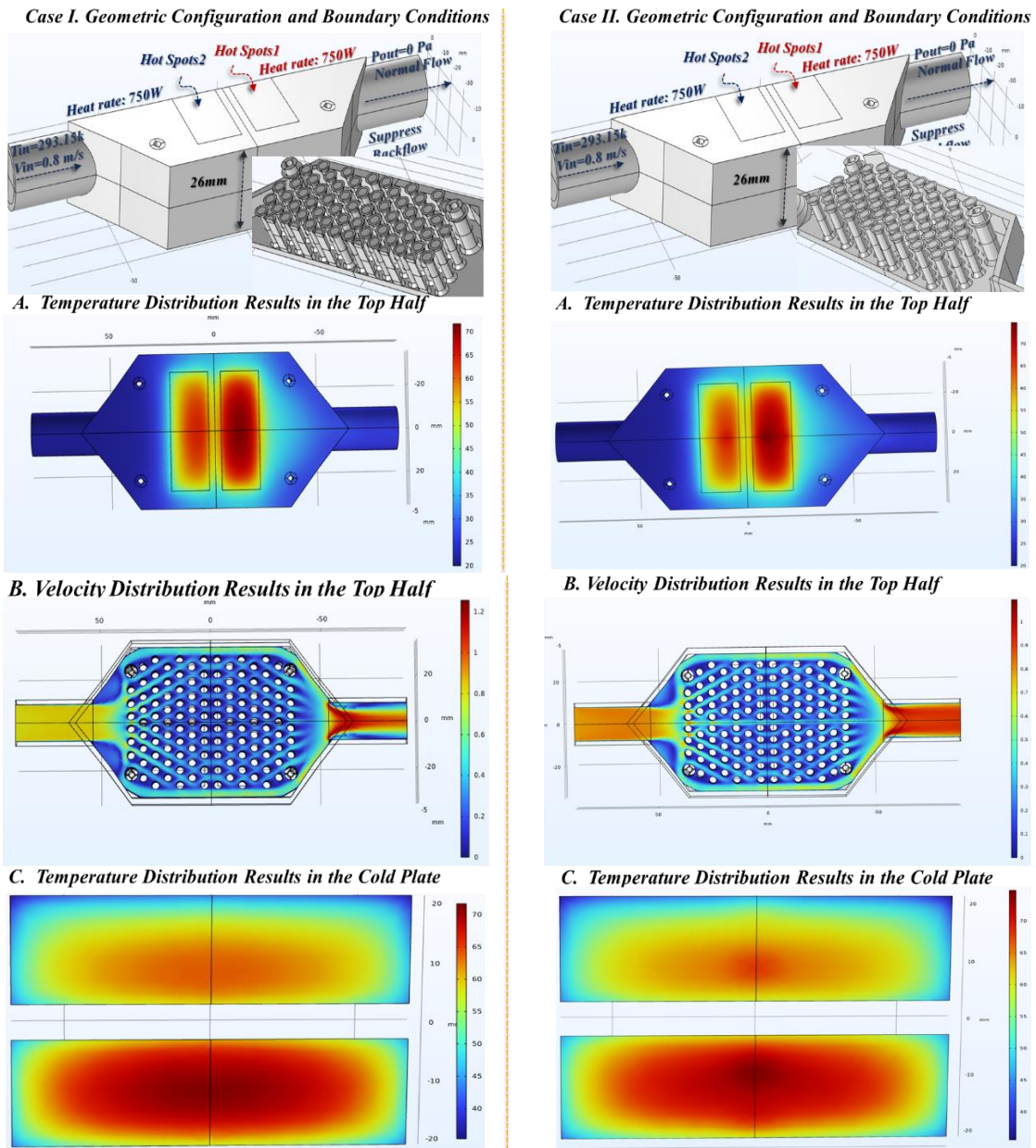


Figure 15 - Comparison results between symmetrical and asymmetrical pin arrangements in the heatsink geometry.

After finalizing the heatsink shape and pin arrangement for the high-power liquid-cooled heatsink, a new version was designed to comply with the RHODAS grant agreement. This version accommodates the design of the high-power heatsink board and the size of the inverter housing. Three heatsinks were designed, each corresponding to one phase of the power converter. As depicted in Figure 16, each heatsink is specifically designed to cover the SiC and GaN module regions of the power converter.

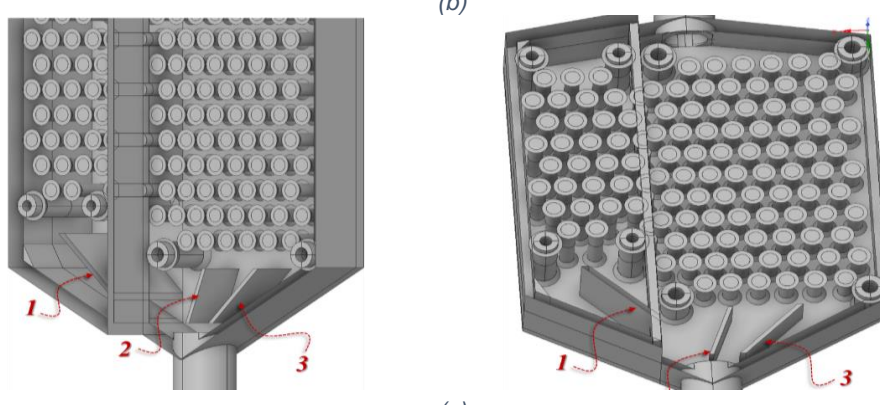
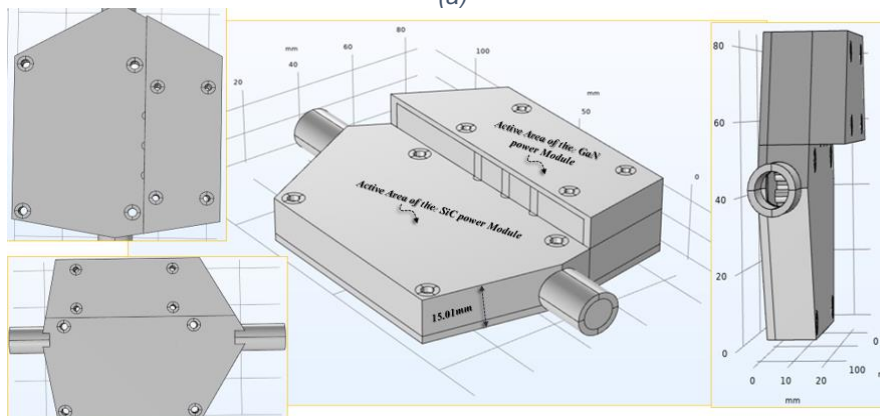
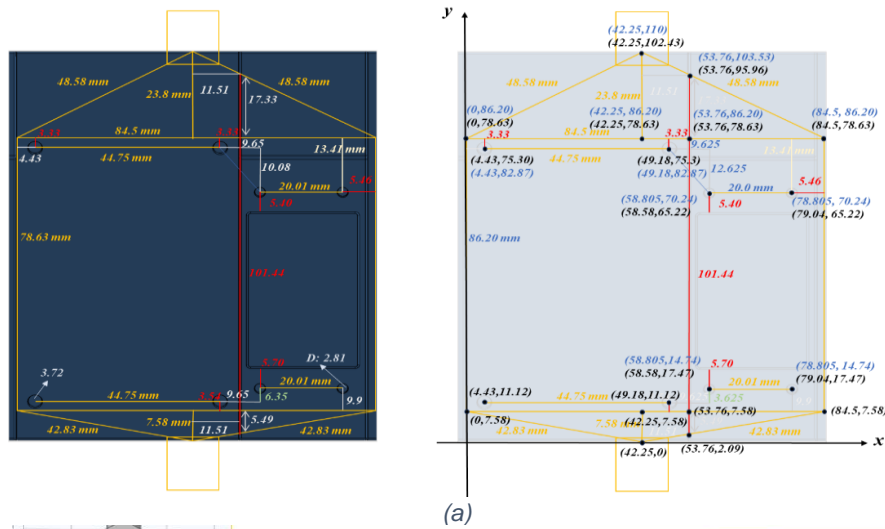


Figure 16 - Final version of the high-power liquid-cooled heatsink, designed with a step to accommodate height differences between the SiC and GaN sections of the power converter board: a) Design the main dimensions of the heatsink body b) Design and simulate the 3D model of the heatsink, including all pins c) Design support at the input side of the heatsink to comply with mechanical restrictions

This step creates a height difference in the pins beneath the SiC and GaN regions of the power converter board. Figure 16 also illustrates the boundary conditions and heat source rates applied in the simulations.

Figure 17 presents the results of this final version of the high-power heatsink, which covers both the SiC and GaN parts of the power converter.

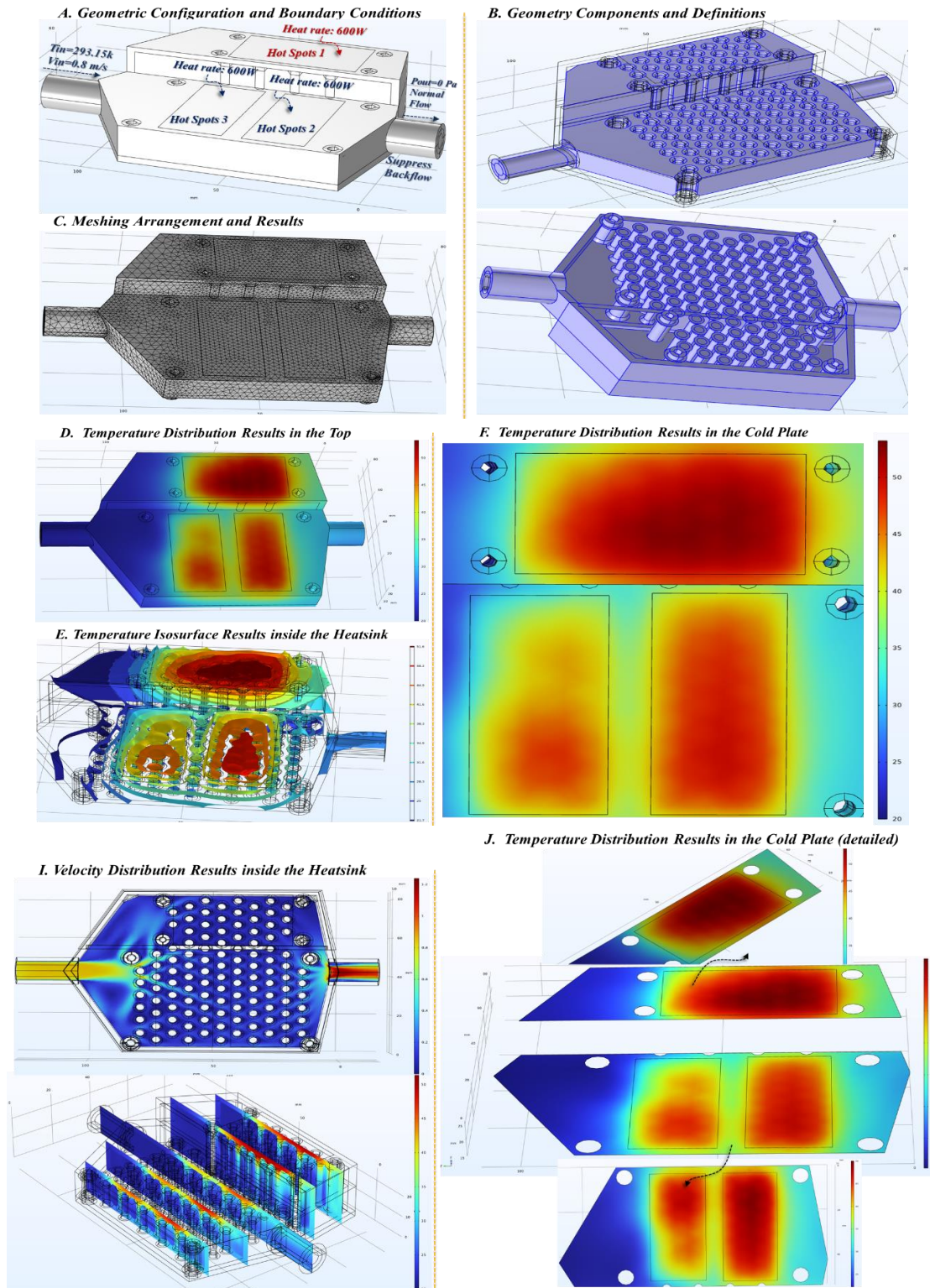


Figure 17 - Multiphysics simulation results for the final version of the high-power heatsink.

For each phase of the power board, there is one SiC module and six parallel GaN transistors. To address the height difference between the GaN and SiC parts of the high-power board and to optimize the height of the thermal interface material - critical for effective heat dissipation - a step was incorporated into the heatsink design.

This figure shows the temperature and velocity distributions in the top half of the heatsink, including temperature distribution on the cold plate. It also demonstrates heat dissipation from the top cold plate to the bottom of the heatsink, along with temperature isosurfaces and pressure distribution results within the heatsink.

One of the most critical parameters in operating the high-power heatsink is the inlet velocity, which has a direct and significant relationship with heat dissipation and overall heatsink efficiency.

One of the most critical parameters in operating the high-power heatsink is the inlet velocity, which has a direct and significant relationship with heat dissipation and overall heatsink efficiency.

To identify optimal parameters for the heatsink, the AU team conducted a sensitivity analysis on the inlet velocity, summarized in Figures 18–20. These figures illustrate the variation in maximum cold plate temperature, velocity distribution of the coolant, and average temperatures of the cold plate and outlet, along with their differences, as the inlet velocity changes from 0.3 m/s to 2.7 m/s.

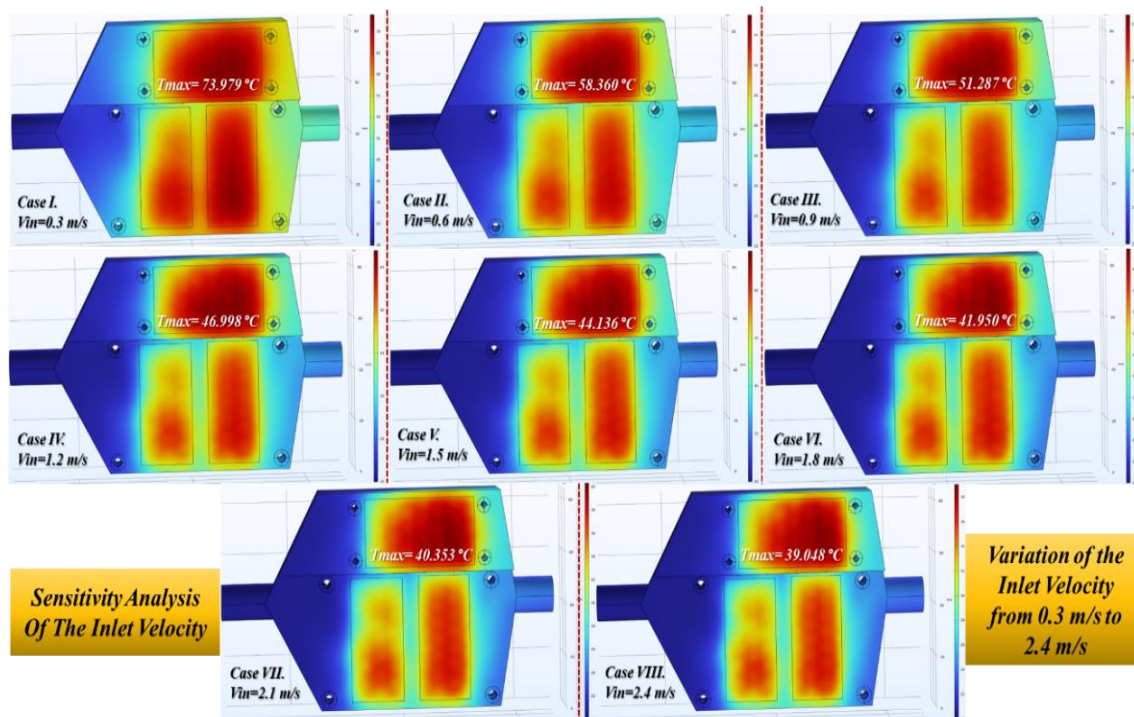


Figure 18 - Multiphysics simulation results for maximum cold plate temperature variation with inlet velocity ranging from 0.3 m/s to 2.7 m/s.

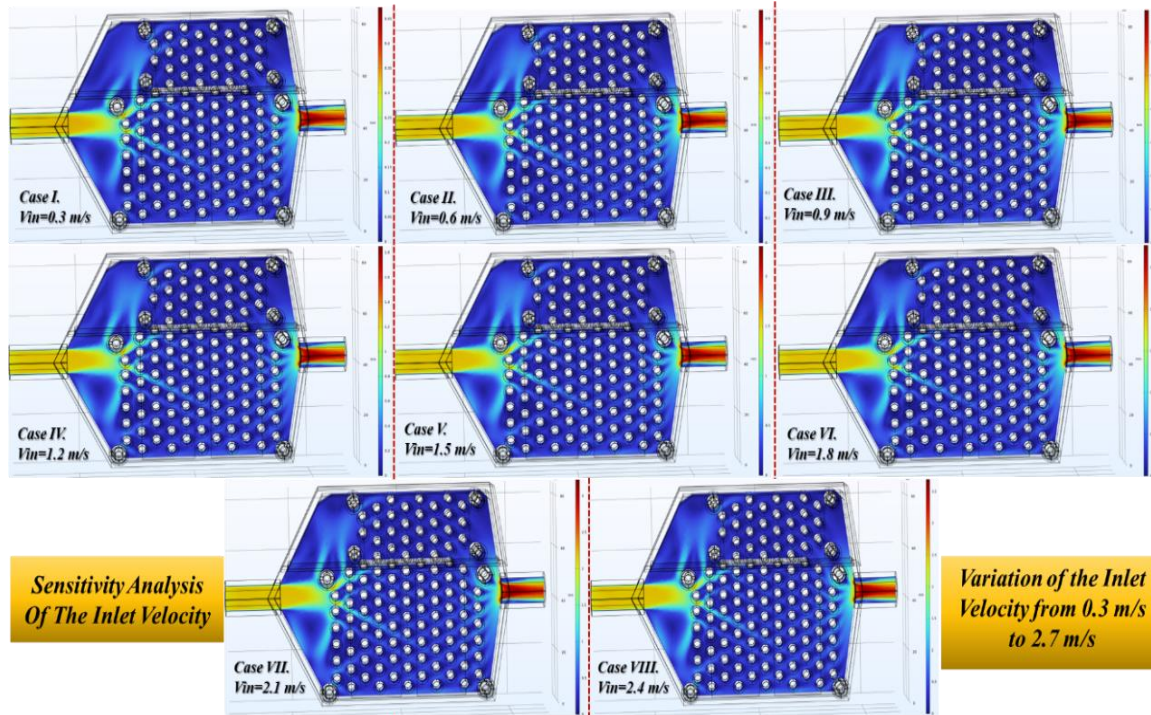


Figure 19 - Multiphysics simulation results for velocity distribution of the coolant within the heatsink at different inlet velocities.

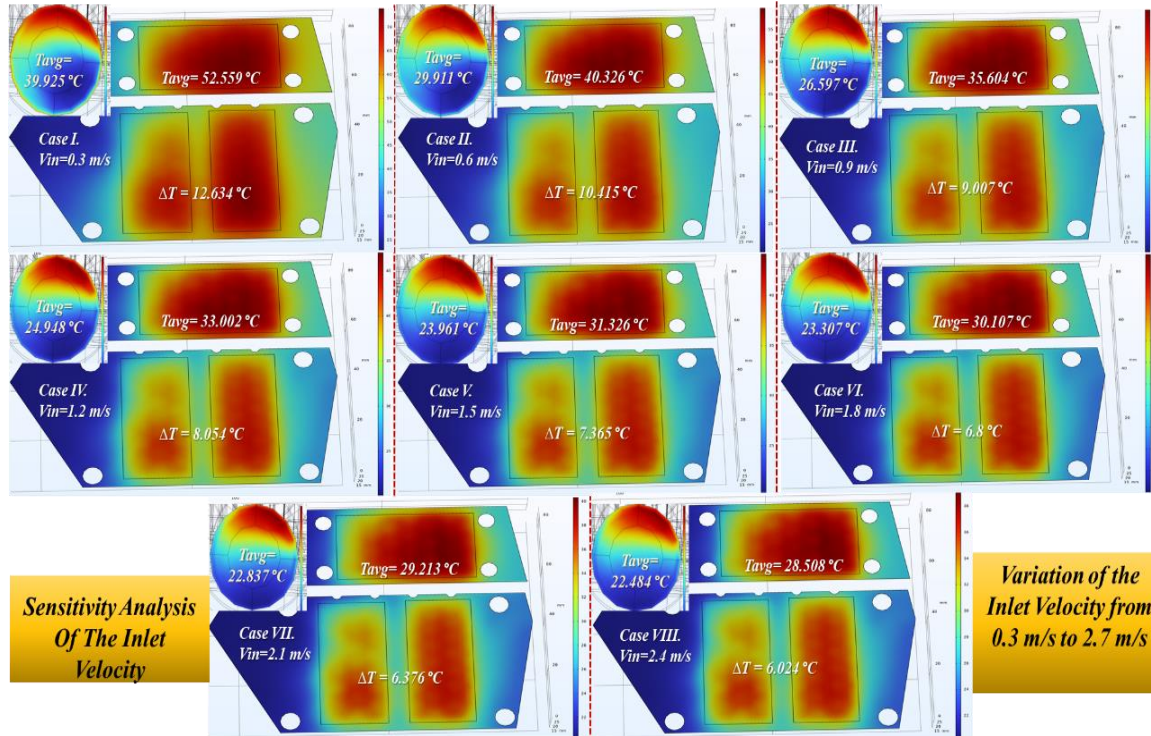


Figure 20 - Multiphysics simulation results for average temperatures of the cold plate and outlet, and their differences, as functions of inlet velocity.

To further investigate the design, the same analysis was performed on the heatsink, with the heat distribution across different layers and the temperature isosurface results inside the heatsink shown in Figures 21 and 22, respectively.

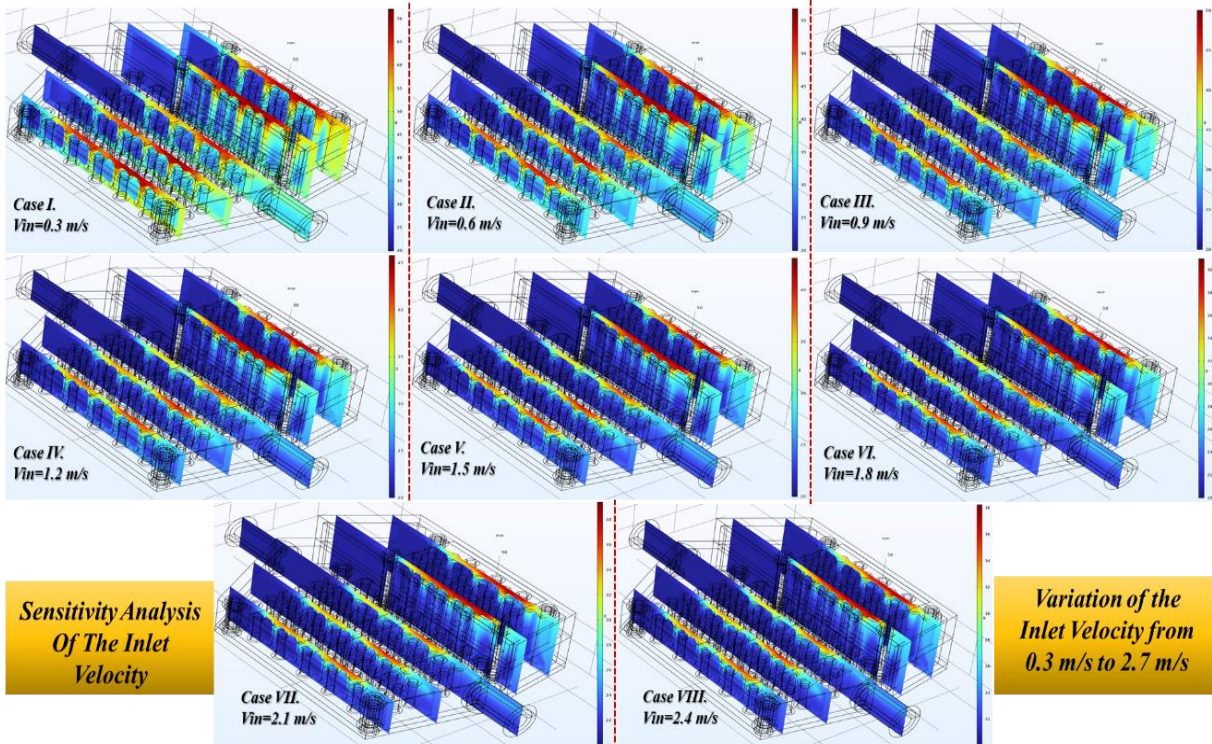


Figure 21 - Multiphysics simulation results for heat distribution across different layers of the heatsink for varying inlet velocities.

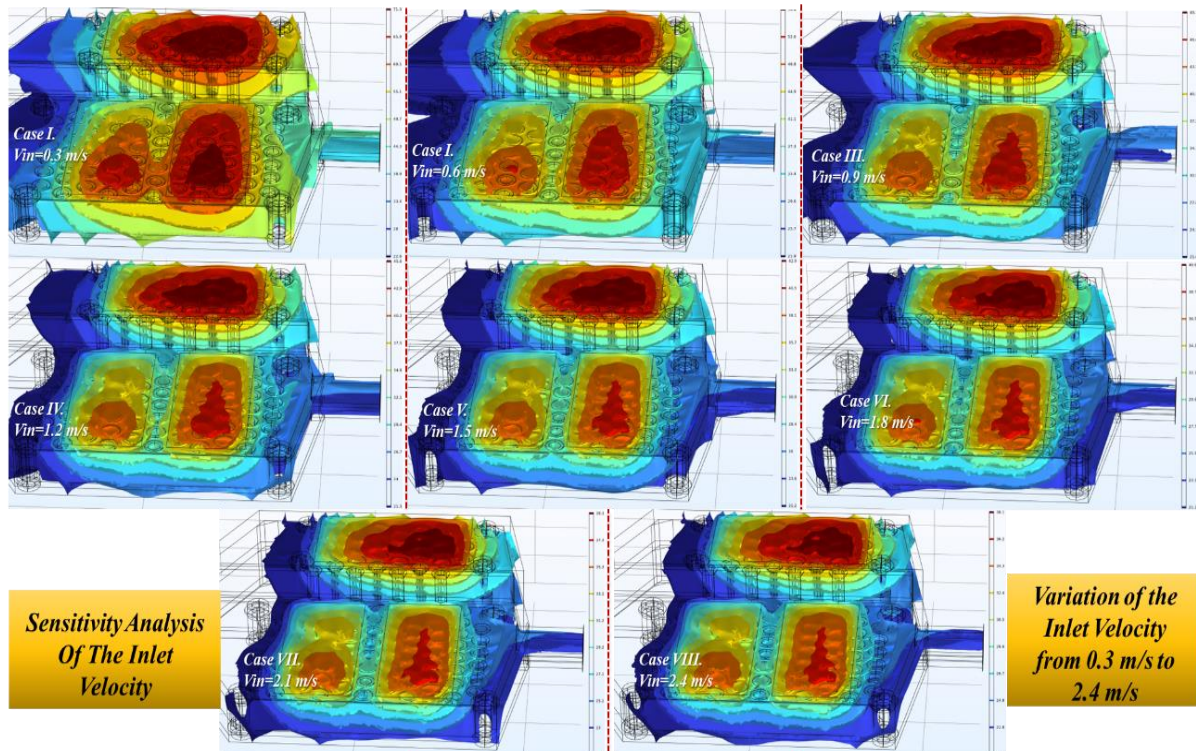


Figure 22 - Multiphysics simulation results for heat distribution across different layers of the heatsink for varying inlet velocities.

2.3 KEY DIFFERENCES BETWEEN HEATSINKS

The air-cooled and liquid-cooled heatsinks solutions were designed to dissipate heat energy generated by the SiC and GaN transistors of the low- and high-power converters correspondingly. The two solutions of heatsinks differ primarily in terms of cooling medium, geometric design, complexity and overall heat dissipation efficiency. It is important to highlight that the TMS for the 15 kW and 150 kW (low- and high-power) converters are neither the same nor directly comparable, as the two systems differ significantly in design and requirements. The 150-kW high-power converter imposes significantly higher heat dissipation requirements, which makes its heatsink design far more critical and necessitates to apply the liquid-cooled heatsink solution.

3 THERMAL MANUFACTURING PROCESS OF LIQUID-COOLED HEATSINKS FOR HIGH-POWER CONVERTER

Within WP3, an order was placed for five liquid-cooled heatsinks designed for a high-power converter system, following the design process detailed in the previous section.

The first heatsink unfortunately failed the required pressure tests. Since these components are liquid-cooled, ensuring water tightness is critical. Any leakage could result in damage to the power boards, causing further delays and increasing project costs. In response to this issue, two potential solutions to resolve the leakage problem were explored.

The first solution involved applying a radiator sealant to the inside of the heatsinks, while the second involved coating the external surface with melted tin. Figures 23 and 24 show the application of these solutions on the printed heatsinks.

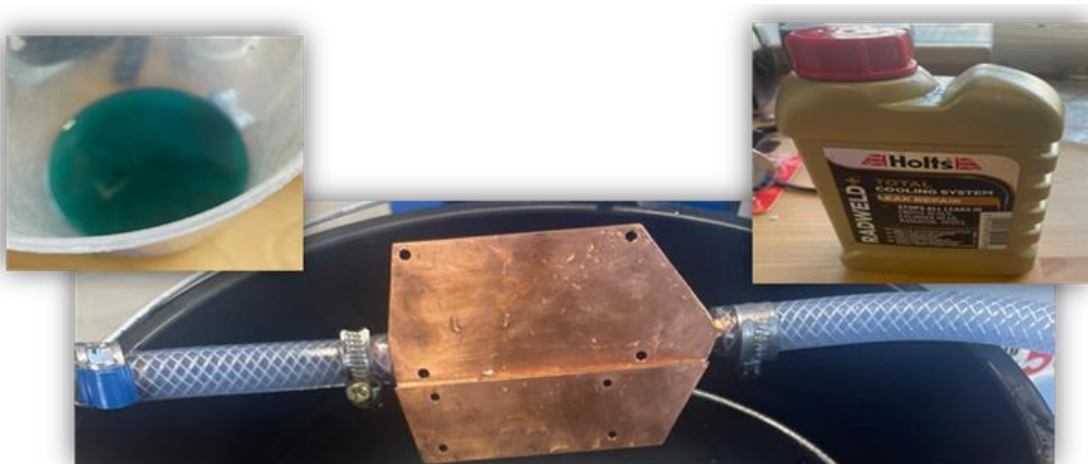


Figure 23 - Application of radiator sealant to the interior surface of the liquid-cooled heatsink.



Figure 24 - Application of melted tin coating to the exterior surface of the liquid-cooled heatsink.

Despite these efforts, neither solution alone could fully resolve the leakage issue, particularly under high-pressure conditions (at least 3.5 bar). As a result, AU combined both approaches - applying the radiator sealant inside and coating the outside with tin on one of the heatsinks.

As shown in Figure 25, this combined approach enabled one of heatsink to pass the 3.5 bar pressure test. However, due to the risk of potential leakage over time, we decided to approach a second supplier to manufacture heatsinks made from aluminum. The second supplier guarantees that these heatsinks will be 100% watertight and gas-tight, even under pressures of 3.5 bar.



Figure 25 - Combined solution of internal sealant and external tin coating, showing acceptable results under 3.5 bar pressure.

To mitigate further delays in the project timeline, the repaired copper heatsink was sent to BOSMAL, the partner responsible for testing the heatsinks. To evaluate the feasibility of replacing copper with aluminium as the heatsink material, a multiphysics simulation as conducted (see Figure 26). The results demonstrate that, despite the material change, the heat dissipation performance remains within acceptable limits. Both the maximum temperature and overall heat dissipation efficiency were maintained. Additionally, the use of aluminium resulted in a significant weight reduction, with the weight of each heatsink decreasing from 485 grams to 122 grams.

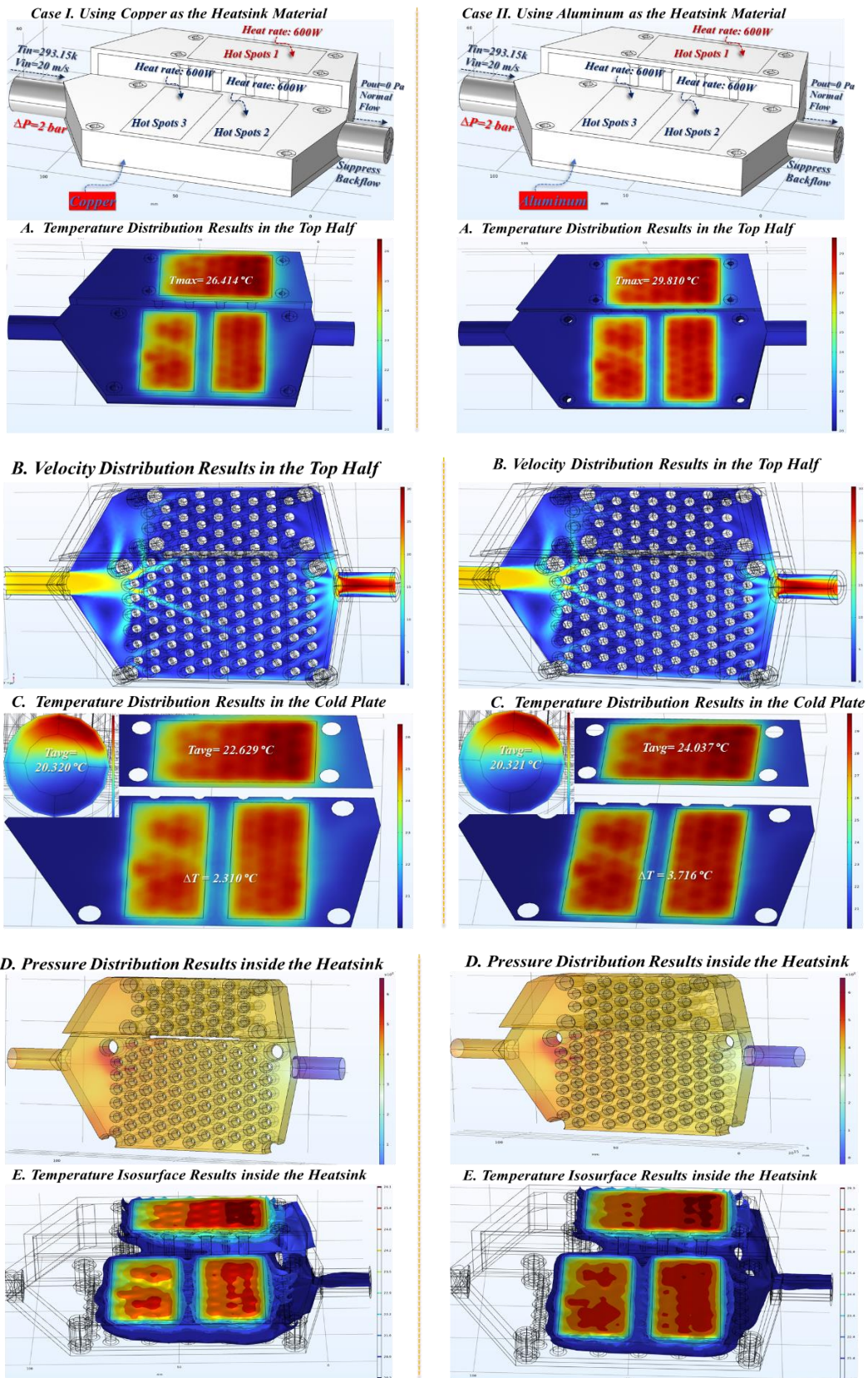


Figure 26 - Multiphysics simulation results comparing the performance of copper and aluminium heatsinks, demonstrating that aluminium maintains effective heat dissipation.

As shown in Figure 27, the aluminium heatsinks were successfully printed and subsequently sent to BOSMAL for testing. The heatsinks were also sent to AIT, to test the three-phase high-power converter system, utilizing one liquid-cooled heatsink per phase. This change in material, along with the manufacturing and testing processes, introduced a delay on the RHODAS project.

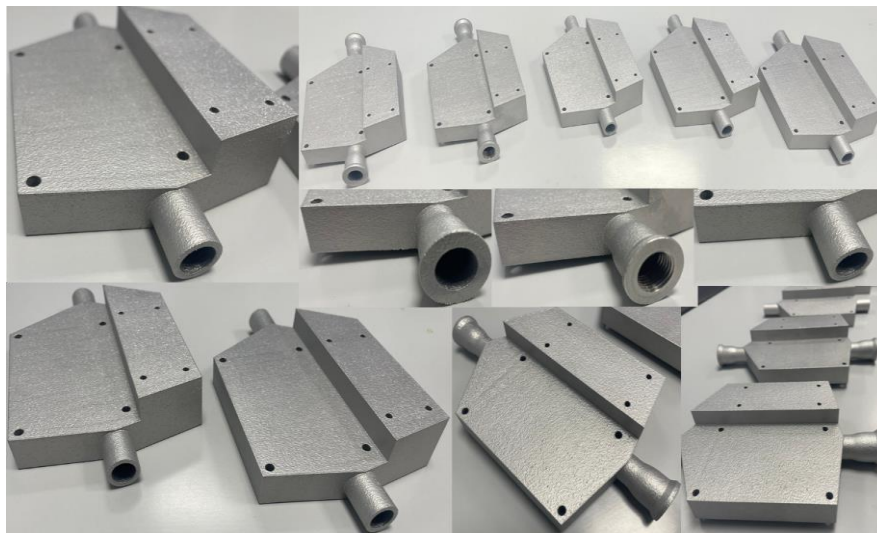


Figure 27 - Printed aluminium high-power, liquid-cooled heatsink heatsinks prepared for testing at BOSMAL and AIT.

4 THERMAL MANAGEMENT SYSTEM UNDER TEST

The Thermal Management System under test was designed to meet the requirements of a prototype high-power converter with a maximum power 150 kW. The TMS consisted of a radiator, fan system, coolant pump and liquid-cooled aluminum heatsink as shown in Figure 28 (a). The TMS components were designated and selected to maintain the required operating temperature of a power converter and to prevent overheating and hot spots under various loading conditions.

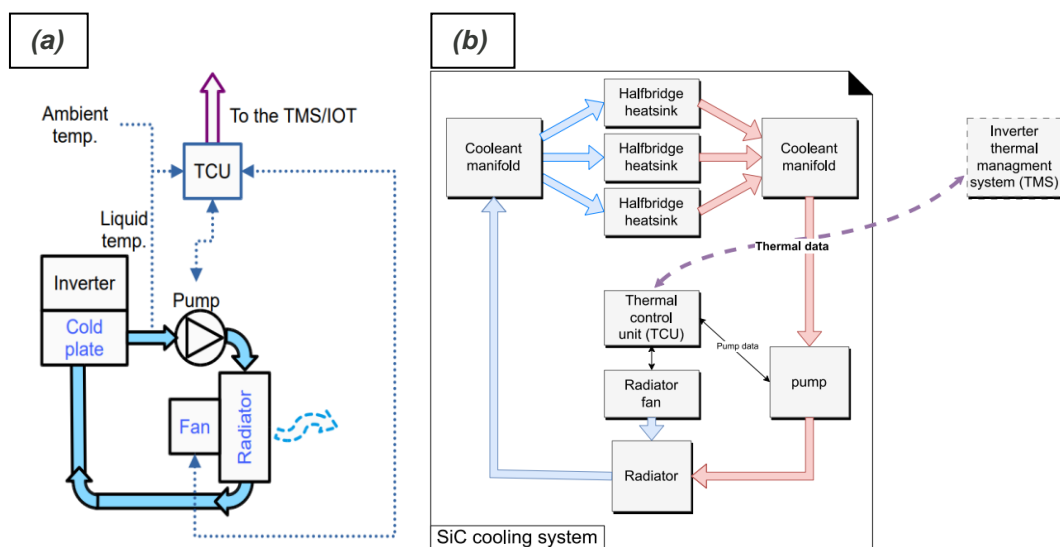


Figure 28 – TMS layout: a) Simplified and b) Detailed

In this system, the coolant pump circulates a water/glycol (50/50) mixture through the radiator, where heat is rejected into ambient air. The fan system helps to increase the air flow rate through the radiator to improve the heat dissipation in a scenario where the natural air flow is insufficient, such as during low-speed driving conditions. The prototype liquid-cooled heatsink was designed to efficiently remove heat from the GaN and SiC modules. Detailed TMS layout is presented in Figure 28 (b).

5 TEST PROGRAM DESCRIPTION

5.1 TEST PHASES

The testing program for the Thermal Management System was divided into two phases: Component-Level Testing and System-Level Validation. The first phase was defined to measure the performance of individual components while the second one aim to validate the operation of the integrated TMS under selected values of the: coolant flow, temperature and thermal load.

5.1.1 PHASE 1: COMPONENT-LEVEL TESTING

The following TMS components were tested under wide operating conditions in order to determine the thermal and hydraulic performance: liquid-cooled heatsink, radiator, fan system and coolant pump. The test methods for the TMS components are summarized as below:

Liquid-cooled heatsink module:

- **Objective:** To evaluate the thermal performance of the heatsink and measure coolant pressure drop curve.
- **Method:** The heatsink was tested under defined test points matrix of varied coolant flow rate and temperature values. The heat losses generated by SiC, GaN semiconductors were simulated by an electric heating element of resistive type, fixed to the cold plate of the heatsink. The aim of the research was to perform the thermal performance and functional tests of the heatsink over wide operating range.
- **Instrumentation:** Flow meters installed for coolant flow measurement, pressure transducers for pressure drop measurement across the heatsink, thermocouples installed between heating elements and the heatsink active surface (cold plate) and at the inlet and outlet of the heatsink.
- **Conditions:** Tests were conducted by stepwise increase in the coolant flow rate and temperature values to measure the heatsink performance and the pressure drop characteristic.

Radiator (without fan system):

- **Objective:** To evaluate the radiator heat dissipation capability over varying coolant and air flow rates.
- **Method:** The radiator was tested by increasing the coolant flow and the air flow rates over the radiator/fins. The tests aimed to reproduce varied cooling demands e.g. during urban driving (low flow rate) or motorway driving (high flow rate).
- **Instrumentation:** Coolant flow meters and anemometer to measure the flow rates across the radiator. Pressure transducers installed to measure pressure drops over the radiator.

- **Conditions:** Tests were conducted by stepwise increase in the air flow and coolant flow rates to measure the radiator performance and pressure drop. The air and coolant temperatures remained at fixed values.

Fan system:

- **Objective:** To determine the fan system cooling capability by forcing the airflow across the radiator.
- **Method:** The fan system was tested at three supply voltage levels: 12V, 13V and 14V. For each voltage level the air flow rate and electric power consumption were measured. Various supply voltage aimed to simulate different operating scenarios affecting the overall efficiency of the cooling system.
- **Instrumentation:** The anemometers for the air flow rate measurement and the power meter to record the electrical energy consumption of the fan system at each voltage level.
- **Conditions:** The fan was tested at various voltages to verify the air flow influence on radiator cooling performance.

Coolant pump:

- **Objective:** To evaluate the coolant pump performance and the ability to maintain the stable flow rate under varying conditions.
- **Method:** The pump was tested at three various Pulse Width Modulation (PWM) settings: 50%, 75% and 100% to determine the functional characteristics of the pump.
- **Instrumentation:** Coolant flow meter and pressure transducers to measure pressure drops across the pump. Control system with data acquisition to execute each PWM setting.
- **Conditions:** The coolant pump was tested under varied flow rate and at constant coolant temperature.

5.1.2 PHASE 2: SYSTEM-LEVEL VALIDATION

The second phase aimed to validate the performance of the integrated TMS system. This test activity allowed to assess the ability of integrated TMS components to manage the heat dissipation in a given test scenarios.

The TMS test method was as follows:

- **Objective:** To validate the thermal performance of an integrated TMS under selected operating points.
- **Method:** The TMS was tested at the fixed values of the coolant flow rate and the heating power (resistive elements), while the coolant temperature was varied.
- **Instrumentation:** The coolant flow meter, thermocouples and pressure transducers were installed across the system.
- **Conditions:** The TMS was tested under steady-state conditions where the coolant temperature was varied.

6 COMPONENTS TESTING

6.1 RADIATOR THERMAL PERFORMANCE TEST

The radiator component of the Thermal Management System is responsible for heat rejection absorbed by the coolant circulating through the TMS. This test aimed to evaluate the heat rate removal, and the pressure drop of the radiator under varied coolant and air flow rates.

6.1.1 TEST OBJECT IDENTIFICATION

The radiator under test was a dual-section design: the low temperature (LT) and high temperature sections (HT). During the test both sections were combined together. The radiator was specifically chosen for the 150-kW high-power converter specification and the component overview is shown in Table 1.

Table 1 - Test object identification

BOSMAL marking	General view	
Sample 1		

6.1.2 SCOPE OF THE TEST

Determination of Functional Characteristics according to BOSMAL instruction BOSMAL/I-7-57/04, Customer standard 18-3716 point 4.4 and requirements:

- Air inlet temperature: 20 °C
- Coolant inlet temperature: 80 °C
- Coolant flow rate on inlet spout: 800; 1000; 1200; 1500; 3000; 5000; 6500; 8000 l/h
- Air flow rate: 0,300; 0,450; 0,600; 0,750; 1,100; 1,500; 2,000 kg/s
- Coolant mixture: water/glycol – 50/50

6.1.3 TEST STAND INSTRUMENTATION

The test bed instrumentation for radiator performance evaluation is shown in Table 2.

Table 2 - Measurement devices identification

Name of device	BOSMAL identification number	Accuracy	Last calibration date	Next calibration date
Atmospheric pressure	F/0700/BW	± 1 hPa	02.2024	02.2026
Cooling air temperature	G/1185/BHW G/1186/BHW G/1187/BHW	$\pm 0.2^\circ\text{C}$	01.2024	01.2025
Cooling air flow rate	F/1220/BHW	$\pm 1,5$ %	08.2022	08.2025
Cooling air pressure drop	F/1212/BHW	± 1 Pa	07.2024	07.2026
Coolant temperature HT section	G/1192/BHW G/1193/BHW G/1194/BHW G/1195/BHW	$\pm 0.2^\circ\text{C}$	01.2024	01.2025
Coolant temperature LT section	G/1567/BHW G/1568/BHW	$\pm 0.2^\circ\text{C}$	01.2024	01.2025
Coolant flow rate on inlet spout	F/0656/BW	± 0.2 %	05.2023	05.2026
Coolant flow rate on outlet spout LT section	F/0164/BW	± 0.2 %	03.2023	03.2026
Coolant pressure drop HT section	F/1109/BHW	± 2 mbar	10.2022	10.2024
Coolant pressure drop LT section	F/1525/BHW	± 2 mbar	10.2022	10.2024

The radiator installation on the test bed with sensor layout is presented in Figure 29.

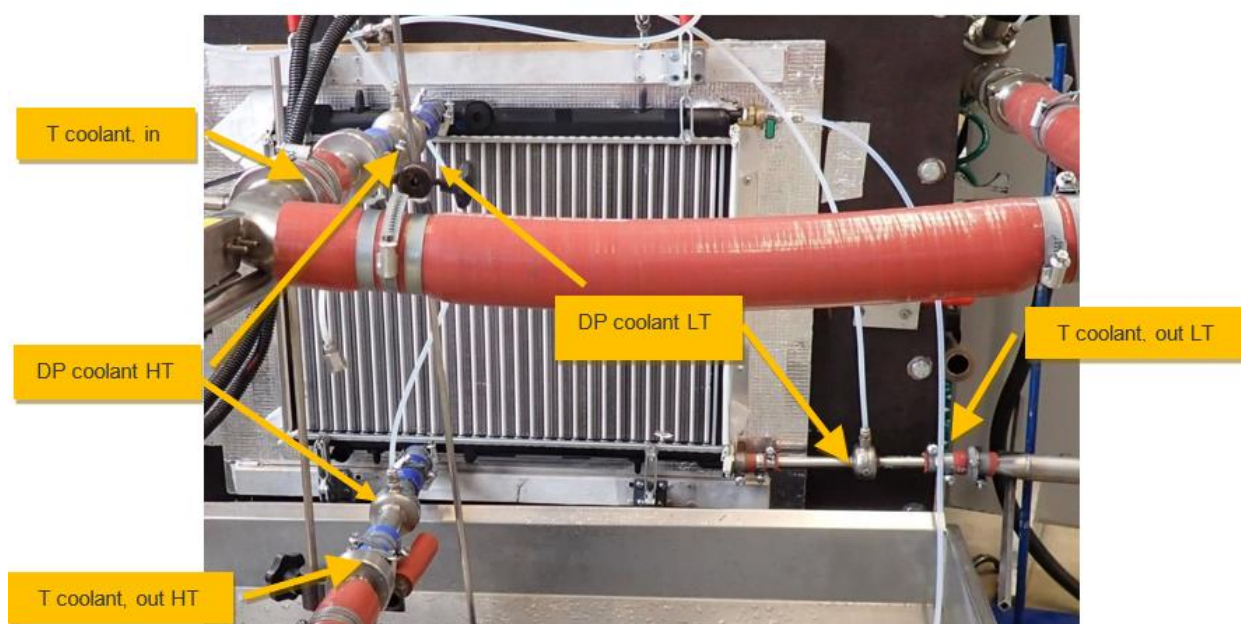


Figure 29 - Test sample assembled on the test bed

6.1.4 TEST RESULTS AND DISCUSSION

The radiator test was performed under conditions where the ambient air and the inlet coolant temperatures remained at constant values. The test parameters varied were the air and coolant flow rates through the radiator. Different coolant flow rates are separated by blank rows in the Table 3 of the summary results.

Table 3 – Thermal performance test results of the radiator

P atm [hPa]	T air [°C]	DP air [Pa]	Q air [kg/s]	T liq in HT [°C]	T liq out HT [°C]	DP liq HT [mbar]	T liq in LT [°C]	T liq out LT [°C]	DP liq LT [mbar]	Q liq inlet – total [l/h]	Q liq LT [l/h]	Q liq HT [l/h]	Q HT [kW]	Q LT [kW]	Q Total [kW]
975,8	20,1	16	0,300	80,0	72,3	5	80,0	67,8	5	800	132	668	5,2	1,6	6,8
975,8	20,0	29	0,449	80,0	71,4	5	80,0	66,7	5	800	132	668	5,8	1,8	7,6
975,9	20,1	46	0,599	80,0	70,8	5	80,0	66,1	5	800	132	668	6,2	1,8	8,1
975,6	20,0	66	0,750	80,0	70,4	5	80,0	65,5	5	801	131	669	6,5	1,9	8,4
975,6	20,0	122	1,100	80,0	69,6	5	80,0	64,7	5	800	131	669	7,0	2,0	9,0
975,6	20,0	208	1,500	80,0	69,1	6	80,0	64,0	5	800	131	669	7,4	2,1	9,5
975,5	20,0	343	2,000	80,0	68,6	6	80,0	63,5	5	800	131	669	7,7	2,2	9,8
976,4	19,9	16	0,301	80,0	73,4	8	80,0	69,7	7	1000	170	831	5,5	1,8	7,3
976,4	20,0	29	0,450	80,0	72,6	8	80,0	68,8	7	1000	169	831	6,2	1,9	8,1
976,3	20,0	47	0,600	80,0	72,0	8	80,0	68,2	7	999	169	830	6,7	2,0	8,7
976,2	20,0	67	0,751	80,0	71,6	8	80,0	67,7	7	1000	169	831	7,0	2,1	9,1
975,9	20,0	123	1,099	80,0	71,0	8	80,0	67,0	7	1001	169	831	7,6	2,2	9,8
975,9	20,0	211	1,500	80,0	70,4	8	80,0	66,4	7	1000	169	831	8,0	2,3	10,3
976,0	20,0	347	2,000	80,0	70,0	8	80,0	65,9	7	1000	169	831	8,4	2,4	10,8
974,9	20,1	17	0,299	80,0	74,2	10	80,0	71,1	8	1200	206	994	5,8	1,9	7,7
974,9	20,0	30	0,452	80,0	73,5	11	80,0	70,3	8	1201	206	995	6,6	2,0	8,6
975,3	20,0	47	0,599	80,0	72,9	11	80,0	69,7	8	1201	206	995	7,1	2,1	9,2
975,8	20,0	67	0,750	80,0	72,5	11	80,0	69,2	8	1200	206	994	7,5	2,2	9,7
976,0	20,0	125	1,100	80,0	71,9	11	80,0	68,5	8	1201	206	995	8,2	2,4	10,5
976,4	20,0	212	1,499	80,0	71,3	11	80,0	68,0	8	1200	206	994	8,7	2,5	11,2
976,2	20,0	348	2,000	80,0	70,9	11	80,0	67,5	8	1199	206	993	9,1	2,6	11,7
975,4	20,1	16	0,300	80,0	75,1	15	80,0	72,5	12	1500	260	1239	6,2	2,0	8,1
975,3	19,9	30	0,450	80,0	74,3	15	80,0	71,7	12	1500	260	1240	7,1	2,2	9,3
975,1	20,0	48	0,601	80,0	73,9	15	80,0	71,2	12	1500	260	1240	7,7	2,3	10,0
975,2	20,0	68	0,749	80,0	73,5	15	80,0	70,8	12	1500	260	1240	8,2	2,4	10,6
975,1	20,0	125	1,100	80,0	72,8	15	80,0	70,2	12	1499	260	1239	9,0	2,6	11,6
974,9	20,0	213	1,502	80,0	72,3	15	80,0	69,7	12	1500	260	1241	9,7	2,7	12,4
974,9	20,0	350	2,000	80,0	71,8	15	80,0	69,3	12	1500	260	1240	10,3	2,8	13,1
976,0	20,1	16	0,299	80,0	75,6	21	80,0	73,5	17	1800	317	1483	6,5	2,1	8,6
975,8	20,0	30	0,450	80,0	75,0	21	80,0	72,8	17	1799	317	1482	7,5	2,3	9,8
975,8	20,0	48	0,599	80,0	74,5	21	80,0	72,3	17	1800	317	1483	8,3	2,5	10,7
975,9	20,0	68	0,750	80,0	74,1	21	80,0	71,9	17	1800	317	1482	8,8	2,6	11,4
975,9	20,0	125	1,100	80,0	73,4	22	80,0	71,3	17	1799	317	1482	9,9	2,8	12,6
975,8	20,0	214	1,499	80,0	72,9	22	80,0	70,9	17	1801	317	1484	10,7	2,9	13,6
975,8	20,0	351	1,997	80,0	72,4	22	80,0	70,5	18	1801	317	1484	11,4	3,1	14,4
975,5	20,1	17	0,299	80,0	77,0	55	80,0	75,4	46	3000	533	2467	7,5	2,5	10,0
975,6	20,0	30	0,450	80,0	76,4	55	80,0	74,8	45	3000	534	2466	8,9	2,8	11,7
975,7	20,0	49	0,600	80,0	76,0	55	80,0	74,4	46	2999	533	2466	9,9	3,0	12,9
975,6	20,0	69	0,750	80,0	75,7	55	80,0	74,0	46	3001	534	2468	10,8	3,2	14,0
975,7	20,0	127	1,099	80,0	75,1	55	80,0	73,4	46	3001	534	2467	12,3	3,5	15,8
975,7	19,9	215	1,501	80,0	74,6	55	80,0	73,0	46	2999	533	2466	13,6	3,8	17,4
975,6	20,0	353	1,999	80,0	74,1	56	80,0	72,5	46	2999	534	2466	14,8	4,0	18,8
975,1	20,0	17	0,299	80,0	78,0	149	80,0	76,7	123	5000	892	4108	8,3	3,0	11,3
975,1	20,0	31	0,451	80,0	77,6	149	80,0	76,1	123	5000	892	4108	10,1	3,5	13,5
975,2	20,0	49	0,600	80,0	77,3	149	80,0	75,8	123	5000	893	4107	11,4	3,8	15,2
975,2	20,0	70	0,751	80,0	77,0	150	80,0	75,4	123	5000	892	4108	12,5	4,1	16,7
975,2	20,0	128	1,099	80,0	76,5	150	80,0	74,8	123	5000	892	4108	14,6	4,7	19,3
975,4	20,0	217	1,498	80,0	76,1	150	80,0	74,3	124	5000	892	4108	16,4	5,2	21,6
975,5	20,0	356	2,000	80,0	75,7	151	80,0	73,8	124	5000	892	4108	18,1	5,6	23,7
974,4	20,1	19	0,300	80,0	78,4	250	80,0	77,2	206	6500	1162	5338	8,7	3,2	11,9
974,4	20,0	32	0,449	80,0	78,1	251	80,0	76,8	207	6502	1162	5340	10,5	3,8	14,3
974,6	20,0	50	0,599	80,0	77,8	251	80,0	76,5	206	6500	1163	5338	12,0	4,2	16,2
974,7	20,0	71	0,750	80,0	77,6	251	80,0	76,1	207	6501	1162	5339	13,2	4,6	17,8
974,8	20,0	130	1,099	80,0	77,2	252	80,0	75,6	207	6501	1163	5338	15,6	5,2	20,9
974,8	20,0	219	1,499	80,0	76,7	253	80,0	75,0	207	6501	1164	5337	17,7	5,9	23,5
974,9	20,0	358	2,002	80,0	76,4	252	80,0	74,6	207	6500	1163	5337	19,7	6,4	26,1
974,2	19,9	17	0,300	80,0	78,7	377	80,0	77,7	310	8001	1434	6567	8,9	3,3	12,2
974,1	20,0	31	0,451	80,0	78,4	379	80,0	77,3	311	7998	1433	6565	10,8	3,9	14,7
974,0	20,1	50	0,602	80,0	78,2	378	80,0	77,0	310	8000	1433	6567	12,4	4,4	16,8
973,9	20,0	70	0,750	80,0	78,0	379	80,0	76,7	311	8000	1434	6566	13,8	4,9	18,6
973,8	20,0	130	1,100	80,0	77,6	379	80,0	76,1	311	7999	1433	6566	16,3	5,6	21,9
974,3	20,0	219	1,500	80,0	77,2	380	80,0	75,7	311	8002	1433	6568	18,5	6,3	24,8
974,2	20,0	361	1,999	80,0	76,9	381	80,0	75,2	312	7999	1434	6565	20,7	7,0	27,6

Where:

- P atm – atmospheric pressure
- T air – temperature of air
- DP air – differential pressure of air measured between test tunnel pressure and ambient pressure
- Q air – quantity of airflow through radiator
- T liq in HT – water temperature measured at inlet of high temperature section
- T liq out HT - water temperature measured at outlet of high temperature section
- DP liq HT – differential pressure between inlet and outlet of high temperature section
- T liq in LT – water temperature measured at inlet of low temperature section
- T liq out LT - water temperature measured at outlet of low temperature section
- DP liq LT – differential pressure between inlet and outlet of low temperature section
- Q liq inlet - total – total quantity of coolant flow through radiator
- Q liq LT – quantity of coolant flow through low temperature section
- Q liq HT – quantity of coolant flow through high temperature section
- Q HT – quantity of heat dissipated through high temperature section
- Q LT - quantity of heat dissipated through low temperature section
- Q Total – summed quantity of heat dissipated through low and high temperature section

Figure 30 compares the heat rejection rates for both sections of the radiator (HT+LT) for varied coolant flow rate. The air pressure drop across the radiator in a function of air speed was measured.

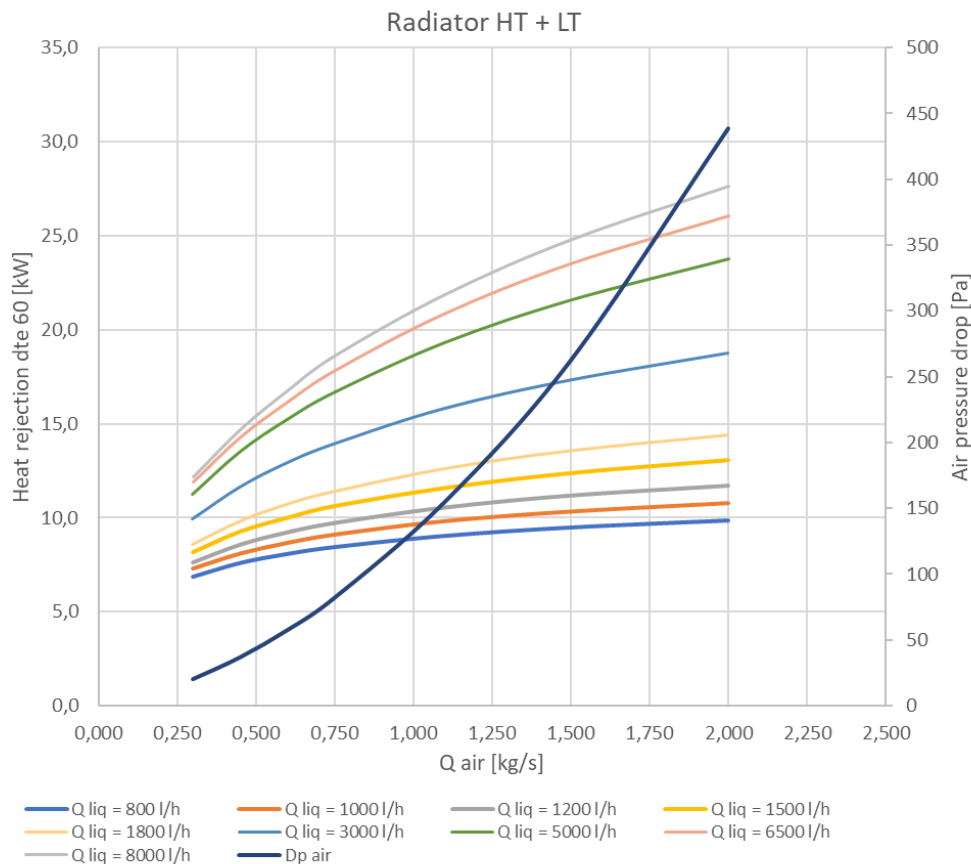


Figure 30 - Heat rejection and air pressure drop vs. air speed

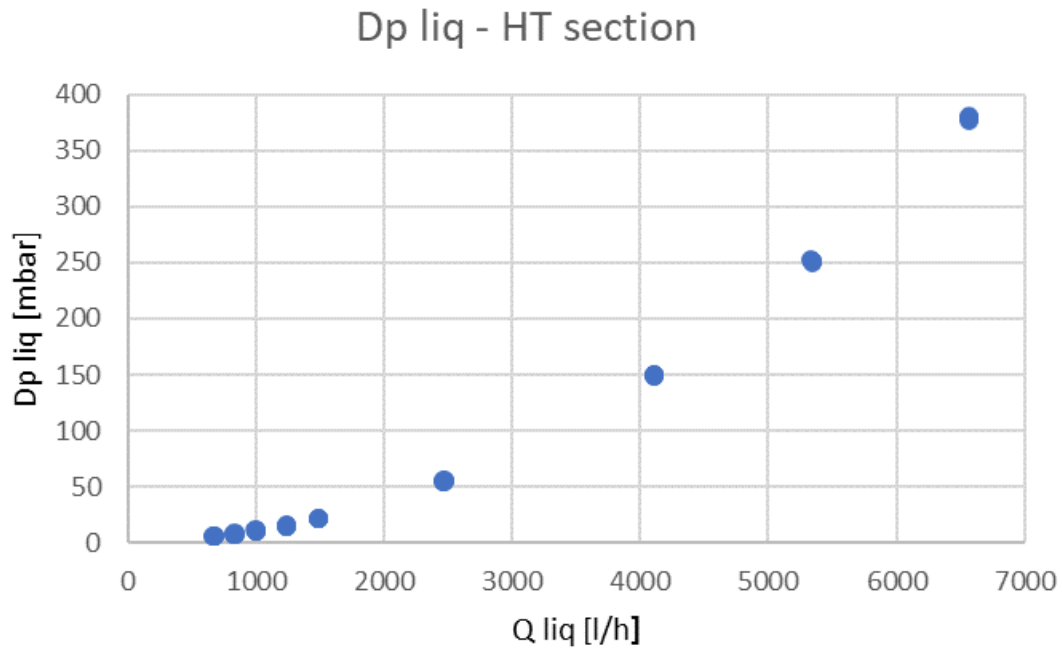


Figure 31 - Coolant pressure drop - HT section

The coolant pressure drop was measured separately for the HT and LT sections as presented in Figures 31-32. The thermal imaging of the HT+LT section was performed at selected operating point of: $Q_{liq} = 1800$ l/h and $Q_{air} = 0,3$ kg/s (Figure 33).

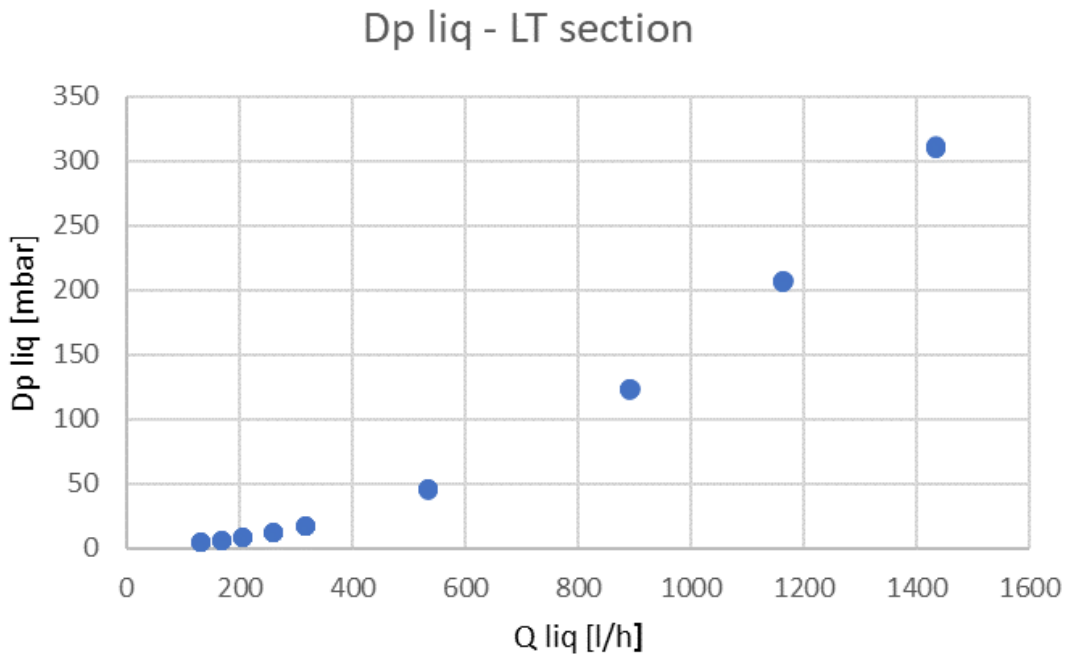


Figure 32 - Coolant pressure drop - LT section

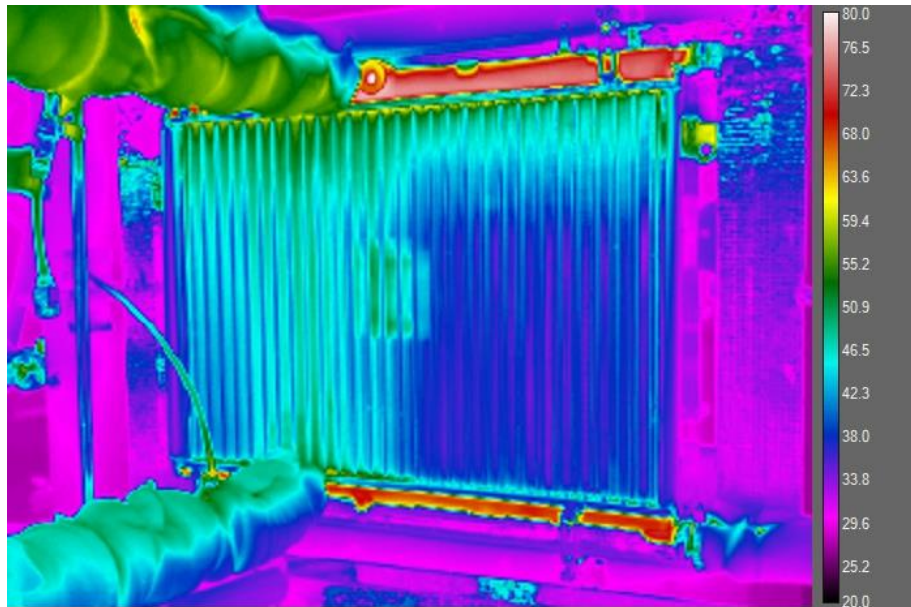


Figure 33 - Thermal imaging of the radiator under test

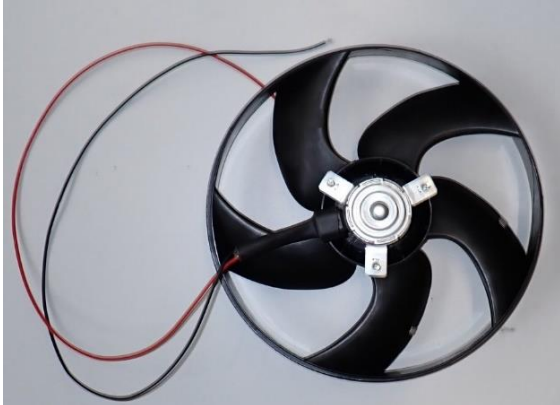
The dual-section radiator exhibited robust heat rejection capabilities across the different coolant flow rates tested. It maintained required performance across a range of thermal loads. However, further optimization of the radiator design, such as enhancing fin density or improving air flow distribution, may improve overall efficiency, particularly at higher coolant flow rates. The maximum heat rejection capacity of two sections of the radiator exceeded 26 kW at 8 000 l/h coolant flow providing safety margin for the TMS designed for 15 kW heat losses. However, a coolant pump of adequate flow rate need to be applied into the system.

6.2 FAN SYSTEM FUNCTIONAL CHARACTERISTIC TEST

6.2.1 TEST OBJECT IDENTIFICATION

The fan system was decoupled from the radiator unit, and it was put under test as a separate component.

Table 4 - Test object identification

BOSMAL marking	General view
Sample 1	

6.2.2 SCOPE OF THE TEST

Determination of Functional Characteristics according to BOSMAL instruction BOSMAL/I-7-57/04, Customer standard 18-3716 point 4.4 and requirements:

- Air inlet temperature: 20 °C
- Air flow rate: 0,280; 0,300; 0,320; 0,340; 0,360; 0,380; 0,400; 0,450; 0,600; 0,750; 1,100 kg/s
- Fan supply voltage: 12; 13; 14 V

6.2.3 TEST STAND INSTRUMENTATION

Table 5 - Measurement devices identification

Name of device	BOSMAL identification number	Accuracy	Last calibration date	Next calibration date
Atmospheric pressure	F/0700/BW	± 1 hPa	02.2024	02.2026
Cooling air temperature	G/1185/BHW G/1186/BHW G/1187/BHW	± 0,2°C	01.2024	01.2025
Cooling air flow rate	F/1220/BHW	± 1,5 %	08.2022	08.2025
Cooling air pressure drop	F/1212/BHW	± 1 Pa	07.2022	07.2024
Power Supply	H/1031/BE	± 0,01 V	01.2023	01.2025
Voltage	H/0555/BE	± 0,1 V	12.2022	12.2024
Fan speed	C/0377/BEE	± 1 rpm	06.2023	06.2025

The fan system installation on the test bed is presented in Figure 34.

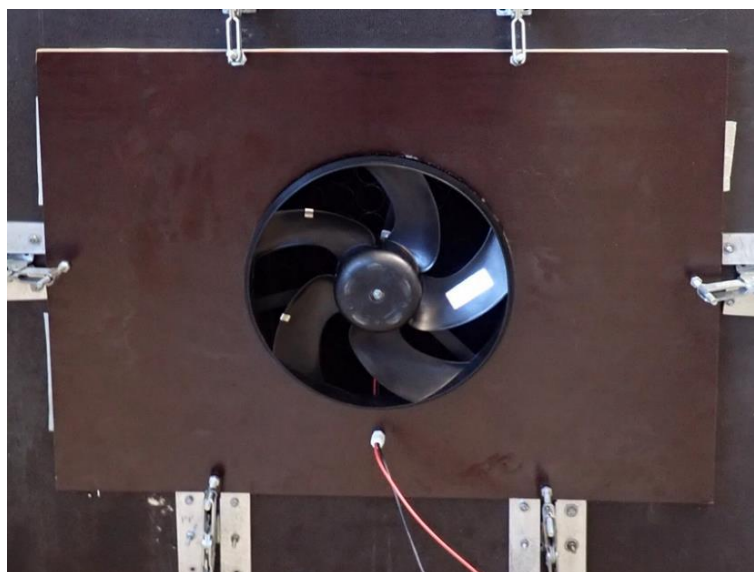


Figure 34 – Fan system mounted on test bed

6.2.4 TEST RESULTS AND DISCUSSION

The fan system was mounted in the test tunnel where the air flow and air pressure were measured. Test tunnel contains test bed fan to simulate air flow of a moving vehicle. The test results for 12 V supply voltage are presented in Table 6.

Table 6 - Test results obtained for 12 V supply voltage

P atm [hPa]	T air [°C]	Dp air [Pa]	Q air [kg/s]	Air density [kg/m ³]	Q air [m ³ /h]	P air [W]	U [V]	I [A]	P el. [W]	Speed [rpm]	Efficiency [%]
Air flow produced by fan system only – e.g. vehicle is at standstill											
977,4	23,3	50	0,275	1,149	862,0	12,0	12,0	8,0	96,0	1578,0	12,5
977,5	23,5	47	0,304	1,148	952,4	12,4	12,0	7,8	93,6	1587,0	13,3
Air flow produced by fan system and test bed fan – e.g. vehicle is moving											
977,4	23,6	45	0,322	1,147	1011,0	12,5	12,0	7,8	93,6	1588,0	13,3
977,5	23,7	41	0,338	1,147	1059,2	12,2	12,0	7,7	92,4	1613,0	13,2
977,4	23,8	38	0,357	1,147	1121,6	11,9	12,0	7,7	92,4	1617,0	12,9
977,7	23,8	34	0,382	1,147	1198,1	11,3	12,0	7,6	91,2	1625,0	12,4
977,6	23,8	30	0,396	1,147	1244,0	10,5	12,0	7,5	90,0	1636,0	11,6
977,6	23,9	16	0,451	1,147	1417,1	6,4	12,0	7,4	88,8	1673,0	7,2
977,5	24,0	-26	0,600	1,146	1883,8	-13,5	12,0	7,0	84,0	1795,0	-
977,7	24,0	-82	0,754	1,146	2369,5	-53,6	12,0	6,2	74,4	1955,0	-
977,6	24,2	-247	1,099	1,145	3455,7	-237,2	12,0	3,2	38,4	2429,0	-

Where:

P atm – atmospheric pressure

T air – ambient air temperature

Dp air – differential air pressure measured and calculated as ambient air pressure minus tunnel air pressure. Positive values mean pressure inside of tunnel is lower than ambient pressure

Q air – quantity of airflow through fan

Air density – air density measured

P air – calculated power of air stream, it is a product of Dp air and Q air

U – fan voltage supply measurement

I – fan electric current flow measurement

P el. – electrical power consumed by fan

Speed – rotational speed of fan

Efficiency – ratio of P air to P el. used by the fan system

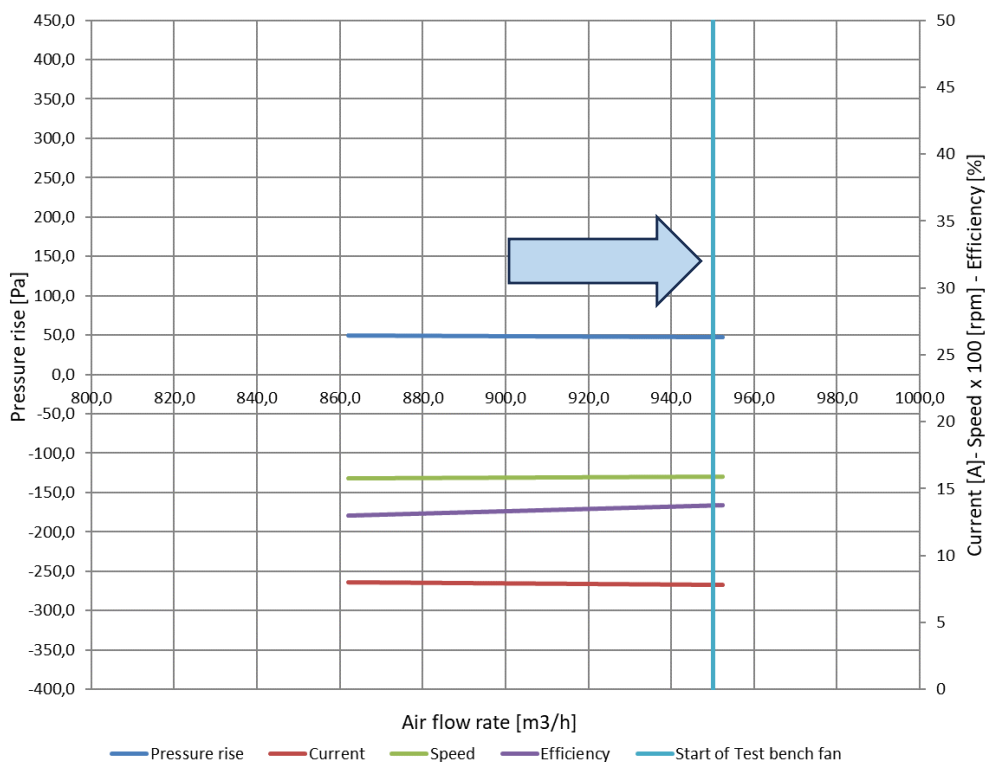


Figure 35 - Fan performance of at 12 V supply voltage, air flow produced only by fan system - e.g. vehicle is at standstill

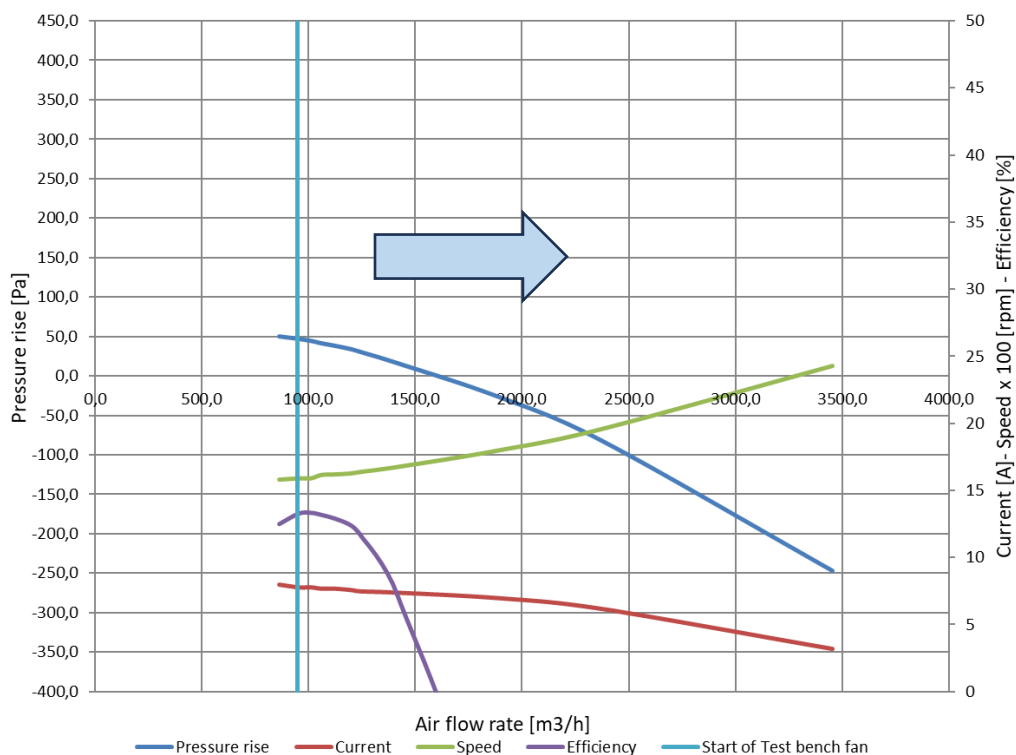


Figure 36 - Fan performance of at 12 V supply voltage, air flow produced by fan system and test bench fan - e.g. vehicle is moving

The fan system test results for 13 V supply voltage are presented in Table 7.

Table 7 - Test results obtained for 13V supply voltage

P atm [hPa]	T air [°C]	Dp air [Pa]	Q air [kg/s]	Air density [kg/m³]	Q air [m³/h]	P air [W]	U [V]	I [A]	P el. [W]	Speed [rpm]	Efficiency [%]
Air flow produced by fan system by only – e.g. vehicle is at standstill											
977,9	20,9	53	0,278	1,158	864	12,8	13,0	8,2	106,6	1589	12,0
978,0	21,2	51	0,300	1,157	934	13,1	13,0	8,2	106,6	1603	12,3
Air flow produced by fan system and fan on the test bench – e.g. vehicle is moving											
977,8	21,3	49	0,317	1,157	988	13,4	13,0	8,1	105,3	1610	12,7
978,0	21,3	46	0,340	1,157	1056	13,5	13,0	8,1	105,3	1620	12,8
977,9	21,3	42	0,361	1,157	1123	13,2	13,0	8,1	105,3	1636	12,6
977,9	21,3	40	0,383	1,157	1193	13,1	13,0	8,1	105,3	1655	12,5
977,9	21,3	36	0,401	1,157	1247	12,6	13,0	8,1	105,3	1666	12,0
977,8	21,3	23	0,453	1,157	1410	8,9	13,0	7,9	102,7	1701	8,7
977,8	21,3	-18	0,599	1,157	1865	-9,4	13,0	7,7	100,1	1839	-
977,8	21,3	-70	0,751	1,157	2335	-45,4	13,0	7,1	92,3	2002	-
977,8	21,3	-233	1,100	1,157	3423	-221,7	13,0	4,4	57,2	2464	-

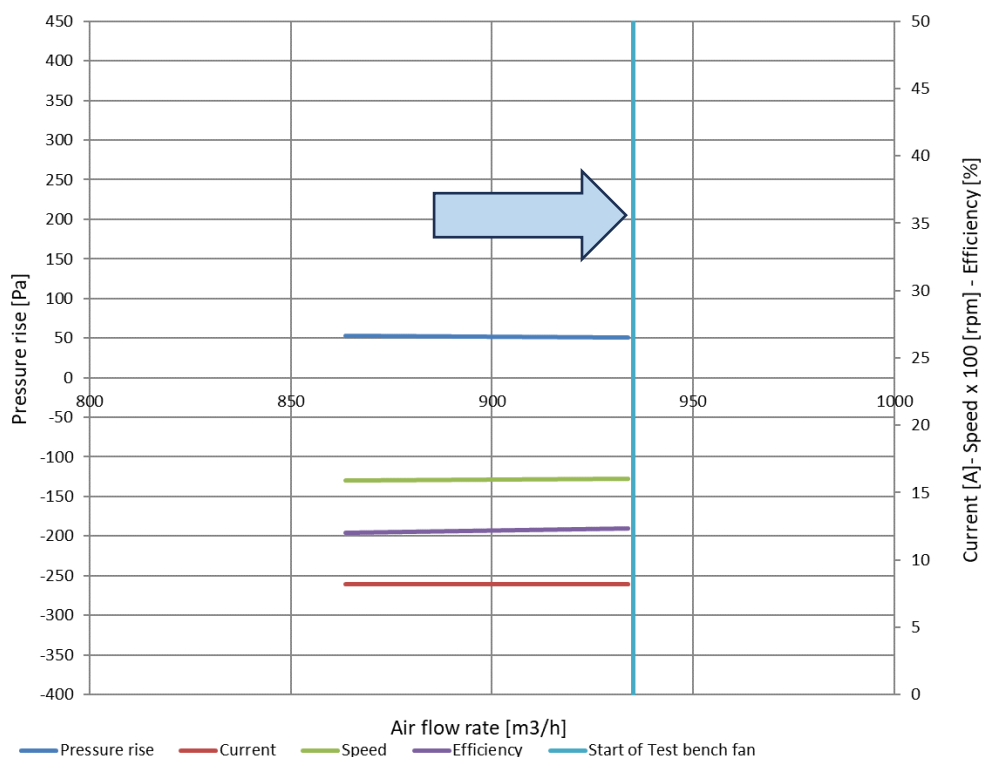


Figure 37 - Fan performance of at 13 V supply voltage, air flow produced only by fan system - e.g. vehicle is at standstill

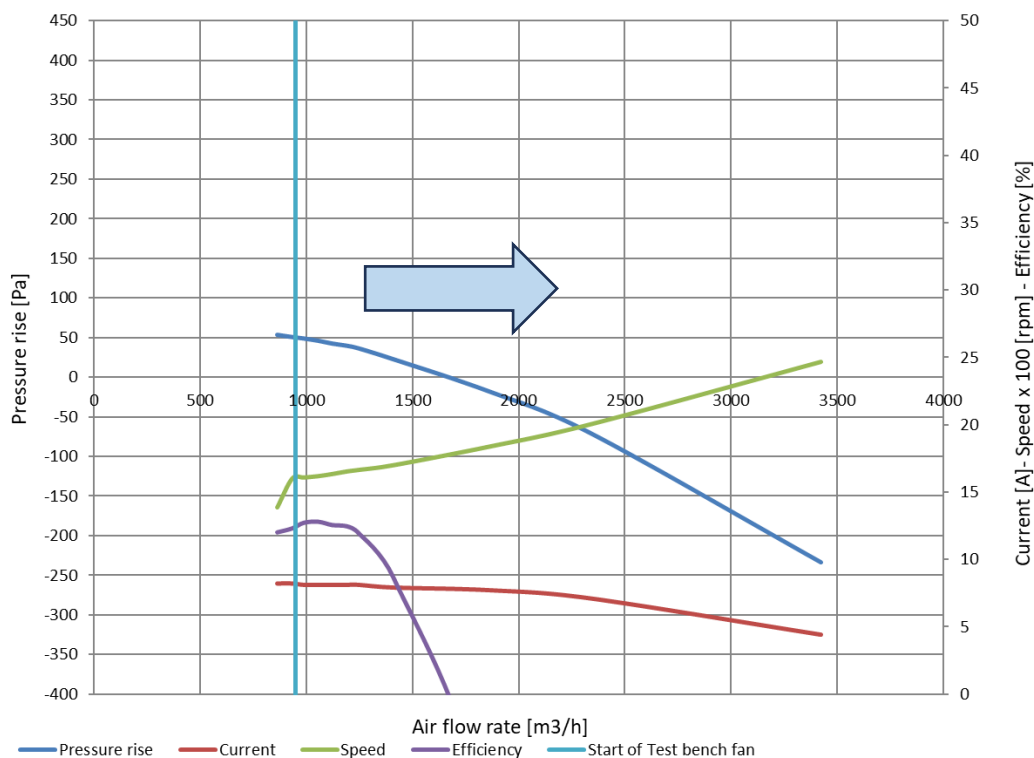


Figure 38 - Fan performance of at 13 V supply voltage, air flow produced by fan system and test bench fan – e.g. vehicle is moving

Table 8 - Test results obtained for 14 V supply voltage

P atm [hPa]	T air [°C]	Dp air [Pa]	Q air [kg/s]	Air density [kg/m ³]	Q air [m ³ /h]	P air [W]	U [V]	I [A]	P el. [W]	Speed [rpm]	Efficiency [%]
Air flow produced by fan system by itself – e.g. car is staying											
977,7	21,7	57	0,282	1,155	877	13,9	14,0	9,0	128,8	1648	11,2
977,7	21,6	54	0,303	1,155	944	14,3	14,0	9,0	126,0	1669	11,7
Air flow produced by fan system and fan on the test bench – e.g. car is moving											
977,6	21,6	55	0,317	1,155	987	15,1	14,0	9,2	128,8	1675	12,2
977,7	21,6	54	0,341	1,155	1062	15,9	14,0	9,2	128,8	1703	12,8
977,5	21,6	51	0,363	1,155	1133	16,2	14,0	9,3	130,2	1719	12,9
977,8	21,6	49	0,382	1,156	1189	16,2	14,0	9,3	130,2	1739	12,9
977,6	21,6	46	0,405	1,155	1262	16,0	14,0	9,4	131,6	1765	12,6
977,8	21,6	37	0,452	1,156	1410	14,6	14,0	9,4	131,6	1802	11,5
978,0	21,6	-4	0,599	1,156	1865	-1,9	14,0	9,2	128,8	1932	1,5
977,8	21,6	-57	0,753	1,156	2346	-37,4	14,0	8,6	120,4	2090	32,2
977,8	21,5	-223	1,101	1,156	3425	-212,2	14,0	5,7	79,8	2532	274,8

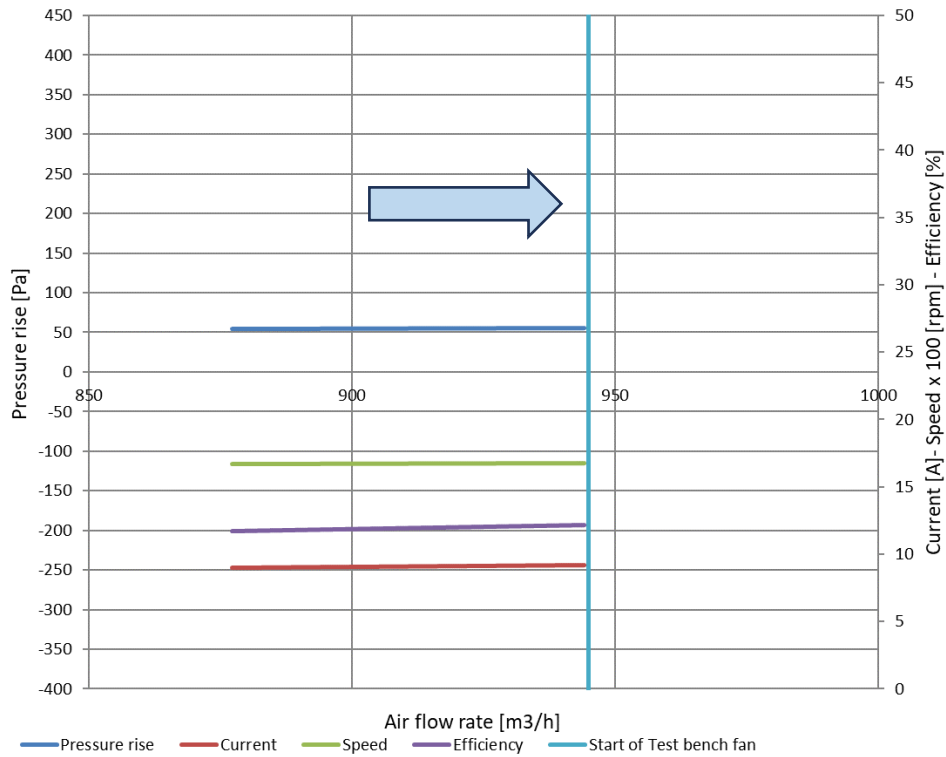


Figure 39 - Fan performance of at 14 V supply voltage, air flow produced only by fan system - e.g. vehicle is at standstill

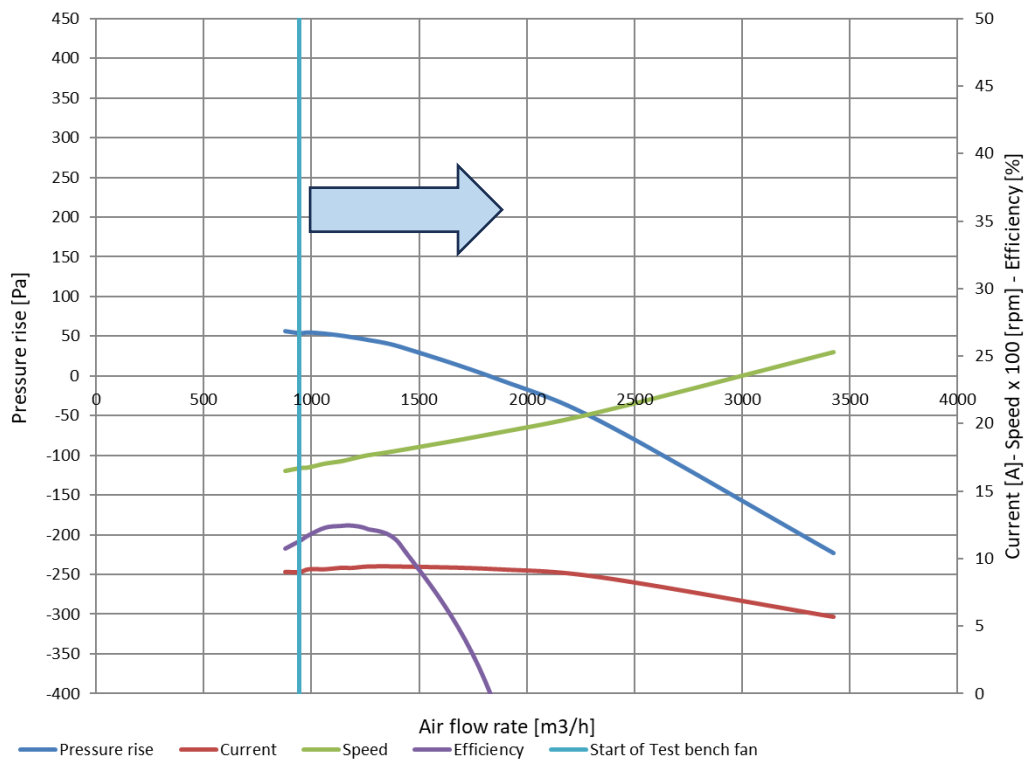


Figure 40 - Fan performance of at 14 V supply voltage, air flow produced by fan system and test bed fan – e.g. vehicle is moving

The fan system test aimed to assess the system ability to provide sufficient airflow over the radiator, particularly during low-speed and high-speed driving conditions. The tests were conducted at varying voltage levels of: 12 V, 13 V and 14 V to simulate different operating scenarios.

The results showed that the fan system achieved required performance across all tested voltage settings. At 12 V the fan provided sufficient airflow rate to support cooling capabilities at use case scenario where the natural airflow is limited. As the voltage increased to 13 V and 14 V, the airflow improved significantly, matching the higher cooling demands.

Despite the increase in supply voltage and the airflow, the electrical power level remained relatively low, with no significant spikes as the voltage increased. This indicates that the fan system can provide the necessary cooling capacity without excessive increase in energy consumption being an effective and energy-efficient solution for thermal management.

In summary, the fan system effectively contributed to radiator cooling across varying operational conditions ensuring stable thermal. The balance between airflow and power consumption highlights its suitability for integration into larger, more demanding power converter systems.

6.3 COOLANT PUMP PERFORMANCE TEST

6.3.1 TEST OBJECT IDENTIFICATION

Table 9 - Test object identification

BOSMAL marking	General view
Sample 1	

6.3.2 SCOPE OF THE TEST

Determination of Functional Characteristics according to BOSMAL instruction BOSMAL/I-7-57/04, Customer standard 18-3716 point 4.4 and requirements:

- Coolant inlet temperature: 80 °C
- Coolant flow rate: 0; 400; 800; 1000; 1200; 1400; 1500; 1800 l/h
- Coolant: water/glycol – 50/50
- Voltage supply: 12 V,
- Signal frequency: 100 Hz,
- Signal PWM: 50%; 75%; 100%

6.3.3 TEST STAND INSTRUMENTATION

Table 10 - Measurement devices identification

Name of device	BOSMAL identification number	Accuracy	Last calibration date	Next calibration date
Atmospheric pressure	F/0700/BW	± 1 hPa	02.2024	02.2026
Ambient air temperature	G/1185/BHW	± 0.2°C	01.2024	01.2025
Coolant temperature	G/1192/BHW G/1193/BHW	± 0.2°C	01.2024	01.2025
Coolant flow rate	F/0655/BW	± 0.2 %	05.2023	05.2026
Coolant pressure	F/1111/BHW	± 4 mbar	12.2021	12.2024
Power Supply	H/1031/BE	0,1A	12.2022	12.2024
Voltage	H/0555/BE	0.01V	06.2023	06.2025

The coolant pump installation on the test bed is presented in Figure 41.

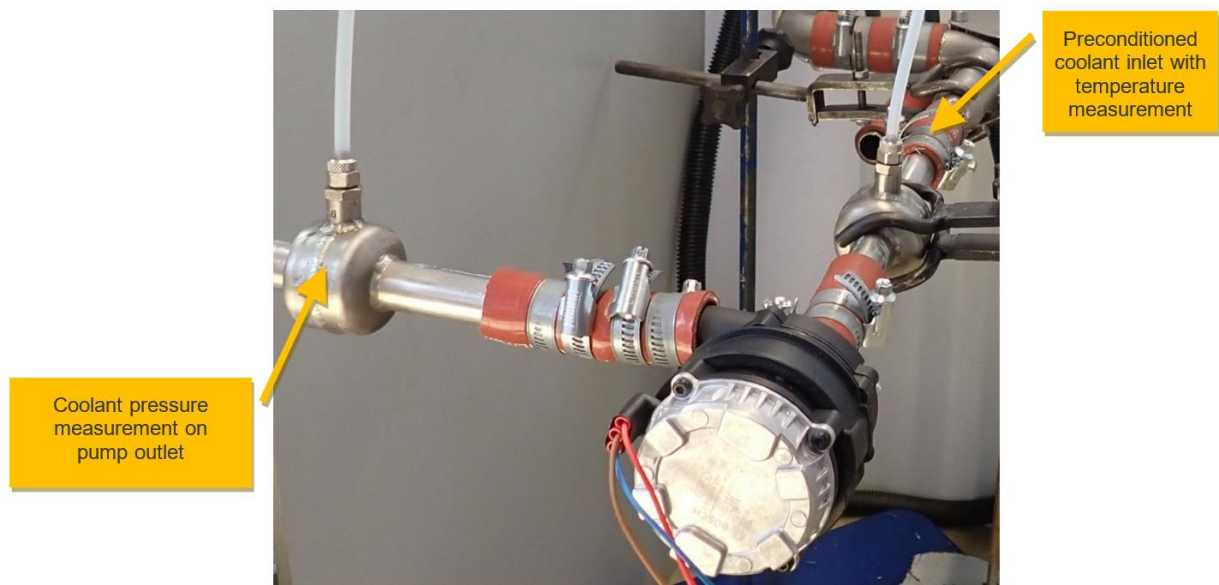


Figure 41 - Coolant pump mounted on test bed

6.3.4 TEST RESULTS AND DISCUSSION

The coolant pump was tested at three PWM settings in consecutive steps. At each PWM level the metering valve at the pump outlet was adjusted to obtain the desired coolant flow rate.

The results of coolant pump performance test for three PWM levels are summarized in Table 11.

Table 11 – Coolant pump test results

P atm [hPa]	T air ambient[°C]	P liq [mbar]	T liq in [°C]	Q liq [l/h]	Current [A]	Voltage [V]
PWM 50%						
975,3	24,6	146	80,0	823	0,59	12,0
975,2	24,7	203	80,0	595	0,54	12,0
975,2	24,7	227	79,8	395	0,50	12,0
974,9	24,9	235	79,9	203	0,43	12,0
974,9	24,9	235	79,7	0	0,38	12,0
PWM 75%						
975,3	24,4	215	80,0	1396	2,15	12,0
975,3	24,5	303	80,2	1202	2,03	12,0
975,5	24,5	373	80,3	1001	1,90	12,0
975,3	24,5	419	80,4	796	1,77	12,0
975,5	24,6	458	79,9	403	1,42	12,0
975,3	24,6	459	80,0	0	1,02	12,0
PWM 100%						
975,7	23,8	285	80,0	1813	4,72	12,0
975,7	23,8	464	80,0	1498	4,65	12,0
975,7	23,8	584	80,0	1196	4,29	12,0
975,5	23,9	636	80,0	997	3,93	12,0
975,5	24,3	670	80,1	802	3,46	12,0
975,4	24,2	698	80,0	402	2,77	12,0
975,4	24,3	696	79,9	0	2,14	12,0

Where:

- P atm – atmospheric pressure measured
- T air ambient – ambient air temperature measured
- T liq in – inlet coolant temperature measured
- Q liq – quantity of coolant flow measured
- Current – pump electrical current measured
- Voltage – pump electrical voltage measured

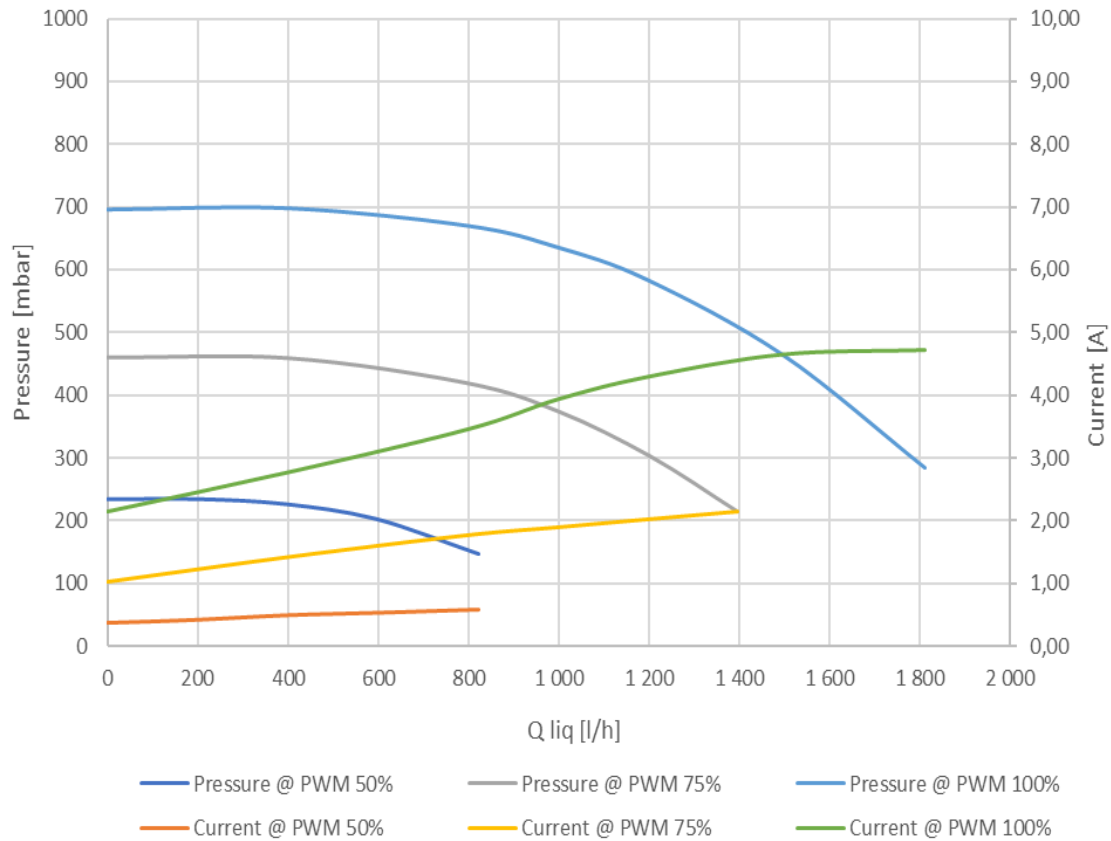


Figure 42 –Coolant pump performance characteristics

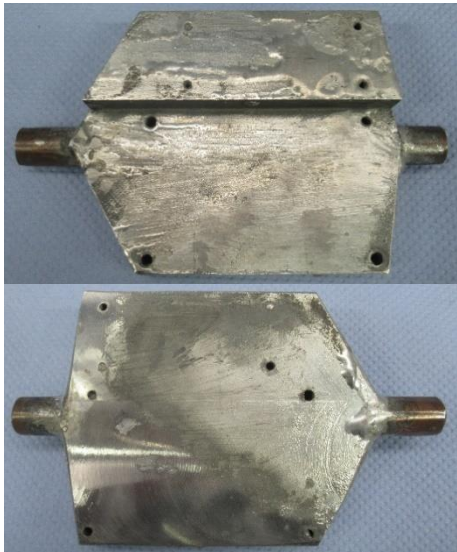
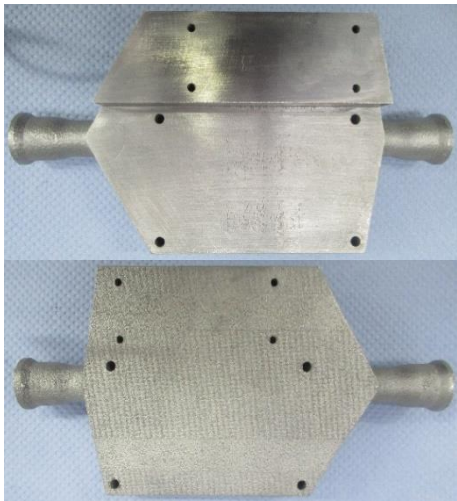
The coolant pump demonstrated consistent performance providing stable coolant flow rates and pressure characteristics under tested conditions. The obtained test results confirmed however, that the coolant pump was underperforming in terms of coolant flow rate during the TMS functional tests run at a later stage (section 6.5). For this reason the TMS coolant pump was replaced with a test bench version.

6.4 HEATSINK FUNCTIONAL CHARACTERISTIC TEST

6.4.1 TEST OBJECT IDENTIFICATION

Two samples of the liquid-cooled heatsink were manufactured and put under the test. Heatsink marked as Sample 1 was made of copper alloy while the Sample 2 was an aluminium alloy version, as depicted in Table 12.

Table 12 - Test object identification

BOSMAL marking	General view
Sample 1	
Sample 2	

6.4.2 SCOPE OF THE TEST

Determination of Functional Characteristics according to BOSMAL instruction BOSMAL/I-7-57/04 and requirements:

- Coolant inlet temperature: 80; 60; 40; 20 °C
- Coolant flow rate on inlet spout: 400; 800; 1000; 1200; 1400; 1500; 1800; 2500 l/h
- Electrical heating: 600; 1200; 1800 W
- Coolant: water/glycol – 50/50

6.4.3 TEST STAND INSTRUMENTATION

Table 13 - Measurement devices identification

Name of device	BOSMAL identification number	Accuracy	Last calibration date	Next calibration date
Atmospheric pressure	F/0700/BW	± 1 hPa	02.2024	02.2026
Ambient air temperature	G/1186/BHW	$\pm 0.3^\circ\text{C}$	10.2024	10.2025
Coolant temperature	G/1565/BHW G/1566/BHW G/1567/BHW G/1568/BHW	$\pm 0.3^\circ\text{C}$	10.2024	10.2025
Coolant flow rate	F/0656/BW	$\pm 0.2\%$	05.2023	05.2026
Coolant pressure	F/1111/BHW	± 6 mbar	10.2024	10.2026
Coolant pressure drop	F/1109/BHW	± 2 mbar	10.2024	10.2026
Electrical heating	H/1017/BE	$\pm 0.2\%$	09.2023	09.2025
Heatsink surface temperature	H/0988/BE	$\pm 0.3^\circ\text{C}$	07.2024	07.2025

The heatsink mounted on the test rig and heating elements installation on the heatsink active surface (cold plate) are presented on figures 43 and 44.

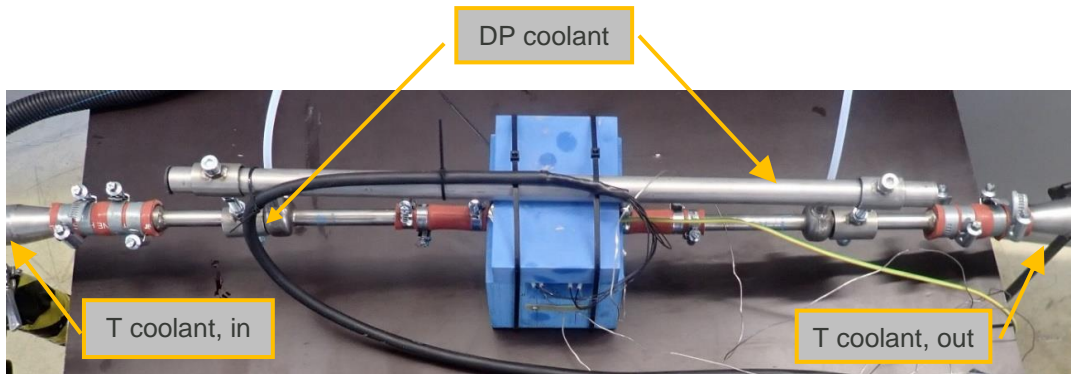


Figure 43 – Heatsink mounted on test bed

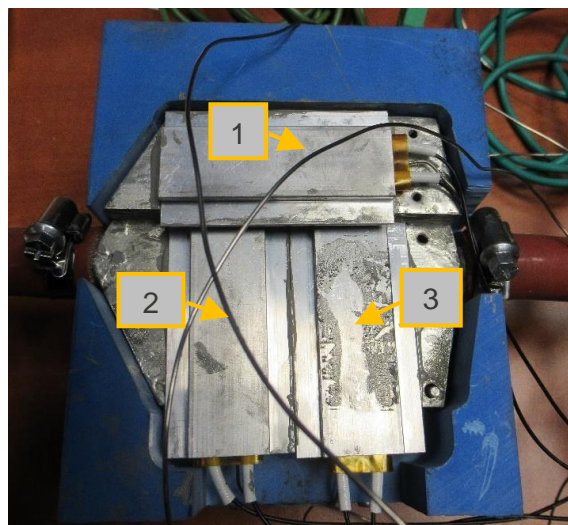


Figure 44 – Heating elements placed on heatsink with identification of mounting spot

6.4.4 TEST RESULTS – HEATSINK SAMPLE 1

Three electrical heating elements were mounted on heatsink in designated places where the SiC and GaN modules are going to be installed in the final inverter version. Three thermocouples were mounted in-between the heating elements and heatsink active surface. Heating elements were installed using thermal interface material type: TermoPasty HPX, with thermal conductivity index of > 2,8 W/mK. Testing proceeded with constant coolant temperature and varying coolant flow in each testing step.

Heatsink test results for 20 °C coolant temperature are presented in Table 14.

Table 14 - Test results obtained for 20 [°C] coolant temperature

P atm [hPa]	T air [°C]	Electrical heat [kW]	Heatsink surface temperature			Q liq [l/h]	P liq [mbar]	DP liq [mbar]	T liq in [°C]	T liq out [°C]	Q coolant [kW]
			T1 [°C]	T2 [°C]	T3 [°C]						
976,7	19,62	0,10	35,58	45,67	66,93	2502	2643	1335	20,00	20,07	0,17
976,7	19,57	0,20	53,40	68,74	96,10	2502	2640	1334	20,00	20,10	0,25
976,7	19,52	0,30	68,19	93,05	111,23	2502	2641	1334	20,00	20,12	0,30
976,7	19,47	0,32	71,30	98,41	116,28	2501	2639	1333	20,00	20,13	0,32
976,7	19,41	0,10	34,09	46,10	62,78	1800	1936	701	20,00	20,07	0,13
976,7	19,37	0,20	52,00	68,90	90,00	1800	1937	700	20,00	20,13	0,23
976,7	19,3	0,30	67,71	93,40	109,99	1798	1935	699	20,0	20,17	0,30
976,7	19,32	0,32	70,94	99,02	115,42	1800	1935	701	20,00	20,17	0,30
976,7	19,31	0,10	33,82	46,18	62,22	1500	1698	492	20,00	20,07	0,10
976,7	19,31	0,20	50,95	69,01	90,09	1499	1697	491	20,00	20,17	0,25
976,7	19,26	0,30	66,97	92,82	110,14	1500	1697	492	20,03	20,27	0,35
976,7	19,26	0,32	70,40	98,37	115,58	1499	1697	490	20,00	20,21	0,31
976,7	19,22	0,10	33,27	46,31	62,18	1399	1628	429	20,00	20,07	0,10
976,7	19,17	0,20	49,45	68,64	89,63	1400	1627	430	20,00	20,17	0,23
976,7	19,16	0,30	65,84	92,55	110,13	1400	1627	430	20,01	20,27	0,35
976,7	19,13	0,32	69,40	98,10	115,57	1400	1626	430	20,05	20,29	0,32
976,7	19,07	0,10	32,90	46,49	62,23	1200	1499	319	20,01	20,10	0,11
976,7	19,07	0,20	48,32	68,60	89,13	1200	1498	319	20,02	20,20	0,21
976,7	19,02	0,30	65,00	92,44	110,57	1200	1498	319	20,00	20,25	0,29
976,7	18,99	0,32	68,70	97,97	115,90	1200	1498	319	20,04	20,31	0,32
976,7	18,96	0,10	32,67	46,43	62,50	1000	1387	224	20,00	20,10	0,10
976,7	18,92	0,20	47,75	68,67	89,19	1000	1387	224	20,05	20,26	0,20
976,7	18,87	0,30	64,44	92,56	110,31	1000	1386	224	20,05	20,36	0,30
976,7	18,87	0,32	67,90	98,00	115,70	1000	1386	224	20,02	20,36	0,32
976,7	18,92	0,10	32,60	46,80	62,35	800	1292	146	19,97	20,10	0,10
976,7	18,96	0,20	47,01	69,16	89,65	800	1291	146	20,04	20,30	0,20
976,7	18,96	0,30	63,69	93,02	110,80	800	1291	146	20,01	20,40	0,30
976,7	18,96	0,32	67,08	98,16	115,90	800	1291	146	20,05	20,46	0,32
976,7	18,96	0,10	33,25	47,30	62,15	400	1151	38	20,04	20,31	0,10
976,7	18,92	0,20	48,22	69,84	89,13	400	1152	38	19,98	20,50	0,20
976,7	18,89	0,30	65,19	94,84	112,30	400	1151	38	19,97	20,73	0,30
976,7	18,84	0,32	68,25	99,33	116,73	400	1151	38	20,04	20,86	0,32

Where:

- P atm – atmospheric pressure measured
- T air – ambient air temperature
- Electrical heat – electrical heat applied to the heatsink surface
- Heatsink surface temperature T1, T2, T3 – heatsink surface temperature measured in spots shown on figure 42
- Q liq – coolant flow through heatsink
- P liq – coolant pressure measured in the cooling system
- DP liq – differential pressure measured at the inlet and outlet of the heatsink
- T liq in – temperature of coolant at the inlet of heatsink
- T liq out – temperature of coolant at the outlet of heatsink
- Q coolant – electrical heat absorbed by coolant

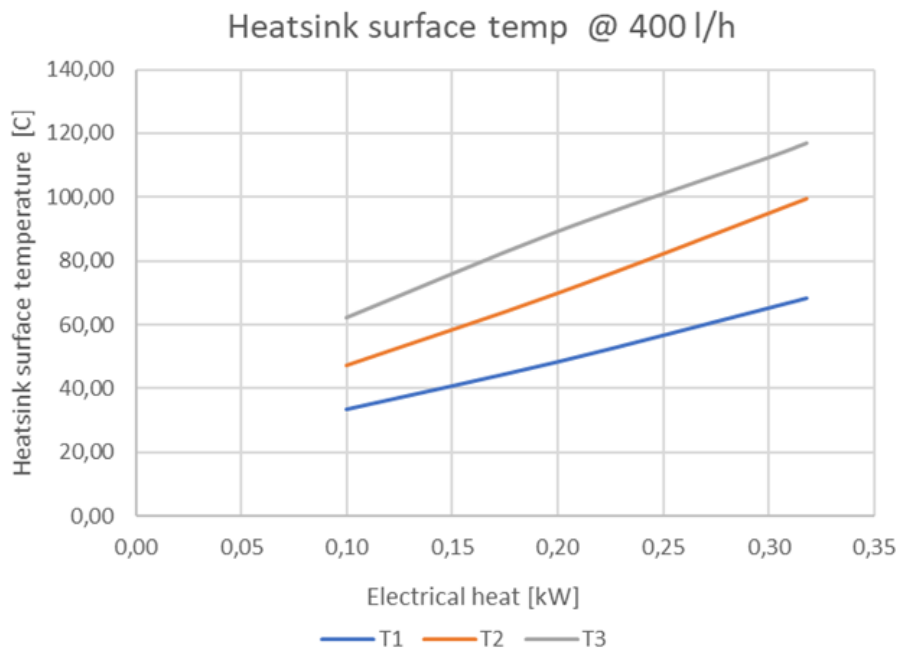


Figure 45 – Heatsink performance at 20 [°C] coolant temperature and 400 l/min coolant flow

Heatsink test results for 40 °C coolant temperature are presented in Table 15.

Table 15 - Test results obtained for 40 [°C] coolant temperature

P atm [hPa]	T air [°C]	Electrical heat [kW]	Heatsink surface temperature			Q liq [l/h]	P liq [mbar]	DP liq [mbar]	T liq in [°C]	T liq out [°C]	Q coolant [kW]
			T1 [°C]	T2 [°C]	T3 [°C]						
977,6	18,83	0,10	51,66	63,39	74,80	2500	2509	1286	40,10	40,14	0,10
977,6	18,87	0,20	67,81	84,99	99,88	2500	2509	1286	40,10	40,18	0,20
977,7	18,92	0,30	82,18	107,80	123,99	2500	2508	1287	40,03	40,18	0,37
977,9	19,02	0,10	52,36	64,15	73,85	1800	1850	677	40,02	40,10	0,15
978,2	19,16	0,20	67,51	83,14	99,40	1800	1851	677	40,06	40,18	0,20
978,0	19,22	0,30	82,16	106,50	123,99	1800	1851	677	40,04	40,20	0,29
978,0	19,32	0,10	52,33	64,33	73,29	1500	1629	474	40,01	40,10	0,13
978,0	19,37	0,20	66,68	84,89	99,40	1500	1629	474	40,00	40,17	0,25
978,0	19,40	0,30	81,12	106,53	124,03	1500	1629	474	40,02	40,22	0,29

978,0	19,46	0,10	51,76	64,65	73,59	1400	1563	414	40,02	40,10	0,11
978,1	19,51	0,20	65,99	85,15	99,52	1400	1563	414	40,04	40,18	0,19
978,1	19,52	0,30	80,26	106,30	123,96	1400	1563	414	39,98	40,20	0,30
979,2	19,62	0,10	51,60	64,10	76,50	1200	1415	278	40,04	40,13	0,10
979,2	19,67	0,20	67,87	84,75	102,08	1200	1447	307	40,04	40,21	0,20
979,6	19,82	0,29	79,96	108,61	125,42	1200	1448	306	40,06	40,30	0,28
979,6	19,92	0,10	51,60	65,34	75,55	1000	1346	215	40,07	40,17	0,10
979,9	20,07	0,20	66,98	84,35	100,40	1000	1346	215	40,10	40,30	0,20
980,0	20,26	0,29	81,10	106,92	124,48	1000	1346	215	40,00	40,30	0,29
980,2	20,42	0,10	51,54	65,79	75,44	800	1260	140	40,08	40,20	0,10
980,4	20,56	0,20	63,96	84,38	98,07	800	1260	140	40,02	40,27	0,20
980,5	20,81	0,29	80,91	107,02	124,35	800	1260	140	40,00	40,37	0,29
980,6	20,86	0,10	51,92	67,83	80,32	400	1139	37	40,02	40,28	0,10
980,8	20,92	0,20	64,89	90,52	107,20	400	1139	37	40,00	40,50	0,20
980,8	20,96	0,29	80,86	109,50	126,97	400	1139	37	40,01	40,70	0,27
968,4	21,12	0,37	68,83	113,89	63,05	400	1130	41	39,95	40,87	0,36

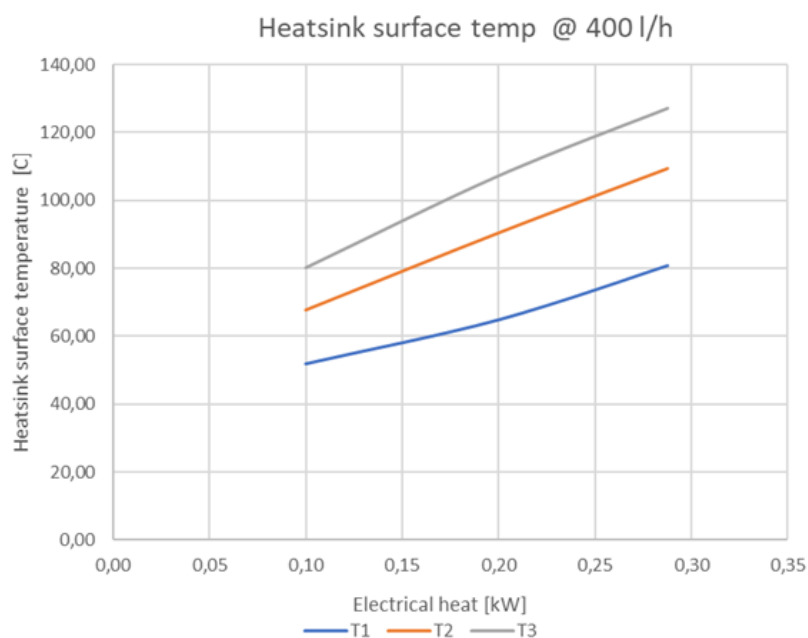


Figure 46 – Heatsink performance at 40 [°C] coolant temperature and 400 l/min coolant flow

Heatsink test results for 60 °C coolant temperature are presented in Table 16.

Table 16 - Test results obtained for 60 [°C] coolant temperature

P atm [hPa]	T air [°C]	Electrical heat [kW]	Heatsink surface temperature			Q liq [l/h]	P liq [mbar]	DP liq [mbar]	T liq in [°C]	T liq out [°C]	Q coolant [kW]
			T1 [°C]	T2 [°C]	T3 [°C]						
981,0	21,53	0,10	70,20	83,59	90,01	2500	2438	1246	59,90	59,95	0,11
981,1	21,58	0,20	85,00	102,29	116,49	2499	2437	1244	60,10	60,18	0,20
981,1	21,62	0,27	94,97	117,58	133,70	2500	2438	1246	60,09	60,20	0,27
981,1	21,62	0,10	70,60	83,36	90,01	1800	1808	655	60,02	60,08	0,11
981,1	21,56	0,20	84,35	102,49	116,60	1800	1808	655	60,05	60,17	0,20
981,1	21,54	0,27	95,12	117,34	133,77	1800	1808	656	60,04	60,18	0,25
981,3	21,48	0,10	70,49	83,65	90,29	1500	1597	459	60,04	60,10	0,09
981,4	21,46	0,20	84,23	102,30	116,67	1500	1597	459	60,05	60,18	0,20
981,6	21,46	0,27	95,11	117,24	133,80	1500	1597	459	60,03	60,20	0,25
981,6	21,46	0,10	70,41	83,61	90,37	1400	1535	401	60,03	60,12	0,11
981,8	21,46	0,20	83,63	102,32	116,74	1400	1535	402	60,04	60,19	0,20
981,8	21,46	0,27	95,00	117,00	133,72	1400	1535	401	60,00	60,18	0,26
982,0	21,46	0,10	70,39	83,47	90,55	1200	1423	297	60,01	60,08	0,09
982,0	21,46	0,20	83,45	102,15	116,84	1200	1422	297	60,03	60,20	0,20
982,1	21,46	0,27	94,93	116,99	133,90	1200	1423	297	60,05	60,25	0,24

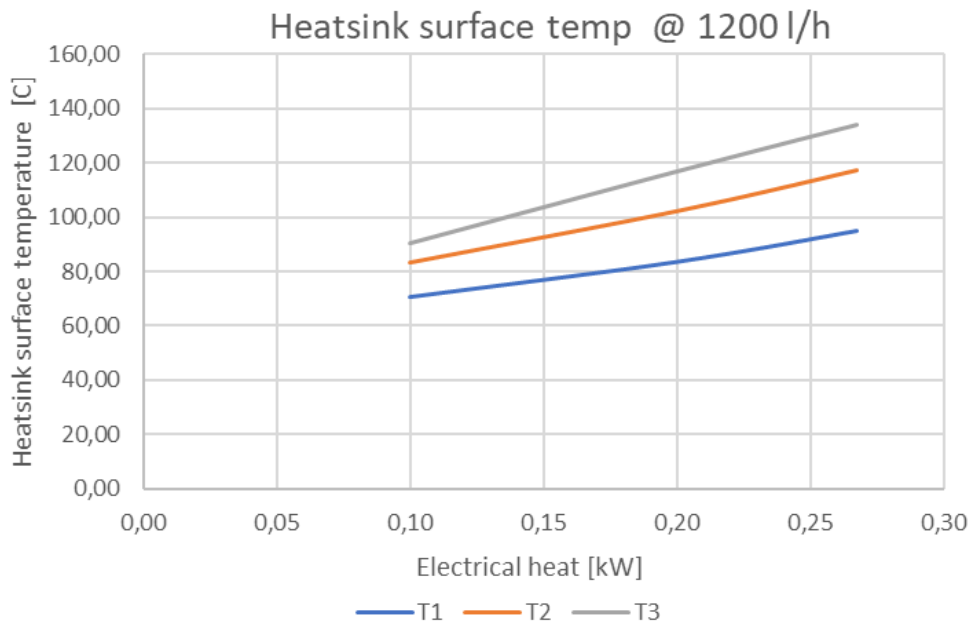


Figure 47 - Heatsink performance at 60 [°C] coolant temperature and 1200 l/min coolant flow

Heatsink test results for 80 °C coolant temperature are presented in Table 17.

Table 17 - Test results obtained for 80 [°C] coolant temperature

P atm [hPa]	T air [°C]	Electrical heat [kW]	Heatsink surface temperature			Q liq [l/h]	P liq [mbar]	DP liq [mbar]	T liq in [°C]	T liq out [°C]	Q coolant [kW]
			T1 [°C]	T2 [°C]	T3 [°C]						
982,7	21,73	0,10	90,20	101,45	108,70	2500	2387	1214	79,99	80,03	0,10
982,7	21,83	0,20	105,50	120,60	133,95	2500	2388	1215	80,04	80,12	0,19
982,8	21,86	0,24	110,82	129,15	143,23	2499	2389	1215	80,04	80,14	0,24
982,9	21,91	0,10	90,44	101,74	109,10	1800	1776	639	80,02	80,07	0,09
983,0	21,96	0,20	105,10	120,76	134,50	1800	1778	638	80,03	80,14	0,20
983,1	22,02	0,24	110,54	128,90	143,60	1800	1777	638	80,01	80,13	0,22
983,2	21,97	0,10	90,20	101,45	109,38	1500	1574	447	80,02	80,08	0,09
983,2	21,96	0,20	105,14	120,69	134,72	1500	1574	447	79,96	80,10	0,20
983,3	21,94	0,24	110,50	128,80	143,70	1500	1574	447	79,98	80,14	0,24
983,3	21,86	0,10	90,10	101,82	109,37	1400	1514	391	79,98	80,05	0,10
983,5	21,86	0,20	105,39	120,74	134,80	1400	1514	391	80,01	80,14	0,19
983,6	21,86	0,24	110,62	128,75	143,81	1400	1514	391	79,99	80,16	0,24
983,7	21,92	0,10	90,13	101,68	109,43	1200	1406	289	79,95	80,02	0,09
983,9	21,92	0,20	104,27	119,59	133,29	1200	1406	290	79,98	80,15	0,20
983,9	21,93	0,24	110,90	128,52	143,99	1200	1406	289	80,00	80,19	0,23

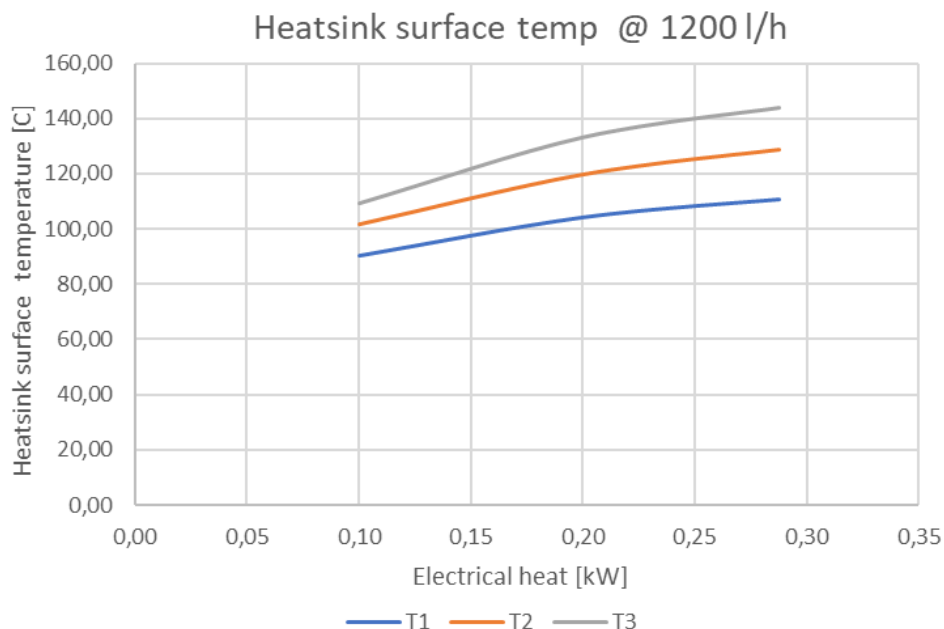


Figure 48 - Heatsink performance at 80 [°C] coolant temperature and 1200 l/min coolant flow

6.4.5 TEST RESULTS - HEATSINK SAMPLE 2

Three electrical heating elements were mounted on heatsink in designated places where the SiC and GaN modules are going to be installed in the final inverter version. Three thermocouples were mounted in-between the heating elements and heatsink active surface. Heating elements were installed using thermal interface material type:

TermoPasty HPX, with thermal conductivity index of > 2,8 W/mK. Testing proceeded with constant coolant temperature and varying coolant flow in each testing step.

Heatsink test results for 20 °C coolant temperature are presented in Table 18.

Table 18 - Test results obtained for 20 [°C] coolant temperature

P atm [hPa]	T air [°C]	Electrical heat [kW]	Heatsink surface temperature			Q liq [l/h]	P liq [mbar]	DP liq [mbar]	T liq in [°C]	T liq out [°C]	Q coolant [kW]
			T1 [°C]	T2 [°C]	T3 [°C]						
967,6	20,63	0,10	27,25	42,10	25,91	2500	2783	1481	20,00	20,07	0,17
967,5	20,75	0,20	31,90	65,41	32,30	2500	2783	1481	20,10	20,18	0,20
967,4	20,83	0,30	38,32	81,60	36,61	2500	2783	1481	20,00	20,17	0,41
967,3	20,90	0,40	45,70	96,30	40,11	2500	2782	1481	20,00	20,20	0,49
967,2	21,00	0,10	26,60	42,89	25,85	1800	2008	779	19,95	20,02	0,12
967,0	20,97	0,20	32,13	65,93	32,32	1800	2007	779	19,93	20,05	0,20
966,8	21,06	0,30	38,97	82,76	37,20	1800	2006	779	19,99	20,18	0,32
966,4	21,09	0,40	46,66	97,38	40,79	1800	2004	779	20,01	20,24	0,40
966,3	21,15	0,10	27,10	43,02	25,93	1500	1742	545	20,00	20,10	0,14
966,7	21,12	0,20	32,69	66,30	32,40	1500	1740	545	20,06	20,19	0,20
966,9	21,07	0,30	39,82	83,20	37,35	1500	1745	546	19,85	20,05	0,30
967,1	21,09	0,40	47,18	97,73	41,17	1500	1741	545	20,00	20,27	0,39
967,2	21,02	0,10	27,01	43,41	25,92	1400	1662	476	20,04	20,12	0,10
967,1	20,93	0,20	32,61	66,50	32,50	1400	1663	476	20,03	20,18	0,20
967,1	20,88	0,30	39,82	83,62	37,53	1400	1661	476	20,01	20,27	0,36
967,0	20,93	0,40	47,44	98,19	41,18	1400	1666	476	19,97	20,26	0,40
970,0	20,28	0,10	27,90	42,90	26,25	1200	1522	352	20,04	20,12	0,10
970,0	20,32	0,20	32,93	66,96	32,92	1200	1522	352	20,04	20,21	0,20
970,0	20,26	0,30	40,96	84,07	37,99	1200	1522	352	20,10	20,37	0,31
970,2	20,42	0,40	48,78	99,00	41,70	1200	1522	352	20,02	20,37	0,41
970,2	20,52	0,10	27,71	43,50	26,20	1000	1400	247	20,04	20,14	0,10
970,3	20,50	0,20	33,28	67,28	33,00	1000	1400	247	20,10	20,30	0,19
970,2	20,56	0,30	41,00	84,70	38,07	1000	1400	247	20,01	20,33	0,30
970,3	20,66	0,40	49,14	99,60	42,06	1000	1399	247	20,09	20,49	0,39
970,4	20,75	0,10	27,99	43,80	26,32	800	1297	161	20,06	20,19	0,10
970,5	20,81	0,20	33,77	67,60	33,20	800	1296	161	20,05	20,31	0,20
970,5	20,74	0,30	41,68	85,02	38,49	800	1296	161	20,09	20,48	0,30
970,6	20,73	0,40	49,94	100,01	42,61	800	1296	161	20,06	20,57	0,40
970,9	20,70	0,10	28,70	44,31	27,20	400	1146	44	20,09	20,32	0,09
971,0	20,65	0,20	35,00	68,81	34,79	400	1146	44	20,10	20,60	0,19
970,9	20,55	0,30	44,21	86,59	40,54	400	1145	44	20,10	20,83	0,29
970,9	20,63	0,40	53,25	102,50	45,28	400	1145	44	20,08	21,10	0,40

Where:

P atm – atmospheric pressure measured

T air – ambient air temperature

Electrical heat – electrical heat applied to the heatsink surface

Heatsink surface temperature T1, T2, T3 – heatsink surface temperature measured in spots shown on figure 42

Q liq – coolant flow through heatsink

P liq – coolant pressure measured in the cooling system

DP liq – differential pressure measured at the inlet and outlet of the heatsink

T liq in – temperature of coolant at the inlet of heatsink

T liq out – temperature of coolant at the outlet of heatsink

Q coolant – electrical heat absorbed by coolant

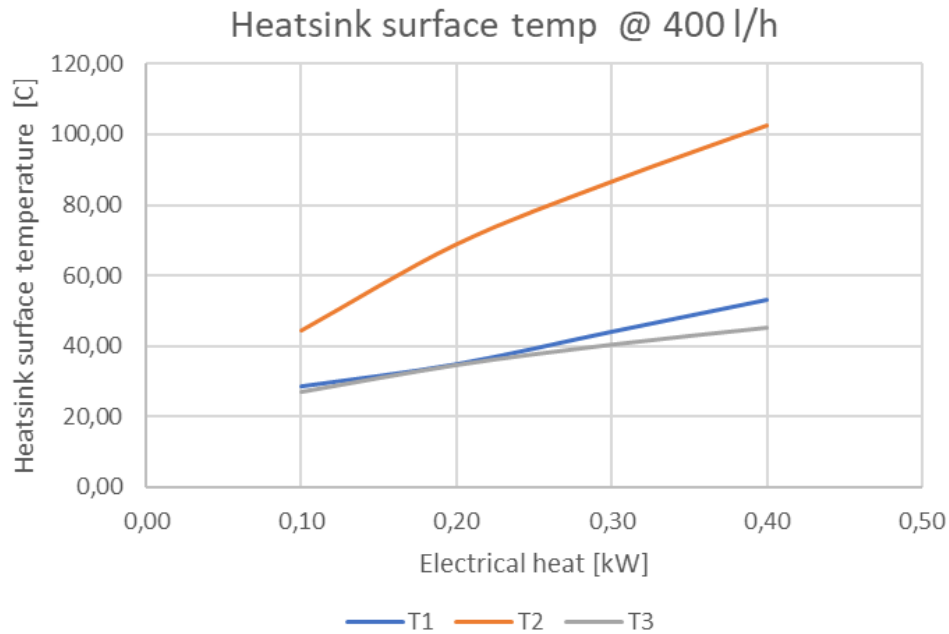


Figure 49 – Heatsink performance at 20 [°C] coolant temperature and 400 l/min coolant flow

Heatsink test results for 40 °C coolant temperature are presented in Table 19.

Table 19 - Test results obtained for 40 [°C] coolant temperature

P atm [hPa]	T air [°C]	Electrical heat [kW]	Heatsink surface temperature			Q liq [l/h]	P liq [mbar]	DP liq [mbar]	T liq in [°C]	T liq out [°C]	Q coolant [kW]
			T1 [°C]	T2 [°C]	T3 [°C]						
977,6	20,16	0,10	45,21	62,10	45,79	2500	2662	1431	40,02	40,11	0,20
977,5	19,98	0,20	50,76	83,42	51,82	2500	2661	1430	40,09	40,17	0,20
977,3	19,86	0,30	58,06	99,10	56,01	2500	2663	1430	40,07	40,19	0,30
976,9	19,76	0,38	63,11	111,54	59,00	2500	2662	1430	40,07	40,22	0,38
976,8	19,72	0,10	45,59	62,35	45,58	1800	1932	754	40,04	40,10	0,11
976,7	19,76	0,20	51,06	83,79	51,65	1800	1931	754	40,05	40,17	0,20
975,9	19,87	0,30	58,60	100,00	56,35	1800	1931	754	40,05	40,22	0,30
975,9	19,90	0,38	63,79	111,90	59,39	1800	1930	754	40,07	40,29	0,38
975,5	19,92	0,10	45,70	62,40	45,61	1500	1685	528	40,01	40,08	0,10
975,4	19,98	0,20	51,21	84,00	51,81	1500	1684	528	40,03	40,17	0,20
975,0	20,07	0,30	59,00	100,29	56,69	1500	1684	528	40,01	40,21	0,29
974,6	20,12	0,38	64,20	112,00	59,70	1500	1683	528	40,05	40,30	0,37
974,4	20,12	0,10	45,73	62,50	45,69	1400	1610	461	40,05	40,11	0,09
974,2	20,07	0,20	51,40	84,10	51,90	1400	1611	461	40,03	40,17	0,20

973,8	20,07	0,30	59,20	100,31	56,76	1400	1610	461	40,01	40,23	0,30
973,5	20,02	0,38	64,38	111,97	59,84	1400	1610	461	40,03	40,30	0,38
973,2	19,96	0,10	45,90	62,48	45,71	1200	1477	341	40,01	40,10	0,11
972,7	19,91	0,20	51,71	84,20	52,00	1200	1477	341	40,02	40,19	0,20
972,5	19,87	0,30	59,67	100,70	57,10	1200	1476	341	40,04	40,30	0,30
972,1	19,82	0,38	64,80	112,39	60,13	1200	1476	341	40,03	40,34	0,37
971,3	19,76	0,10	46,09	62,67	45,86	1000	1362	239	40,01	40,10	0,09
971,2	19,76	0,20	52,07	84,49	52,28	1000	1361	239	40,01	40,22	0,20
971,1	19,76	0,30	60,24	101,00	57,43	1000	1362	239	40,00	40,30	0,29
971,0	19,88	0,38	65,45	112,51	60,50	1000	1361	239	40,02	40,40	0,37
970,2	20,39	0,10	46,31	62,74	46,02	800	1265	154	40,05	40,17	0,09
969,7	20,63	0,20	52,55	84,67	52,55	800	1265	155	40,05	40,30	0,20
969,5	20,73	0,30	61,07	101,38	57,90	800	1265	155	40,00	40,37	0,29
969,4	20,85	0,37	66,30	113,10	61,09	800	1265	155	40,03	40,50	0,37
969,4	20,96	0,10	47,07	63,49	46,85	400	1132	41	40,14	40,40	0,10
968,9	21,06	0,20	54,13	85,83	54,00	400	1131	41	40,13	40,60	0,19
968,4	21,07	0,30	63,18	102,81	59,78	400	1131	41	40,00	40,75	0,30
968,4	21,12	0,37	68,83	113,89	63,05	400	1130	41	39,95	40,87	0,36

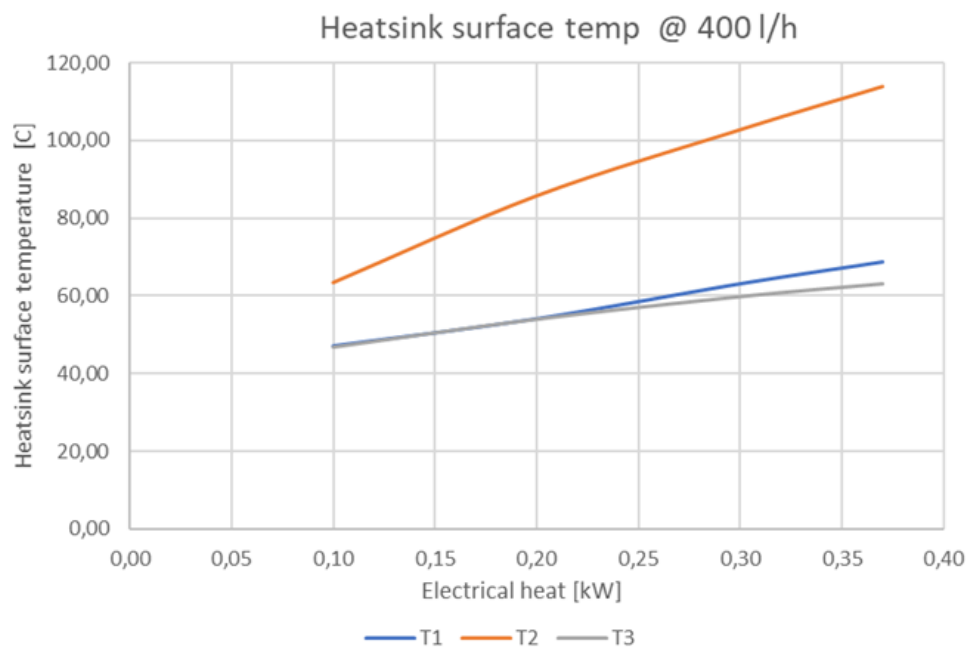


Figure 50 – Heatsink performance at 40 [°C] coolant temperature and 400 l/min coolant flow

Heatsink test results for 60 °C coolant temperature are presented in Table 20.

Table 20 - Test results obtained for 60 [°C] coolant temperature

P atm [hPa]	T air [°C]	Electrical heat [kW]	Heatsink surface temperature			Q liq [l/h]	P liq [mbar]	DP liq [mbar]	T liq in [°C]	T liq out [°C]	Q coolant [kW]
			T1 [°C]	T2 [°C]	T3 [°C]						
981,9	21,99	0,10	64,90	81,31	65,30	2500	2584	1385	60,01	60,08	0,16
981,7	21,52	0,20	70,70	101,36	70,81	2501	2585	1386	60,02	60,11	0,24
981,6	21,22	0,30	77,70	117,76	75,61	2500	2584	1385	60,05	60,17	0,30
981,5	21,06	0,34	79,83	123,76	77,02	2500	2583	1385	60,04	60,18	0,34
981,5	20,92	0,10	65,08	82,01	65,40	1800	1885	729	60,03	60,09	0,09
981,4	20,82	0,20	71,14	102,20	71,02	1800	1887	730	60,04	60,16	0,20
981,3	20,75	0,30	78,30	118,56	75,88	1800	1884	730	60,03	60,20	0,30
981,2	20,72	0,34	80,40	124,10	77,29	1800	1885	729	60,05	60,23	0,33
981,1	20,63	0,10	65,28	81,99	65,51	1500	1650	511	60,06	60,12	0,10
981,1	20,56	0,20	71,44	102,36	71,23	1500	1650	511	60,07	60,19	0,18
980,8	20,52	0,30	78,71	118,88	76,10	1500	1650	511	60,03	60,23	0,29
980,8	20,47	0,33	80,80	124,35	77,50	1500	1650	511	60,06	60,27	0,32
980,7	20,45	0,10	65,30	82,11	65,52	1400	1581	447	60,04	60,10	0,09
980,7	20,37	0,20	71,59	102,47	71,27	1400	1581	447	60,04	60,18	0,20
980,0	20,22	0,30	78,81	118,90	76,11	1400	1580	446	60,02	60,22	0,28
979,6	20,22	0,34	81,00	124,48	77,55	1400	1579	446	60,02	60,27	0,34
979,3	20,16	0,10	65,50	82,10	65,50	1200	1455	331	60,00	60,08	0,10
979,1	20,16	0,20	71,80	102,63	71,42	1200	1454	331	60,01	60,17	0,20
978,9	20,13	0,30	79,37	119,50	76,39	1200	1454	331	60,02	60,27	0,30
978,9	20,07	0,33	81,48	124,90	77,84	1200	1454	331	60,03	60,31	0,33

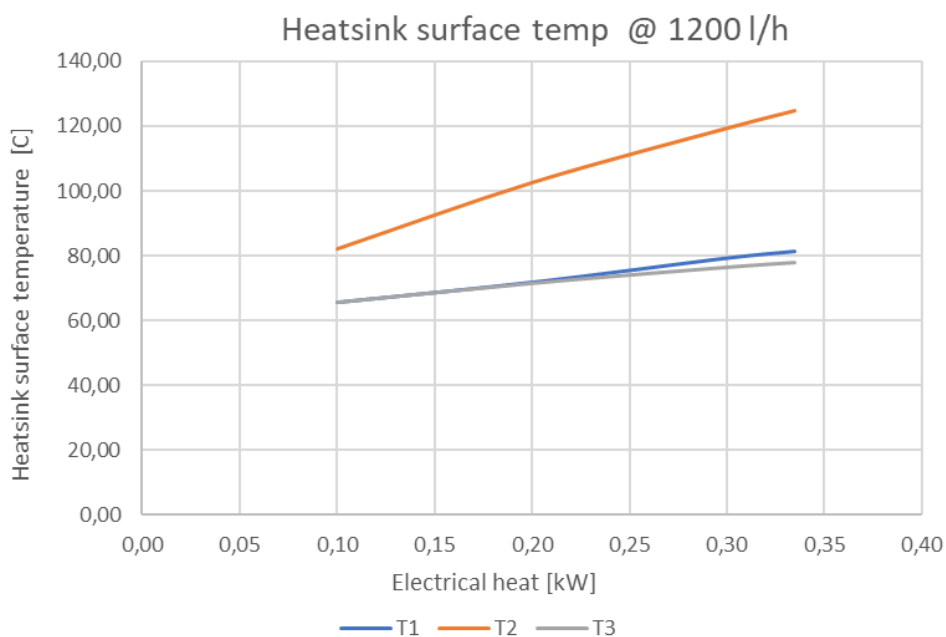


Figure 51 – Heatsink performance at 60 [°C] coolant temperature and 1200 l/min coolant flow

Heatsink test results for 80 °C coolant temperature are presented in Table 21.

Table 21 - Test results obtained for 80 [°C] coolant temperature

P atm [hPa]	T air [°C]	Electrical heat [kW]	Heatsink surface temperature			Q liq [l/h]	P liq [mbar]	DP liq [mbar]	T liq in [°C]	T liq out [°C]	Q coolant [kW]
			T1 [°C]	T2 [°C]	T3 [°C]						
983,3	21,87	0,10	84,97	100,80	86,60	2500	2518	1337	80,00	80,03	0,09
983,2	22,01	0,20	91,40	119,70	93,08	2500	2519	1339	80,00	80,08	0,20
983,3	22,14	0,29	97,51	134,76	98,59	2500	2520	1342	80,00	80,11	0,28
983,2	22,23	0,10	85,16	100,80	86,23	1800	1848	706	79,98	80,03	0,09
983,1	22,35	0,20	91,80	119,70	92,84	1800	1850	707	79,96	80,07	0,20
983,1	22,44	0,29	98,16	135,00	98,74	1800	1849	708	79,97	80,13	0,29
982,9	22,46	0,10	85,30	100,84	86,20	1500	1624	495	79,95	80,01	0,09
982,9	22,52	0,20	92,06	120,62	89,81	1500	1623	494	79,95	80,09	0,20
982,9	22,56	0,29	98,50	136,10	94,29	1500	1622	494	79,98	80,17	0,28
982,8	22,59	0,10	85,32	101,56	84,89	1400	1556	432	79,94	80,00	0,08
982,8	22,62	0,20	92,27	121,20	90,10	1400	1557	433	80,01	80,15	0,20
982,6	22,62	0,29	98,70	136,64	94,62	1400	1557	433	80,01	80,21	0,28
982,5	22,64	0,10	85,48	101,85	85,09	1200	1437	321	80,00	80,07	0,09
982,4	22,57	0,20	92,43	121,46	90,48	1200	1436	320	80,02	80,18	0,19
982,4	22,56	0,29	98,94	136,80	95,03	1200	1436	320	79,99	80,21	0,27

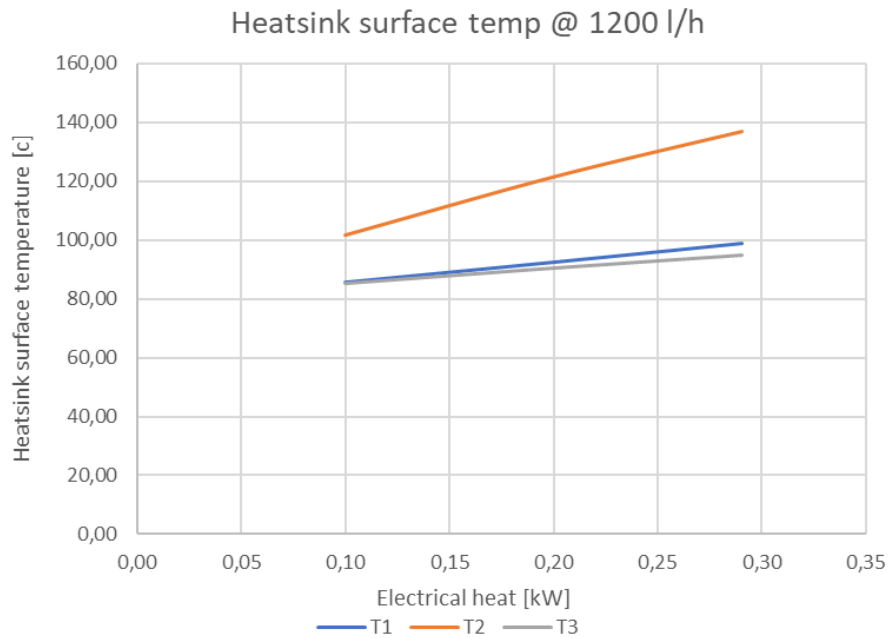


Figure 52 – Heatsink performance at 80 [°C] coolant temperature and 1200 l/min coolant flow

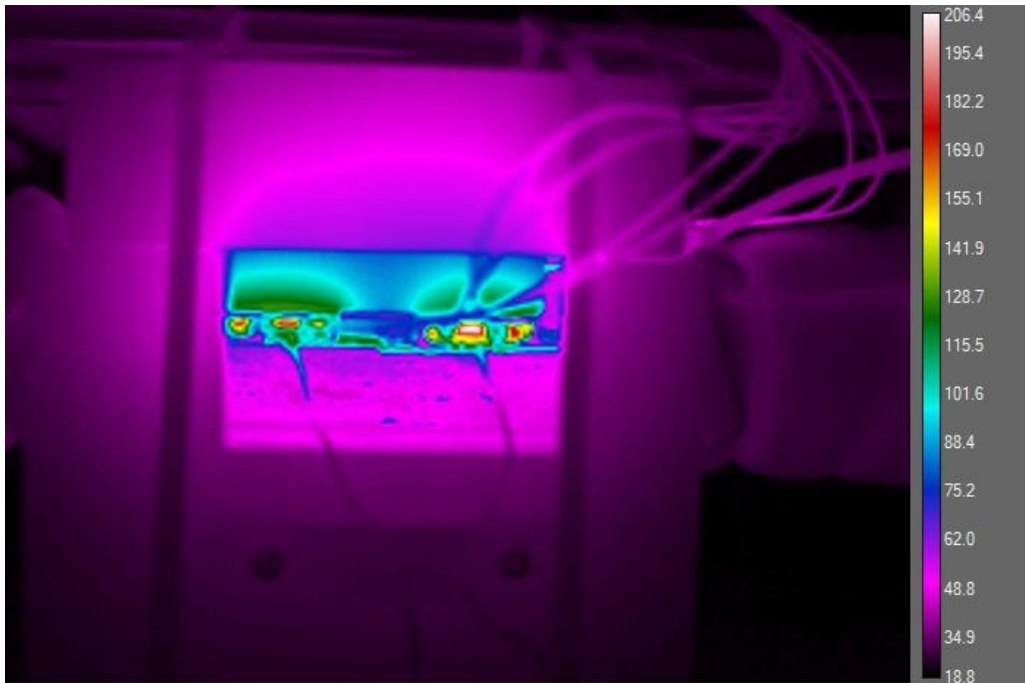


Figure 53 - Thermal imaging of heating elements on heatsink sample 1



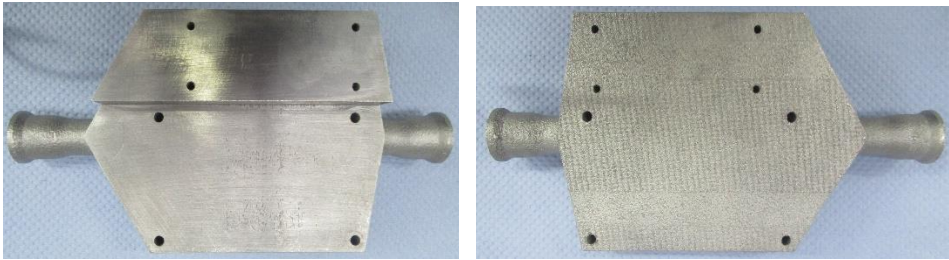
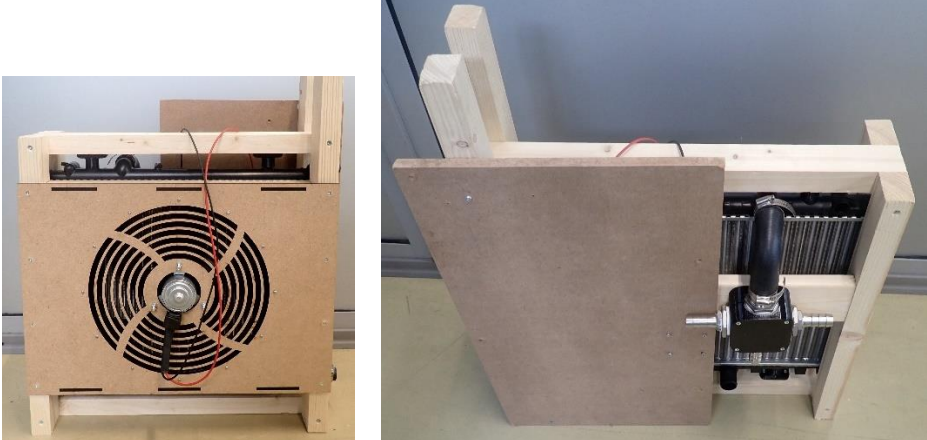
Figure 54 - Thermal imaging of heating elements on heatsink sample 2

6.5 THERMAL MANAGEMENT SYSTEM FUNCTIONAL CHARACTERISTIC TEST

6.5.1 TEST OBJECT IDENTIFICATION

The heatsink Sample 2 was chosen for the functional tests of integrated TMS. The TMS coolant pump was substituted with a test bed device to increase the coolant flow rate to 1500 l/h, as agreed upon between BOS and AU.

Table 22 - Test object identification

BOSMAL marking	General view	
Sample 2		
Integrated TMS module		

6.5.2 SCOPE OF THE TEST

Determination of Functional Characteristics according to BOSMAL instruction BOSMAL/I-7-57/04 and requirements:

- Coolant inlet temperature: 20; 40; 60 °C
- Coolant flow rate on inlet spout: 1500 l/h
- Electrical heating: 100; 200; 300; 400 W
- Fan supply voltage: 14 V
- Coolant: water/glycol – 50/50

6.5.3 TEST STAND INSTRUMENTATION

The test stand instrumentation is presented in Table 23.

Table 23 - Measurement devices identification

Name of device	BOSMAL identification number	Accuracy	Last calibration date	Next calibration date
Atmospheric pressure	F/0700/BW	± 1 hPa	02.2024	02.2026
Ambient air temperature	G/1186/BHW	$\pm 0.3^\circ\text{C}$	10.2024	10.2025
Coolant temperature	G/1565/BHW G/1566/BHW G/1567/BHW G/1568/BHW	$\pm 0.3^\circ\text{C}$	10.2024	10.2025
Coolant flow rate	F/0656/BW	$\pm 0.2\%$	05.2023	05.2026
Coolant pressure	F/1111/BHW	± 6 mbar	10.2024	10.2026
Coolant pressure drop	F/1109/BHW	± 2 mbar	10.2024	10.2026
Electrical heating	H/0879/BE	$\pm 0.2\%$	09.2024	09.2026
Heatsink surface temperature	H/0988/BE	$\pm 0.3^\circ\text{C}$	07.2024	07.2025
Fan Power Supply	H/0459/BE	$\pm 0,01$ V	09.2023	09.2025
Fan Voltage	H/0555/BE	± 0.1 V	12.2022	12.2024

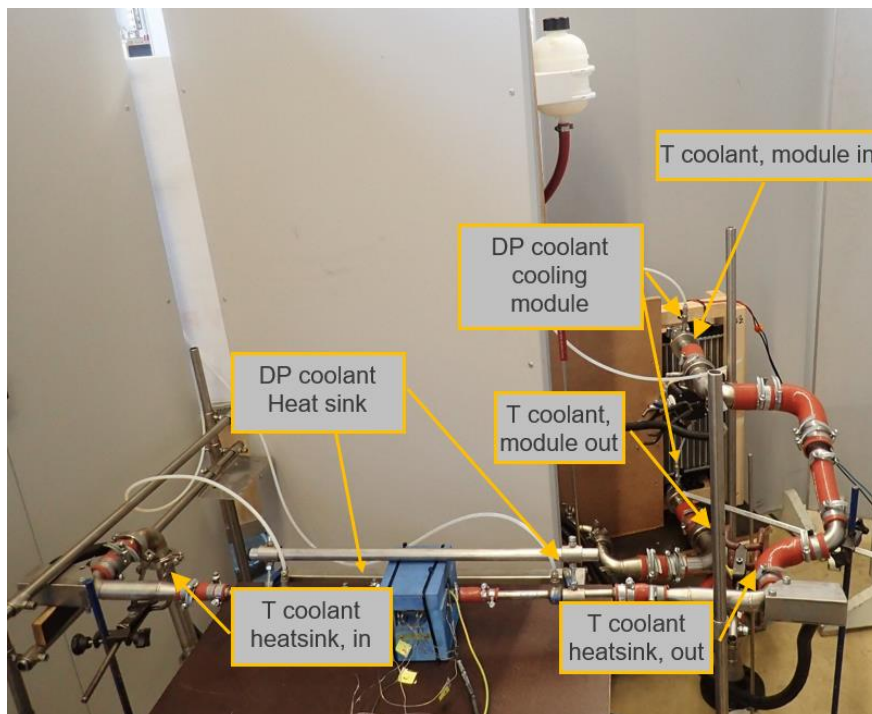


Figure 55 – TMS assembled on the test bench for the functional tests

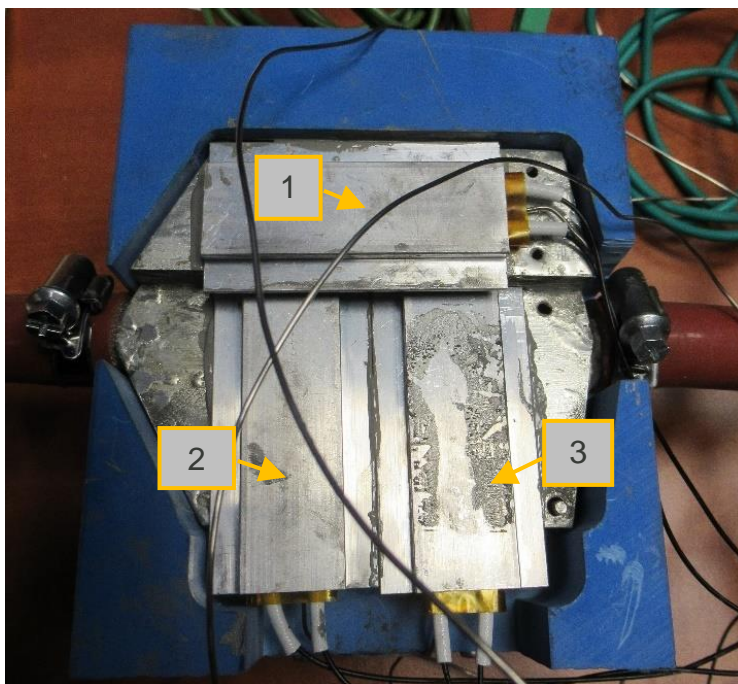


Figure 56 - Heating elements with heatsink surface temperature sensors

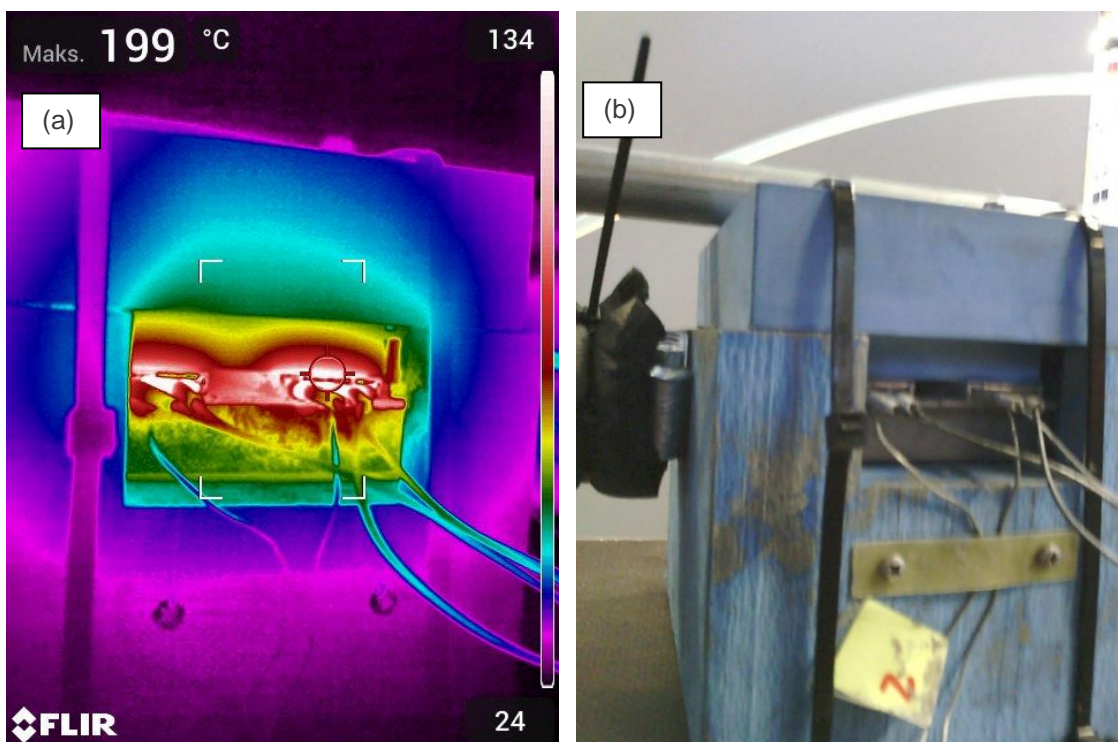


Figure 57 - Heatsink: a) Thermal imaging, b) Mounting presentation during the testing

6.5.4 TEST RESULTS – TMS

Test results for coolant temperature of 20 °C are presented in Table 24.

Table 24 - Test results obtained for 20 [°C] coolant temperature

Ambient		Heatsink				Coolant side of heatsink					Coolant side of cooling module				Fan system		
P atm [hPa]	T air [°C]	Electrical heat [kW]	heatsink surface temperature			Q liq [l/h]	P liq [mbar]	DP liq [mbar]	T liq in [°C]	T liq out [°C]	Q coolant of Heat sink [kW]	T liq in [°C]	T liq out [°C]	DP liq [mbar]	Q coolant of radiator in module [kW]	U [V]	I [A]
			T 1 [°C]	T 2 [°C]	T 3 [°C]												
972,7	22,2	0,10	30,52	27,30	27,00	1498	789	541	20,00	20,07	0,10	20,17	20,19	20	0	0	0
972,7	21,8	0,20	41,10	34,08	32,82	1497	790	541	20,00	20,14	0,20	20,24	20,25	20	0	0	0
972,4	21,4	0,30	50,22	42,42	39,69	1497	789	541	20,00	20,21	0,30	20,30	20,34	20	0	0	0
972,4	21,2	0,40	57,30	51,47	47,60	1497	790	541	20,00	20,27	0,39	20,38	20,38	20	0	0	0
Fan system switched off because of Tair ambient > T liq in																	

Where:

P atm – atmospheric pressure

T air – ambient air temperature

Electrical heat – electrical heat applied to heatsink surface

Heatsink surface temperature T1, T2, T3 – heatsink surface temperature measured with thermocouple between electrical heating pad and heatsink cold plate

Coolant side of heatsink:

Q liq – coolant flow measured

P liq – coolant pressure measured

DP liq – differential coolant pressure measured between inlet and outlet of heatsink

T liq in – coolant temperature measured at heatsink inlet

T liq out – coolant temperature measured at heatsink outlet

Q coolant of Heatsink – energy absorbed by coolant flowing through heatsink

Coolant side of cooling module:

T liq in – coolant temperature measured at inlet of radiator

T liq out – coolant temperature measured at outlet of radiator

DP liq – differential coolant pressure measured between inlet and outlet of radiator

Q coolant of radiator in module – coolant energy dissipated by radiator

Fan system:

U – voltage applied to cooling fan

I – electrical current flow through cooling fan

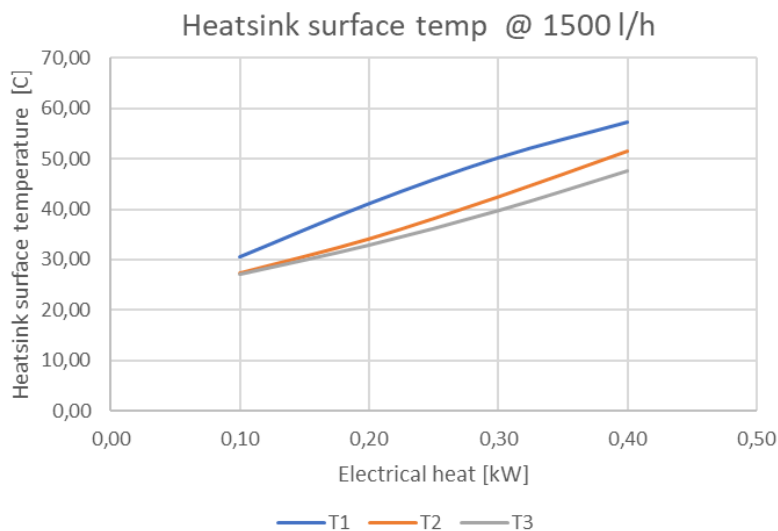


Figure 58 – TMS performance at 20 [°C] coolant temperature and 1500 l/h coolant flow

Test results for coolant temperature of 40 °C are presented in Table 25.

Table 25 - Test results obtained for 40 [°C] coolant temperature

Ambient		Heatsink				Coolant side of heatsink					Coolant side of cooling module				Fan system		
P atm [hPa]	T air [°C]	Electrical hest [kW]	heatsink surface temperature			Q liq [l/h]	P liq [mbar]	DP liq [mbar]	T liq in [°C]	T liq out [°C]	Q coolant of Heat sink [kW]	T liq in [°C]	T liq out [°C]	DP liq [mbar]	Q coolant of radiator in module [kW]	U [V]	I [A]
			T 1 [°C]	T 2 [°C]	T 3 [°C]												
967,6	20,0	0,10	50,80	47,20	46,39	1500	724	524	39,97	40,08	0,10	40,09	38,65	19	2,11	14,0	9,02
967,3	20,2	0,20	61,76	54,70	52,79	1500	724	523	39,98	40,13	0,20	40,18	38,71	19	2,16	14,0	8,83
967,2	20,3	0,30	68,23	63,48	60,00	1500	724	524	39,98	40,18	0,30	40,24	38,75	19	2,18	14,0	8,81
967,2	20,4	0,38	72,28	70,49	65,91	1500	723	523	39,98	40,27	0,38	40,29	38,84	19	2,12	14,0	8,81

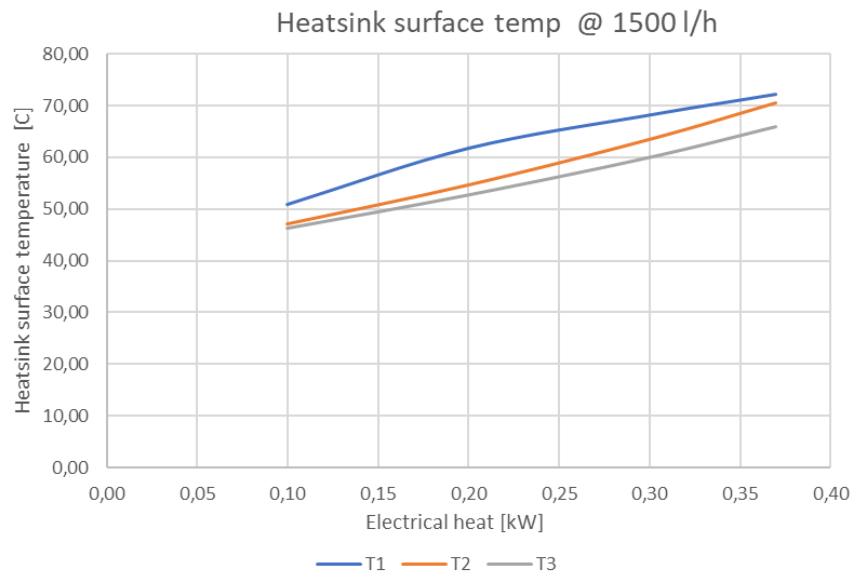


Figure 59 – TMS performance at 40 [°C] coolant temperature and 1500 l/h coolant flow

Test results for coolant temperature of 60 °C are presented in Table 26.

Table 26 - Test results obtained for 60 [°C] coolant temperature

Ambient		Heatsink				Coolant side of heatsink					Coolant side of cooling module				Fan system		
P atm [hPa]	T air [°C]	Electrical hest [kW]	heatsink surface temperature			Q liq [l/h]	P liq [mbar]	DP liq [mbar]	T liq in [°C]	T liq out [°C]	Q coolant of Heat sink [kW]	T liq in [°C]	T liq out [°C]	DP liq [mbar]	Q coolant of radiator in module [kW]	U [V]	I [A]
			T 1 [°C]	T 2 [°C]	T 3 [°C]												
967,6	20,0	0,10	50,80	47,20	46,39	1500	724	524	39,97	40,08	0,10	40,09	38,65	19	2,11	14,0	9,02
967,3	20,2	0,20	61,76	54,70	52,79	1500	724	523	39,98	40,13	0,20	40,18	38,71	19	2,16	14,0	8,83
967,2	20,3	0,30	68,23	63,48	60,00	1500	724	524	39,98	40,18	0,30	40,24	38,75	19	2,18	14,0	8,81
967,2	20,4	0,38	72,28	70,49	65,91	1500	723	523	39,98	40,27	0,38	40,29	38,84	19	2,12	14,0	8,81

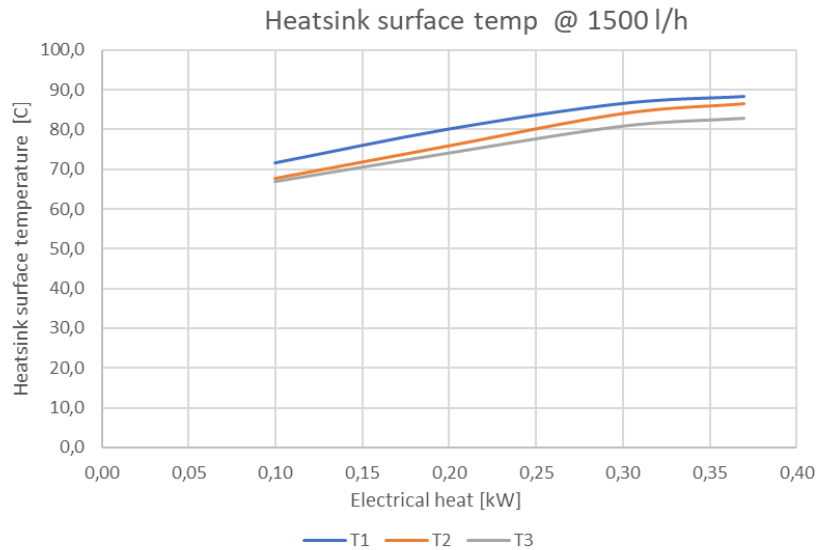


Figure 60 – TMS performance at 60 [°C] coolant temperature and 1500 l/h coolant flow

7 ANALYSIS OF THE THERMAL PERFORMANCE OF THE LIQUID-COOLED HEATSINK

This section presents a mathematical analysis of the experimental results obtained from heatsinks testing at BOSMAL. The primary focus was on the aluminium heatsink as it represented the final version intended for application in the RHODAS project.

7.1 ALUMINUM VS. COPPER HEATSINK PERFORMANCE

The test results indicate that the aluminium heatsink outperforms the copper heatsink in terms of heat dissipation rate under identical test conditions. This outcome is attributed to the high active surface roughness of the copper heatsink, including visible air bubbles in thin layer. These surface imperfections resulted from the rectification process made to resolve a coolant leakage issue before the copper heatsink was sent to BOSMAL.

A detailed comparison also reveals a significant temperature variation at the regions marked as points 2 and 3 on the copper heatsink in Figure 46. This temperature variation as in Figure 46 arises from the asymmetric distribution of air bubbles and the tin layer on the copper heatsink surface (marked as Sample 1). In contrast, the aluminium heatsink shows much closer temperature distribution values between these points, reflecting the superior design and manufacturing processes of the aluminium heatsink.

7.2 DATA ANOMALIES IN SAMPLE 2

Upon reviewing the test data for Sample 2, an error in either the recorded measurements or the labelling of T1 and T2 values was inferred. This assumption was based on the expectation that the highest temperature should correspond to the largest cold plate area for the GaN semiconductor, denoted as T1 in Figure 56. Following an investigation, it was stated that the differences in T1, T2 measurements derived from the thermocouples mounting differences between different tests of heatsinks. The thermocouples were installed in-between the heatsink cold plate and a heating element surface using thermal interface material and clamping force. Slight differences in positioning (e.g. closer or farther away from heating element) could influence the measurement result. As a further

improvement a dedicated channel for thermocouple could be machined into the heatsink surface to provide repeatable contact area for the temperature measurement.

7.3 PERFORMANCE EVALUATION OF THE ALUMINUM HEATSINK

Since the aluminium heatsink was intended to be used in the final prototype, the analysis focuses on test results reported for Sample 2. Key performance metrics derived from the data are as follows:

Based on figures extracted from the datasheets for the SiC and GaN modules (see Figures 5–6), the junction temperature limits are 175 °C and 150 °C, respectively.

Under coolant temperatures of 20 °C and 40 °C, the calculated heatsink surface and junction temperatures remain well below these limits, demonstrating the aluminium heatsink effectiveness.

7.4 SYSTEM CHARACTERIZATION AND WORST-CASE SCENARIO

According to the system characteristics defined in WP1 for TMS characterization, the thermal management system (TMS) must be capable of:

- A total heat loss of 3 kW.
- Operating temperature range of -20 °C to 50 °C.

Assuming the worst-case scenario of a coolant temperature at 60 °C, the summarized results in Table 9 show that the aluminium heatsink can adequately manage the heat dissipation requirements of the SiC module. Supporting calculations confirm that the design meets the system operational needs.

$$P_{max} = 150kW \quad (1)$$

$$P_{max,phase} = 50kW \quad (2)$$

$$P_{Loss,2\%,phase} = 2\% * 50kW = 1kW \quad (3)$$

$$P_{Loss,2\%,phase,SiC} = 0.50 * P_{Loss,2\%,phase} = 500W \quad (4)$$

$$R_{th,J2C} = 0.13 K/W \text{ (datasheet)} \quad (5)$$

$$\Delta T_{L2H,max,test} = T_{C,max,test} - T_{L,max,test} = 81°C - 60°C = 21°C \quad (6)$$

$$P_{Loss,SiC,test} = 340W \quad (7)$$

$$R_{th,max,L2H} = \frac{\Delta T_{L2H,max,test}}{P_{Loss,SiC,test}} = \frac{21}{340} = 0.06 \frac{K}{W} \quad (8)$$

The calculation of the junction temperature if: $P_{Loss,2\%,phase} = 2\% * 50kW = 1kW$:

$$\Delta T_{L2H,2\%} = R_{th,max,L2H} * P_{Loss,2\%,phase,SiC} = 0.06 * 500 = 31^{\circ}\text{C} \quad (9)$$

$$\Delta T_{j2C,2\%} = R_{th,j2C} * P_{Loss,2\%,phase,SiC} = 0.13 * 500 = 65^{\circ}\text{C} \quad (10)$$

$$T_{j,max,SiC} = \Delta T_{j2C,2\%} + \Delta T_{L2H,2\%} + T_{L,max,test} = 156^{\circ}\text{C} < 175^{\circ}\text{C} \quad (11)$$

The above calculations demonstrate that the aluminium heatsink version is capable of handling the 3 kW power losses and the ambient temperature range of -20 °C to 50 °C, with a considerable safety margin relative to the defined operational boundaries.

Regarding the GaN module, as expected based on the calculations in T3.1 of WP3, the design limitations - specifically the requirement for an interconnected heatsink to cover both the SiC and GaN boards - result in a larger height behind the GaN board and a lower Tj restriction for the GaN module. Consequently, the heatsink can effectively manage GaN losses up to 350 W, positioning the GaN module in areas with lower power loss requirements.

While the test shows that the heatsink can overcome to the goals that was defined for the TMS, in the next step we want to calculate two scenario that we have 2.4% and 3% losses in the converter. Please see the following calculations:

The calculations for **2.4%** Power losses:

$$P_{max} = 150kW \quad (12)$$

$$P_{max,phase} = 50kW \quad (13)$$

$$P_{Loss,2.4\%,phase} = 2.4\% * 50kW = 1.2kW \quad (14)$$

$$P_{Loss,2.4\%,phase,SiC} = 0.50 * P_{Loss,2.4\%,phase} = 600W \quad (15)$$

$$R_{th,j2C} = 0.13 \text{ K/W (datasheet)} \quad (16)$$

$$\Delta T_{L2H,max,test} = T_{C,max,test} - T_{L,max,test} = 81^{\circ}\text{C} - 60^{\circ}\text{C} = 21^{\circ}\text{C} \quad (17)$$

$$P_{Loss,SiC,test} = 340W \quad (18)$$

$$R_{th,max,L2H} = \frac{\Delta T_{L2H,max,test}}{P_{Loss,SiC,test}} = \frac{21}{340} = 0.06 \frac{\text{K}}{\text{W}} \quad (19)$$

The calculation of the junction temperature if: $P_{Loss,2.4\%,phase} = 1.2kW$:

$$\Delta T_{L2H,2.4\%} = R_{th,max,L2H} * P_{Loss,2.4\%,phase,SiC} = 0.06 * 600 = 37.08^{\circ}\text{C} \quad (20)$$

$$\Delta T_{j2C,2.4\%} = R_{th,j2C} * P_{Loss,2.4\%,phase,SiC} = 0.13 * 600 = 78^{\circ}\text{C} \quad (21)$$

$$T_{j,max,SiC,2.4\%} = \Delta T_{j2C,2.4\%} + \Delta T_{L2H,2.4\%} + T_{L,max,test} = 175.08 \cong 175^{\circ}\text{C} \quad (22)$$

The calculations for **3%** Power losses:

$$P_{max} = 150kW \quad (23)$$

$$P_{max,phase} = 50kW \quad (24)$$

$$P_{Loss,3\%,phase} = 3\% * 50kW = 1.5kW \quad (25)$$

$$P_{Loss,3\%,phase,SiC} = 0.50 * P_{Loss,3\%,phase} = 750W \quad (26)$$

$$R_{th,j2C} = 0.13 \text{ K/W (datasheet)} \quad (27)$$

$$\Delta T_{L2H,max,test} = T_{C,max,test} - T_{L,max,test} = 81^{\circ}\text{C} - 60^{\circ}\text{C} = 21^{\circ}\text{C} \quad (28)$$

$$P_{Loss,SiC,test} = 340\text{W} \quad (29)$$

$$R_{th,max,L2H} = \frac{\Delta T_{L2H,max,test}}{P_{Loss,SiC,test}} = \frac{21}{340} = 0.06 \frac{\text{K}}{\text{W}} \quad (30)$$

The calculation of the junction temperature if: $P_{Loss,3\%,phase} = 1.5\text{kW}$:

$$\Delta T_{L2H,3\%} = R_{th,max,L2H} * P_{Loss,3\%,phase,SiC} = 0.06 * 750 = 46.35^{\circ}\text{C} \quad (31)$$

$$\Delta T_{j2C,3\%} = R_{th,j2C} * P_{Loss,3\%,phase,SiC} = 0.13 * 750 = 97.50^{\circ}\text{C} \quad (32)$$

$$T_{J,max,SiC,3\%} = \Delta T_{j2C,3\%} + \Delta T_{L2H,3\%} + T_{L,max,test} = 203.85^{\circ}\text{C} > 175^{\circ}\text{C} \quad (33)$$

The following calculations show that in the case of 2.4%, the system approximately touches the boundary, and for the case of 3%, it exceeds the boundary, meaning the heatsink cannot support the operation of the SiC modules. Attention to the ΔT_{j2C} value is crucial in this calculation, as it stems from the physical restrictions of the SiC power modules and cannot be compensated. Additionally, these calculations are based on the highest ambient temperature as the worst-case scenario. The only parameter that can be improved is $R_{th,L2H}$ which can be reduced by using an appropriate thermal interface material and applying high mounting pressure. After calculation, it is determined that by reducing $R_{th,L2H}$ from $0.06 \frac{\text{K}}{\text{W}}$ to the $0.02 \frac{\text{K}}{\text{W}}$ we have:

$$T_{J,max,SiC,3\%} = \Delta T_{j2C,3\%} + \Delta T_{L2H,3\%} + T_{L,max,test} = 173^{\circ}\text{C} < 175^{\circ}\text{C} \quad (34)$$

In this regard, AU suggests that to improve the overall efficiency of the TMS system, a **graphite-based thermal interface material** should be used, coupled with high mounting pressure.

8 CONCLUSION

The deliverable D3.3 provides a comprehensive analysis of the Thermal Management System testing and validation activities undertaken as part of the RHODAS project and focusing on a 150kW high-power converter version. The findings presented in this report are valuable for advancing the development of efficient and reliable thermal management solutions for heavy-duty electric transportation.

The findings and recommendations outlined in this deliverable have significant implications for the development of next-generation electric transport technologies. The innovative liquid-cooled heatsink design represent an advancement in thermal management solutions dedicated for the high-power GaN and SiC modules applied for the state-of-art-electric motors inverters.

The obtained test results positively validate the TMS design for the high-power converter solution. The final system-level test results and analysis are detailed in the WP5 deliverables.

Note: A delay in the delivery of this deliverable occurred, mainly due to delays in the manufacturing and testing of the 15kW base converter, and technical problems in the design of the internal cooling channels of the heatsinks of the 150kW high power converter.

However, these delays have not affected either the development of the modulations and cooling of the low power converter (15kW), or the final design of the heatsinks for the high-power converter (150 kW). The developments and conclusions in modulation and cooling have been able to be incorporated into the design and manufacturing of the 150kW high power converter, currently in the electrical testing phase prior to its integration into the demonstrator.